Assessing the Potential of Activated Bauxite Residue (ABR) to Remove PFAS in the Water Column

by

Jingya Pang

A thesis submitted in partial fulfillment of the requirements for the degree of

Master of Science

in

Environmental Science

Department of Civil and Environmental Engineering
University of Alberta

Abstract

Per- and polyfluoroalkyl substances (PFAS) belong to a group of synthetic organic compounds characterized by the substitution of at least one hydrogen atom with fluorine and the presence of other functional groups. Their high thermal and chemical stability makes PFAS resistant to removal and degradation. PFAS have been widely detected in the environment and food chain, with potential effects on humans. Wastewater treatment plant (**WWTP**) effluent is a significant source of PFAS emissions, and conventional wastewater treatment processes have proven ineffective against PFAS. This has sparked a growing interest in adsorption as a potential treatment option. Bauxite residue (**BR**), a by-product of alumina extraction, is highly alkaline material that poses environmental and health risks due to the potential release of toxic materials. However, BR has a potential to be reused for other purposes including wastewater treatment. This study investigates the efficacy of activated bauxite residue (**ABR**) as an adsorbent material for removing PFAS in the water column and evaluates its capacity as a viable solution for PFAS treatment technology. The potential of ABR for PFAS removal from wastewater was evaluated using a comprehensive approach involving three aspects: **(1)** characterization of ABR, focusing on porosity, elemental composition, bond types, and surface charge, **(2)** evaluation of adsorption kinetics and isotherms to quantify adsorption rate, capacity, and PFAS removal efficiency, and **(3)** biological toxicity testing via acute toxicity (*Daphnia magna*) and *in-vitro* bioassays to address cell toxicity pathways (cytotoxicity, estrogenicity, and mutagenicity). Brunauer-Emmett-Teller (**BET**) surface analysis revealed ABR is predominantly mesoporous, which can enhance the adsorption capacity and removal efficiency of PFAS. The pore size distribution indicated the heterogeneity of pore sizes on ABR. X-ray photoelectron spectroscopy (**XPS**) analysis showed an increase in fluorine (F) relative atom concentration from 1.37% to 57.69% after saturation with

100 mg/L PFAS (100 mg/L for individual of 10 PFAS), suggesting surface adsorption. The elemental concentration obtained from XPS and energy-dispersive X-ray spectroscopy (**EDX**) (detection depth of 1–10 nm vs up to 5000 nm) further confirmed the presence of F on the surface. Furthermore, **carbon-fluorine bonds** were detected on the "spent" ABR, supporting this conclusion. The most significant difference in surface charge between "virgin" and "spent" ABR occurred at pH 6–8, emphasizing the need to neutralize ABR solution to improve the removal efficiency. Various dosages of ABR (10, 15, 25, 50, and 100 g/L) and exposure periods (1 h vs 24 h) were tested. The highest sum removals (∑PFAS) of ~91% was achieved at 100 g/L, but even a 10 g/L dosage was nearly as effective (~87%). This was comparable to a commercial powdered activated carbon (**PAC**), suggesting the potential of ABR to exhibit better performance at higher concentrations. The removal efficiency was higher for long-chain PFAS (#C ≥6 for perfluoroalkyl **sulfonic** acids [**PFSAs**] and ≥8 for perfluoroalkyl **carboxylic** acids [**PFCAs**]), where the stronger electrostatic and hydrophobic interactions and higher molecular weight may contribute. Also, the short-term exposure was sufficient for the complete removal of long-chain PFAS, while a longer exposure period may be required for short-chain ones. Pseudo-second-order (**PSO**) adsorption kinetic models fit PFAS slightly better than other models (R^2 ranged from 0.995 to 1), suggesting that chemisorption likely occurred on the ABR surface. However, individual PFAS followed different isotherm models (Langmuir, Freundlich, and Sips) in the mixture. These differences can be attributed to **(1)** the pore blocks of long-chain PFAS, **(2)** the interactions between PFAS molecules, and **(3)** the varying numbers of layers. Finally, no acute toxicity was observed in *Daphnia magna* exposed to standardized environmental water treated with 50 g/L ABR, indicating that the treatment process does not introduce additional toxicity into treated water at practical levels. Furthermore, cytotoxicity assessments using the *Aliivibrio fisheri* assay showed no

significant difference across dosages, with the lowest $1/IC_{10}$ for 10 g/L ABR. Hence, the use of <10 g/L ABR is effective as both removal efficiency is maximized, and the potential toxicity is minimized. Estrogenicity was not impacted by ABR through yeast-estrogen screen (YES) analysis. Similarly, there was no detectable DNA damage via the umuC assay. Overall, the use of ABR adsorption is a promising solution to remove PFAS from the water column, offering environmental and economic benefits for more sustainable water treatment practices.

Preface

This thesis is an original work by Jingya Pang under the supervision of Dr. Maricor Arlos. Experiments related to *Daphnia magna* acute toxicity were run by Demi Meier and part of experiments related to *in-vitro* bioassays were run together with Huixin Qiu. Part of this work has been presented/accepted for poster and oral presentations to conferences including Society of Environmental Toxicology and Chemistry Prairie Northern Chapter (SETAC PNC) 2024 Annual General Meeting and Conference, Faculty of Engineering Graduate Research Symposium (FEGRS) 2024, and National Water and Wastewater Conference (NWWC) 2024. No part of this thesis has been previously published.

Acknowledgments

No words can express my deepest gratitude to my supervisor Dr. Maricor Arlos, for her unwavering dedication in imparting her professional expertise and technical knowledge which has well-equipped me as a Master's student. I am grateful for her constant constructive guidance, invaluable advice, and insightful feedback throughout my Master's study which has always enlightened the journey and next steps of my research, and for her continuous and boundless encouragement, enthusiasm, compassion, patience, kindness and trust over the past two years which have made me more resilient, stronger, and courageous in facing challenges. Also, this work would not have been accomplished without assistance and support from (1) Scott Berggren and his team for their feedback and suggestions on the progress from an industrial perspective; (2) Aaron Boyd and Dr. Tamzin Blewett for their technical support and experimental space for running *Daphnia magna* tests; (3) Nas Yousefi, Shihong Xu, and Peng Li from nanoFAB – Fabrication and Characterization Facility, University of Alberta for their training and help with material characterization tools and running some of the analysis; (4) Ola Jabar from the Department of Chemical and Petroleum Engineering, Research Instrumentation and Technical Support Lab, University of Calgary for part of the material characterization; (5) David (Yupeng) Zhao and Brett Mason for their guidance and kind assistance with the equipment in the teaching and shared lab; (6) Fei Cheng and Demi Meier for their training on the experiments completed in this thesis; (7) Huixin Qiu for her company and help in running some of the *in-vitro* bioassays; (8) Daniela Pulgarin Zapata and Emily Quecke for their helpful discussions and collaborations on the experiments; (9) Mitacs and GRÖN Holding Corporation for the financial support of this project. I am profoundly grateful to all of them. In addition, I would like to extend my thanks to all the lab mates in Arlos Research Lab (present and former) for their company, encouragement, and collaboration which have been essential during this journey. I appreciate the University of Alberta for providing me with the opportunity and resources to continue my study. Finally, special thanks to my family and friends for their companionship, comfort and joy, which have given me the courage to keep moving forward.

Table of Contents

List of Tables

List of Figures

List of Abbreviations

Abbreviation	Full Form
ABR	Activated bauxite residue
AFFF	aqueous film forming foams
A^2O	anaerobic/anoxic/oxic
BET	The Brunauer-Emmett-Teller
BR	Bauxite Residue
CFU	colony-forming unit
DMSO	dimethyl sulfoxide
EC_{50}	half maximal effective concentration
EDX	energy dispersive X-ray
EFSA	European Food Safety Authority
E2	17β-Estradiol
FTOH	fluorotelomer alcohols
GAC	Granular activated carbon
HRT	hydraulic retention time
LHA	lifetime health advisory
MOA	modes of action
MOF	Metal-organic frame
NOM	Natural organic matter
OECD	The Organisation for Economic Co-operation and Development
OM	Organic matter
PAC	Powdered activated carbon
PFAA	perfluoroalkyl acid
PFAS	perfluoroalkyl and polyfluoroalkyl substances
PFBA	Perfluorobutanoic
PFBS	Perfluorobutanesulfonic
PFCA	perfluoroalkyl carboxylic acids
PFDA	Perfluorodecanoic
PFHpA	Perfluoroheptanoic
PFHxA	Perfluorohexanoic
PFHxS	Perfluorohexane sulfonate
PFNA	Perfluorononanoic
PFO	Pseudo-first-order
PFOA	Perfluorooctanoic
PFOS	perfluorooctane sulfonate
PFPeA	Perfluoropentanoic
PFSA	perfluoroalkyl sulfonic acids
PFTEDA	Perfluorotetradecanoic
PFUnA	Perfluoroundecanoic
PMTs	persistent, mobile and toxic substance
POP	persistent organic pollutant
PSO	Pseudo-second order
QA/QC	Quality assurance/quality control
RM	Red mud
SPE	solid phase extraction

SVHC	Substances of Very High Concern
TOP	pre-total oxidizable precursor
TWK	Trinkwasserkommission (German Drinking Water Commission)
US/USA	United States
USEPA	United States Environmental Protection Agency
WWTP	wastewater treatment plant
XPS	X-ray photoelectron spectroscopy
YES	Yeast Estrogen Screen
6:2 FTSA	6:2 Fluorotelomer Sulfonic

1 Introduction

1.1 Brief origin and background of perfluoroalkyl and polyfluoroalkyl substances (PFAS)

Fluorinated substances include a large umbrella of organic and inorganic substances that contain at least one fluorine atom [1]. A subclass of highly fluorinated chemicals known as perfluoroalkyl and polyfluoroalkyl substances (**PFAS)** contain ≥1 carbon atom bonded to F atoms with a general structure of C_nF_{2n+1} [2]. The Organisation for Economic Co-operation and Development (OECD) expanded the definition as any organic substances that contain at least one fully fluorinated methyl (perfluorinated methyl group-CF_3-) or methylene (perfluorinated methylene group-CF_2-) carbon atom, excluding those bonded with any H/Cl/Br/I atom [3]. Today, the "PFAS" terminology is commonly associated with **per- and polyfluoroalkyl** substances, a group of synthetic organic compounds characterized by at least one hydrogen atom substituted by fluorine atoms and the presence of other functional groups [4], [5]. These legacy (e.g., already banned perfluorooctane sulfonate [**PFOS**] and perfluorooctane sulfonic acid) and emerging contaminants have been popularly used in the last several decades [6]. There are now more than 4,700 types of PFAS, with that number continuing to grow [7].

Generally, PFAS could be divided into two categories: perfluoroalkyl **sulfonic** acids (**PFSAs)** and perfluoroalkyl **carboxylic** acids (**PFCAs)** [8]. Based on the carbon chain length that easily differentiates chemical properties (e.g., hydrophobicity and environmental mobility), each subclass of PFAS can be further classified as short- and long-chain. Long-chain PFSAs include substances with ≥6 carbon (e.g., PFOS, $C_8F_{17}SO_3H$) and long-chain PFCAs contain ≥8 carbon (e.g., perfluorooctanoic acid, PFOA, $C_7F_{15}CO_2H$) [9]. PFSA with <6 carbons and PFCA with <8 carbons are called short-chain PFAS. As a result, PFAS now represent a diverse class of compounds unified by the presence of a perfluoroalkyl group. This structural characteristic, combined with many functional groups, leads to different interactions with a wide range of environmental and biotic matrices [10].

In recent years, escalating concerns about PFAS have catalyzed substantial global research interests. More specifically, PFAS are hard to remove from or decompose in the environment, rendering them one of the persistent, mobile and toxic substances (PMTs). PFAS are composed of a hydrophobic carbon chain with halogens and a hydrophilic functional group at one end in their structures, imparting their unique amphiphilic properties. The high electronegativity of fluorine makes carbon-fluorine single bond [11] the strongest covalent bond with a bond energy of 485 kJ/mol, which is much higher than that of C-O single bond (358 KJ/mol) and C-C single bond (348 kJ/mol) [12], [13]. Hence, these characteristics present significantly high thermal and chemical stability [14], with many now referring to PFAS as "forever chemicals" [15]. To illustrate this, two of the most popular PFAS substances, PFOS and PFOA have half-lives of >41 and >92 years, respectively [16]. Additionally, PFAS have been observed to bio-transform into perfluoroalkyl acids (**PFAA**) as "dead end" daughter products, rendering PFAS to be poorly biodegradable (also see **Section 1.4.2**) [10]. In some cases, the so-called precursors transform into non-fluorinated moieties, but a perfluorinated residue always remains in the environment [12].

Subsequently, due to PFAS' high thermal and chemical stability, they are extremely suitable as water and oil repellants and friction-resistant additives [17]. Since the 1940s, PFAS substances have been successfully employed in numerous industrial or consumer products, covering more than 100 sectors. They are widely manufactured as ingredients for surfactants, lubricants, insecticides [18], cosmetics, non-stick pans, food packages, waterproof clothing [19], chromium plating, photolithography [5], aqueous film forming foams (AFFF), and even included in many categories like ammunition, climbing ropes, guitar strings, artificial turf and soil remediation [20] to name a few. The total quantity of worldwide fluoropolymers produced alone is estimated at 320,000 tons annually [21]. Given that PFAS are used in almost all aspects of human life with long-range mobility/transport potential [22] similar to persistent organic pollutants (POPs) [23], [24], PFAS tend to transfer globally through atmospheric and/or oceanic diffusion [25].

PFAS have been detected in every phase of our environment: soil, air, organisms, and sediments, particularly in various aquatic matrixes [11] including surface water, fresh water, rainwater, snow, groundwater, and drinking water [17], [24], [26]. For example, PFAS concentrations in Lake Victoria in Africa revealed PFOA and PFOS levels ranging from 0.4–11.65 ng/L and 0.4–2.53 ng/L respectively [27]. High levels of PFAS concentrations in the water column were observed in different regions and different water bodies in China as well. For example, 12 PFAS substances were detected in Qing River, peaking in summer in a range of 39.44 to 207.59 ng/L [28]. In groundwater, Chen et al. investigated eight rural areas in eastern China and detected 17 PFAS in the groundwater ranging from 5.3 to 615 ng/L. The most abundant PFCAs in the groundwater were PFBA and PFOA, followed by PFNA, PFHpA, and PFHxA while the prevalent PFAS was PFBS, followed by PFOS and PFHxS [29]. Water samples from the South China Sea were also characterized to have a total PFAS concentration in the range of 0.195–4.925 ng/L [30]. Similarly, surface water collected in the Western Mediterranean Sea indicated the presence of 15 different PFAS substances, quite uniformly distributed across the selected area and with total concentrations ranging from 0.246 to 0.515 ng/L [31]. Especially in Canada, PFAS has been observed in diverse aquatic environments. Codling et al. detected a mean concentration of 9 ng/L for ∑17PFAS in the stormwater in Saskatoon, Saskatchewan [32]. An evaluation of risk for PFAS exposure in source water for drinking water in Ontario revealed a mean concentration of 6.4 ng/L ∑10 PFAS [33]. For freshwater samples collected across Canada from 2013 to 2020, 13 PFAS were measured in 566 samples, with a maximum of ~140 ng/L (PFHxA and PFBS) [34].

PFAS does not only pollute and persist in the environment, but can also enter biota such as invertebrates, fish, and humans [35], [36]. For example, PFAS levels in benthic invertebrates can reach levels 1000 times higher than that in the water [8]. In the St. Lawrence River (Quebec, Canada), the mean of ∑60 PFAS concentration in fish was 21–92 ng/g and the highest (~92±34 ng/g) was observed in Smallmouth bass (*Micropterus dolomieu*) [37]. PFAS are extremely bioaccumulative in the food chain via their potential binding to lipoproteins in blood [6]. Hence,

PFAS has been also widely detected in human blood, human breast milk, and animal muscle tissues [13]. Even relatively low levels of PFAS in drinking water can lead to significant burdens in blood serum over a lifetime period [38]. Furthermore, toxic effects (EC_{50}, half maximal effective concentration) of PFCAs have been observed (laboratory settings) on aquatic organisms such as marine mussels (33 to 594 µg/L) [39], microalgae (27.5 to163.6 mg/L) and primary (20 to 110 mg/L) and secondary consumers (0.11 to 15.5 mg/L) [40]. In humans, exposure to PFAS (pre-natal and early-life stages) has been associated with decreased birth weights in new-borns and alterations in the behaviour or accelerated puberty in children [7], [17], [18], [38]. PFOS is linked to a reduction in antibody response to immunization in children and raised blood total cholesterol in adults [38]. Moreover, both acute and chronic diseases in humans such as diabetes, cerebrovascular diseases, myocardial infarction, Alzheimer's and Parkinson's diseases, and asthma have been associated with PFAS exposure even at trace concentrations [7], [17], [18]. Hence, the United States Environmental Protection Agency (USEPA) has classified PFOA as a likely carcinogen [41]. Residents living in sites near significant PFAS contamination have also been found to have higher relative risks for kidney, breast, prostate and testicular cancer [38], [42]. Hence, several jurisdictions around the world have defined guidelines and regulations for PFAS concentrations in drinking water, to protect human health as subsequently described below.

1.2 Regulations on PFAS concentration in drinking water

As attention to PFAS continues to grow and the risks of exposure to PFAS in humans and animals have been widely recognized, many countries and organizations have enacted PFAS regulations/guidelines in different water matrices or different uptake pathways. Nonetheless, it is currently impractical to ban all PFAS use since they are essential in many areas (e.g., surgical gowns) and there appears to be no current alternative. These essential uses were defined under the Montreal Protocol, including the categories related to health, safety and the functioning of our society [20], [43].

PFAS guideline threshold values are influenced by many factors, including social, political, and economic considerations [44]. So far, most response actions have only been focused on a handful of substances such as PFOA and PFOS due to their widespread prevalence and known adverse effects [10]. In industry, PFOA and PFOS have been added to the limited or forbidden list of the Stockholm Convention on Persistent Organic Pollutants and included in the Candidate list of the Substances of Very High Concern (SVHC).

Humans (as the final link in numerous food chains) uptake PFAS primarily through food and drinking water [43]. As a consequence, regulation of PFAS concentration has been implemented for drinking water in many jurisdictions. In Europe, most countries have established different drinking water limits for PFAS intake. For example, the German Drinking Water Commission (Trinkwasserkommission [TWK]) first set the health-based lifelong PFOA and PFOS exposure of 0.3 g/L in drinking water in 2006 [45]. In Italy, the highest amount of PFAS in drinking water was enforced by the Italian National Health Institute with PFOS ≤30 ng/L, PFOA ≤500 ng/L, and other PFAS ≤500 ng/L. The German Ministry of Health proposed a health-based guidance of a maximum of 300 ng/L for the sum of PFOA and PFOS in drinking water. Due to variations in regulations across Europe, the European Food Safety Authority (EFSA) published a tolerable weekly dose of only 4.4 ng/kg body weight for the sum of four representative PFAS: PFOA, PFOS, PFNA and PFHxS in 2020. In Australia, the highest daily intake is 20 ng/person for the sum of PFOS and PFHxS and 160 ng/person for PFOA. Their drinking water quality guidelines specify the levels of 70 ng/L for the sum of PFOS and PFHxS, and 560 ng/L for PFOA [46].

In the United States (US), the United States Environmental Protection Agency (USEPA) recommends a lifetime health advisory (LHA) of 70 ng/L for PFOS and PFOA in drinking water. However, there are significant variations in guidance levels among different states. **Table 1** listed some State advisory levels and reference doses for PFOA and PFOS in the drinking water and compared them with the recommended level according to the EPA. It illustrates that the reference doses in all the states are lower (and therefore more conservative) than that of EPA (20 ng/kg-day)

except for Maine and California (**Table 1**). However, the differences in advisory levels are substantial across different regions. Alaska, Texas and Maine have levels ranging from 2 to 8 times higher than the suggested 70 ng/L, while California has the most stringent regulation, with 5.1 ng/L for PFOA and 6.5 ng/L for PFOS.

Table 1. *Advisory level and reference dose for PFOA and PFOS in drinking water across different states in the USA. Adapted and revised from [44], [47], [48], [49]. USEPA = United States Environmental Protection Agency. Reference dose (ng/kg-day) indicates the maximum daily intake per kilogram of body weight without significant health risks. The States above the broken line have higher Advisory Levels than USEPA.*

Guideline	**Advisory Level**		**Reference Dose**	
(Jurisdiction, Year)	PFOA (ng/L)	PFOS (ng/L)	PFOA (ng/kg-day)	PFOS (ng/kg-day)
USEPA, 2016	70	70	20	20
Alaska, 2016	400	400	20	20
Texas, 2017	290	560	15	20
Maine, 2016	130	560	6	80
Minnesota, 2017	35	27	18	5.1
Vermont,2016	20	20	20	20
New Jersey 2017	14	13	2	1.8
New Hampshire, 2019	12	15	6.1	3.0
California, 2019	5.1	6.5	20	30

As mentioned earlier, guidelines in most countries and regions worldwide focus on the commonly used PFAS substances such as PFOA, PFOS and sometimes PFHxS. However, since long-chain PFAS can degrade into end-products as short-chain ones and PFAA, it is crucial to set up guidelines for a broader range of PFAS in drinking water. Hence, Canada has developed more detailed federal guidelines for a few PFAS substances in the drinking water with each PFAS having its own screening value. As shown in **Table 2**, the highest screening value is 30 ng/L for PFBA, followed by PFBS at 15 ng/L. This is expected given that PFBA and PFBS are among the most

prevalent short-chain compounds in PFCAs and PFSAs with only four carbon atoms. The short carbon chain length makes them more soluble in water and more difficult to remove. The screening values for other PFAS are all under 1 ng/L, significantly lower than the advisory concentration in other countries (e.g., **Table 2**).

***Table 2**. Health-based guidance for PFAS concentrations in drinking water in Canada [11], [47].*

PFAS Name	Abbreviation	Drinking Water Screening Value (ng/L)
Perfluorobutanoate	PFBA	30
Perfluorobutane sulfonate	PFBS	15
Perfluorohexanesulfonate	PFHxS	0.6
Perfluoropentanoate	PFPeA	0.2
Perfluorohexanoate	PFHxA	0.2
Perfluoroheptanoate	PFHpA	0.2
Perfluorononanoate	PFNA	0.02
Fluorotelomer sulfonate	6:2 FTS	0.2
Fluorotelomer sulfonate	8:2 FTS	0.2

1.3 Alternatives for long-chain PFAS — issues associated with short-chain compounds

Since the 1950s, long-chain PFAS has been preferred over short-chain ones due to their higher stability and robustness [17]. After several regulatory changes, PFOA and PFOS have been banned in many countries, with long-chain PFAS being phased out voluntarily from 2000 due to their persistent and bioaccumulative potential [50]. To meet the industry needs/requirements, the replacement of long-chain PFAS involved the use of short-chain alternatives or the insertion of ester functional groups [51] as they are expected to be less hazardous to the environment and humans [50]. Nevertheless, the alternative PFAS showed high global contamination as evidenced by their persistence (P), bioaccumulation potential (B), (eco)toxicity (T) and long-range transport potential (LRTP) [52], [53]. Specifically, short-chain alternatives have similar persistence to the long-chain ones. Although short-chain PFAS are less bioaccumulative than long-chain ones in

animals and humans, they show higher uptake into the leaves, stems, and fruit of plants. Most short-chain PFAS show a less toxic trend except for PFHxA, exhibiting a higher ecotoxicity than PFOA to aquatic species [52]. Lastly, short-chain PFAS are more mobile due to their higher solubility in water and weaker sorption to solids.

These novel alternatives, especially short-chain PFAS, have become important sources of PFAS and PFAA contamination in surface water, which also have been detected in most environmental matrices [54], [55]. In Canada, short-chain PFAS are the most prevalent species detected in both source water and drinking water. Among them, PFBA showed the highest mean concentrations, measuring 2.64 ng/L in source water and 2.49 ng/L in drinking water [33]. Similar results were observed in wastewater treatment plants (WWTPs) in Canada, short-chain, especially PFBA, PFPeA, and PFHxA were dominant in both influent and effluent, exhibiting up to 73% of ∑42 PFAS [56]. In China, short-chain PFAS were observed to dominate PFAS pollution in residential soils and were also detected abundantly in WWTPs by several studies with concentrations up to hundreds of ng/L [54], [57], accounting for up to 89% of the total PFAS in the aquatic environment [53]. On a global scale, PFBS and PFBA are the two most common short-chain PFAS and have been detected widely in drinking water, sediment, and even snow/ice in polar regions.

1.4 Main sources of PFAS emissions in the environment

PFAS could be released into the environment during the manufacturing process, usage and disposal. The sources of PFAS emissions into the environment can be classified into two main catalogues: (1) direct sources and (2) indirect sources as shown in **Figure 1**. The direct sources originate from immediate operations in manufacturing facilities whereas the indirect sources are waste-related. As previously mentioned, PFAS are extensively used in the industry due to their high stability and use as performance enhancers for other products. Therefore, PFAS can be included in (a) primary product ingredients, residuals or impurities, and (b) transformation and

consumer products [58]. The latter include paints, varnishes, cleaning solutions, food packages, paperboard, etc., while the former pertains to electroplating, textile and paper coating.

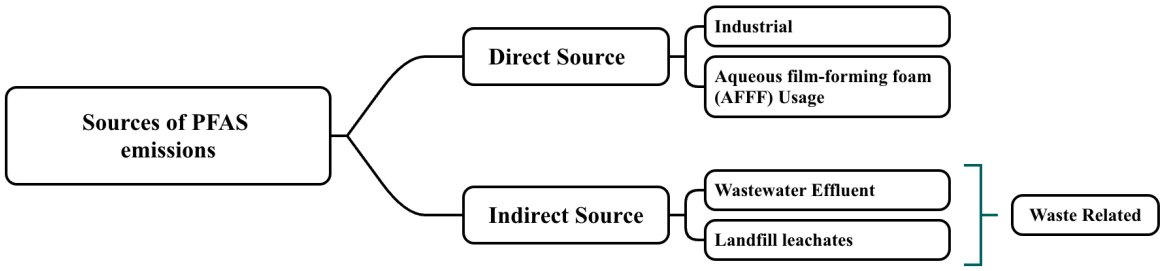

Figure 1. *PFAS emissions sources in the environment. Adapted from [58], created by using X Mind software.*

Aqueous Film Forming Foam (AFFF) is a type of foam used as a fire suppressant, especially for liquid fuel fires (i.e., oil, gasoline, or other flammable liquids). AFFFs are made from complex mixtures of PFAS and other hydrocarbon surfactants which are employed to prevent re-ignition and to lower the surface tension when spreading AFFF spontaneously. Consequently, AFFFs have a widespread use at military sites [59], [60], air force and naval bases for fire-fighting training exercises as well as in airports, emergency response, and oil refineries. Due to the high consumption of AFFF in training or emergencies, severe water contamination can occur and PFAS could be brought to surface water, groundwater and soil [61]. A study conducted in Sweden has detected PFAS in the sediment, lake and pond water located in the surrounding area of a firefighting training facility, with average levels (nine PFAS) of ~1700 ng/L in the lake and were dominated by PFSAs (PFHxS, PFOS and PFBS).

As PFAS have been increasingly difficult to remove by traditional degradation methods, many studies reveal that waste-related sources are significant indirect contributors to PFAS emissions. Landfill is one of the oldest and most common methods of solid waste disposal. Landfills are designed to have a leachate collection system to delineate constituents released via the degradation of solid wastes. PFAS, in particular, can be released from waste through biological transformation

from the PFAS precursors or via abiotic leaching. Compared to normal aliphatic hydrocarbons, PFAS pose more soluble properties due to their functional groups, such as the carboxyl group and sulfonic acid group, facilitating the easy dissolution of PFAS and its subsequent transport in the leachates (and then released to the environment). These features make landfill leachates one of the main sources of these compounds [62] and serve as a significant long-term source to the environment [58], [63].

There were a total of 32 PFAS substances measured in landfill leachate from 17 landfills in Washington State, with pre-total oxidizable precursor (TOP) and post-TOP assays (assays for potential PFAS formation), concentrations ranging from 61 to 172,976 ng/L and 580 to 36,122 ng/L respectively [64]. In Germany, the concentration of total 43 PFAS from 22 landfill sites showed that the untreated leachate contained 31 to 12,819 ng/L and 4 to 8,060 ng/L in treated leachate (with different treatment processes including activated carbon, biological treatment, nanofiltration, wet air oxidation, and external treatment) [65]. A total concentration of 7,280 to 292,000 ng/L of PFAS was observed in raw leachate in China while after treatment (different combinations among membrane bioreactor, anoxic/oxic/oxic, anoxic/oxic, up-flow anaerobic sludge blanket, reverse osmosis, and nanofiltration) the concentration decreased to 98.4 to 282,000 ng/L [66]. In many areas, leachate from landfills is collected and then treated in WWTPs, which is another important indirect source of PFAS emission. In 2013, 563 to 638 kg of PFAS was estimated from landfill leachate to WWTPs in the USA [62].

1.4.1 PFAS fate and transport in wastewater treatment plants (WWTPs)

As the ultimate destination of stormwater, industrial and municipal wastewater and landfill leachate, WWTPs have become one of the most concerning point sources of PFAS [67]. An overview of the PFAS environmental cycle and pathways related to WWTPs is illustrated in **Figure 2**. All residual PFAS in the wastewater are re-emitted to the environment through different pathways. The end-product (i.e., effluent) containing PFAS can enter back into urban water systems and may impact the receiving aquatic environments directly (lakes, rivers, creeks). Many

studies focusing on PFAS in US rivers in particular showed WWTP is an important source of PFAS (34.4 ng/L with increased streamflow and 74.9 ng/L with low flow and up to 315 kg/year of total annual PFAA mass load from WWTP to Long Island Sound) [68], [69]. Through bioaccumulation and ingestion via drinking water, humans are also exposed to PFAS. In Arctic Canada, PFAS concentrations were found to be over 100-fold greater in Cambridge Bay wastewater effluent than previously reported in any Arctic seawater [70]. In China, the concentrations in river water samples were reported approximately 5–12 times smaller than in WWTP effluents [67].

Another waste generated in WWTPs is biosolids which are then applied to agricultural fields (a common practice in Canada [71], [72]). A fraction of PFAS in the water adsorbs on the sludge due to their affinities for solids and are further recalcitrant to the subsequent sludge digestion process. PFAS are frequently detected at concentrations up to hundreds of ng/L in both solid and semi-solid products (sludge). When applied to soil, PFAS can further contaminate groundwater or be taken up by agriculture products.

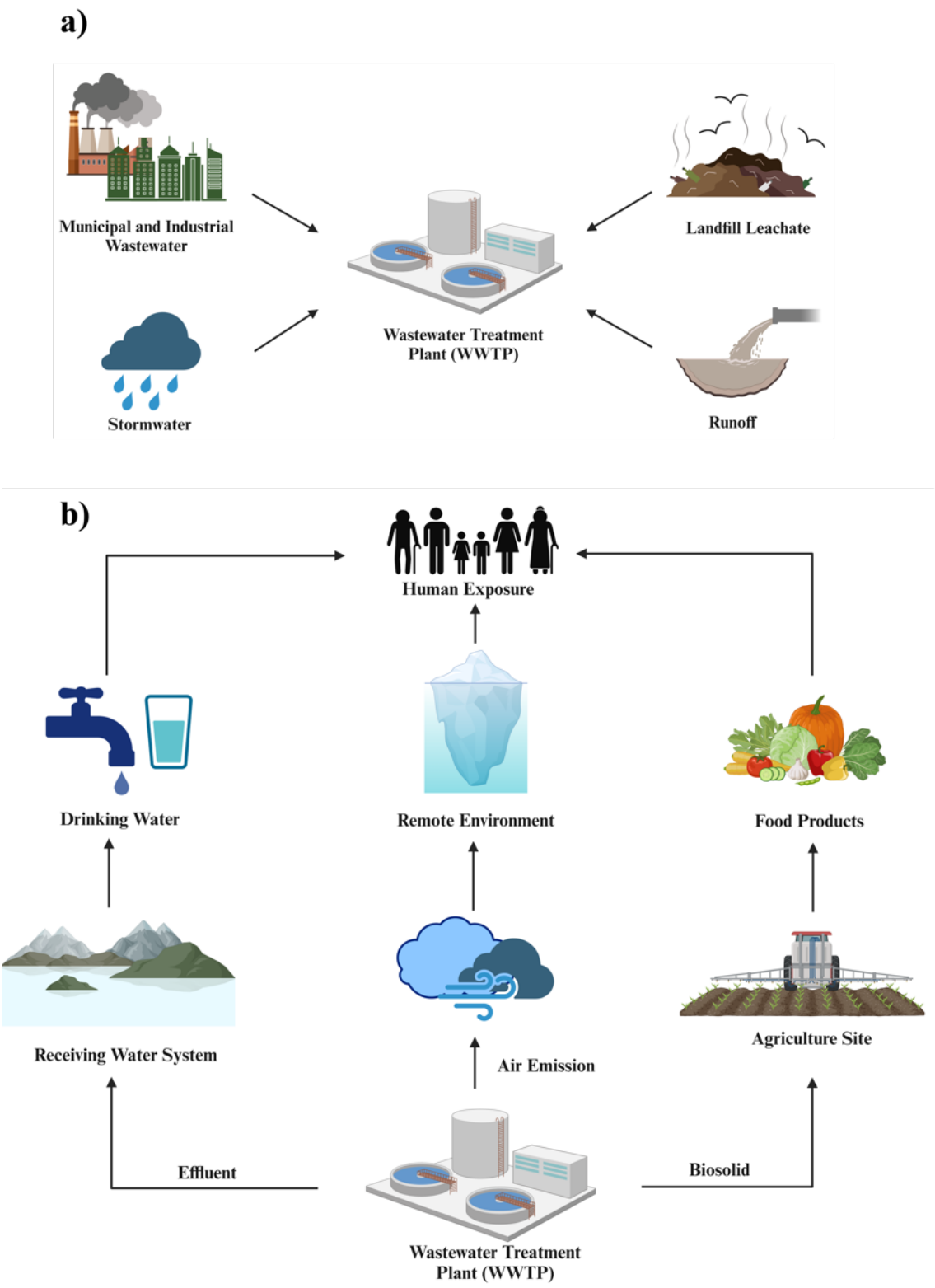

Figure 2. ***(a)*** *Sources of PFAS in WWTP;* ***(b)*** *Environmental pathways of PFAS from WWTP. The image is drawn with BioRender.*

Air emission is another direct pathway during wastewater treatment since the facility is outside, notably semi-volatile and neutral PFAS. WWTPs are estimated to have 1.5–15 times more PFAS in ambient air than in background reference sites [67]. These portions of PFAS can travel over great distances in the atmosphere and possibly lead to the occurrence of PFAS in remote and pristine regions [67].

PFAS precursors (such as fluorotelomer alcohols [FTOHs]) are also commonly used in industry for manufacturing of surfactants, stain-resistant products and firefighting foams [7], [73], [74], [75], [76]. These precursors are of particular concern due to their potential to transform into parent PFAS. Due to the presence of these precursors in the influent (prior to biological treatment), PFAS concentrations after biological treatment are often higher in the effluent than in raw (untreated) wastewater [77]. Simultaneously, the concentration of PFAS precursors was found to decrease from influent to effluent after treatment [78], [79], [80], leading others to suggest that the precursors are responsible for PFAS formation during treatment [7], [81], [82]. This observation has been reported in many WWTPs worldwide, including in China, Europe, and North America [7]. In Australia, the total concentration of nine PFAS increased by an average of 9.8 times in effluent compared to influent in 11 WWTPs [6] while in Singapore, PFOA levels increased after membrane bioreactor treatment [83]. These multiple lines of evidence show that regardless of the treatment, precursors can transform into long-chain PFAS in the WWTPs [84], [85], [86]. Additional insights related to PFAS removal and their precursor substances are discussed subsequently below.

1.4.2 Removal efficiency of PFAS in WWTPs

PFAS are highly recalcitrant to conventional wastewater treatment processes [8]. Preliminary treatment aimed at the physical settling of solids provides very little to no removal of these contaminants, possibly due to lower hydraulic retention time (HRT) and minimum biological activity of such units [87]. Highly variable, and negative removal efficiencies for most of the PFAS were reported during primary treatment [88], and concentrations of PFAS were not also found to

lower after secondary treatment stages (e.g., PFOS with a 58% increasing [89]). As previously indicated, biological treatment often transforms precursors to more persistent chemicals, so no PFAS could technically be biodegraded [10]. In fact, anaerobic/anoxic/oxic (A^2O) treatment has been reported to contribute much higher effluent concentrations of PFOS and PFOA than conventional activated sludge systems, biofilm process and chemical flocculation [67]. Guerra et al. further analyzed the fate of 21 PFAS substances in 20 Canadian WWTPs and found that in the order of high to low PFAS percent formation, the ranking was found to be: advanced biological treatment with nutrient removal (160%) > aerated/facultative lagoon (150%) > secondary biological treatment (55%) > primary treatment with chemical assist (–1%) [90]. They further associate that treatment operating at longer HRTs and at higher temperatures tends to have high PFAS formation.

The concentration of commonly detected PFAS in the influent and effluent from WWTPs in worldwide (10 countries) are shown in **Table 3**. Here, the total concentration of all detected PFAS in almost all studies had negative or zero removals, with values up to a three-fold increase than the influent. This finding further illustrates that existing technologies for wastewater treatment are insufficient for PFAS removals. Note, however, that when focusing on the PFAS sub-groups in the same country, the overall trend observed suggested that longer-chain PFAS had better removals than the short-chain ones (increasing removal efficiency, especially in Sweden). In cases where acceptable treatment was observed (e.g., Sweden), the removal of long-chain PFAS was almost all positive and could reach higher than 70%. Nevertheless, most PFAS removals are lower than 50% or show negative removals. Overall, it appears that currently existing wastewater treatment processes are insufficient in removing PFAS and may even introduce more PFAS into the water after treatment.

Table 3. *Influent and effluent concentrations of various PFAS in WWTPs worldwide (Most studies detected >1 WWTPs and the average was used here). "/" cannot calculate.*

PFAS compounds	Influent conc (ng/L)	Effluent conc (ng/L)	Removal Efficiency (%)	Country	Reference
Total 13	125.69	174.11	-39	Canada	[90]
PFPeA	11.34	12.99	-15		
PFHxA	14.74	21.79	-48		
PFHpA	5.82	7.36	-26		
PFOA	11.69	18.50	-58		
PFNA	2.58	4.13	-60		
PFDA	1.05	3.05	-191		
PFUnA	0.00	0.00	/		
PFDoDa	0.00	0.00	/		
PFBS	6.27	6.17	2		
PFHxS	20.40	22.28	-9		
PFOS	41.45	65.63	-58		
Total 9	55	94	-71	Australia	[91]
PFHxA	9.5	18	-89		
PFHpA	2.5	3.6	-44		
PFOA	2.8	22	-686		
PFNA	0.64	1.3	-103		
PFDA	0.36	3	-733		
PFUnA	0.18	0.49	-172		
PFDoDa	0.03	0.11	-267		
PFHxS	20	20	0		
Total 12	20.14	23.15	-15	Sweden	[92]
PFHxA	5.18	9.17	-77		
PFHpA	1.55	1.77	-14		
PFOA	3.63	5.74	-58		
PFNA	0.81	0.62	23		
PFDA	0.67	0.43	36		

PFUnA	0.37	0.1	73		
PFDoDa	0.27	0.02	93		
PFBS	0.96	0.81	16		
PFHxS	2.07	1.77	13		
PFOS	4.01	2.65	34		
Total PFCA	16.67	40.33	-142	Sweden	[89]
Total PFSA	5.23	5.77	-10		
Total 16	57.95	57.93	0	China	[93]
PFPrA	7.15	5.35	25		
PFBA	5.5	5.5	0		
PFPeA	1.39	1.55	-12		
PFHxA	9.19	8.81	4		
PFHpA	1.33	1.61	-21		
PFOA	13.49	16.6	-23		
PFNA	1.63	2.13	-31		
PFDA	0.79	1.09	-39		
PFUnA	0.42	0.34	19		
PFDoDa	0.2	0.13	37		
PFBS	3.31	3.06	8		
PFOS	6.14	7.3	-19		
Total 12	4410	6640	-51	USA	[94]
PFBA	130	490	-277		
PFPeA	200	1690	-745		
PFHxA	360	1370	-291		
PFHpA	60	940	-1467		
PFOA	120	110	9		
PFNA	10	10	0		
PFDA	20	0	100		
PFUnA	0	0	/		
PFDoDa	0	0	/		

PFBS	80	80	0		
PFHxS	490	500	-2		
PFOS	2950	1450	51		
Total 10	760.2	943.45	-24		
PFPeA	7.45	17.95	-129		
PFHxA	35.05	42.95	-23		
PFHpA	16.5	22.65	-37		
PFOA	74.35	83.35	-12		
PFNA	94.9	187.3	-97	Thailand	[88]
PFDA	32.15	41.6	-29		
PFUnA	42	80.7	-92		
PFDoDa	55.25	3.8	28		
PFHxS	28.75	39.6	-38		
PFOS	423.35	424.5	0		
Total 20 PFAS	10–15	14–24	-40–-60	Jordan	[95]
Total 21	49.8	214.2	-330		
PFBA	4.8	4.4	8		
PFPeA	2.1	1.3	38		
PFHxA	1.8	3.2	-78		
PFHpA	1.9	20.4	-974		
PFOA	3.4	65.3	-1821		
PFNA	0	9.6	/		
PFDA	0	2.8	/	Spain	[96]
PFUnA	0	2.7	/		
PFDoDa	3.2	1.6	50		
PFTEDA	3.2	2.2	31		
PFBS	0	16.7	/		
PFHxS	6.9	17.6	-155		
PFOS	11.1	34.7	-213		

Total 18	121.95	116.785	4		
PFPeA	25.75	65.85	-156		
PFHxA	0.85	0.85	0		
PFHpA	1.7	3.35	-97		
PFOA	10.35	14.15	-37		
PFNA	0.6	1.15	-92		
PFDA	3.3	1.55	53	Greece	[97]
PFUnA	5.95	4	33		
PFDoDa	7.5	2.85	62		
PFTeDA	1.55	5.2	-235		
PFBS	0	0	/		
PFHxS	6.4	1.645	74		
PFOS	8.45	12.58	-49		

1.4.3 Physical-chemical treatment approaches for PFAS removal from water

Many novel approaches have been developed to obtain high removal efficiency of PFAS in the water column as shown in **Table 4**. The latest studies mostly focus on oxidation, ozonation and nanofiltration (i.e., non-biological treatment). Photochemical oxidant and nanofiltration show the best removal performance, reaching 100% for PFCAs. For PFOA, coagulation often offers lower removal efficiency but can achieve ~90% at the optimal dose. In many cases, removal efficiencies are all lower than 80%, which is still not enough for the requirement for WWTPs.

Although these technologies have some ability to remove PFAS, they also have some drawbacks [98]. For example, nano/microfiltration requires high energy and cost. Chemical oxidation has the potential for the formation of short-chain PFAS and the release of adsorbed precursors [10]. There has been an attempt to develop nanomaterials (some were photocatalytic) but the inherent stability of nanomaterials also poses a risk to the environment and humans [99]. Advanced oxidation processes may further generate toxic by-products, creating a new set of

emerging substances of concern [100]. These drawbacks limit the large-scale application of these systems.

Table 4. *Removal efficiency of selected advanced treatment processes for PFAS removal from water (bench-scale studies only).*

Removal technique	Adsorbate	Removal %	Reference
In-situ formed ferric nanoparticles via ozonation	PFAS from the firefighting foam	44	[4]
Use of Persulfate as a Photochemical Oxidant	C4–C8 PFCAs	100	[101]
Nanofiltration NF90	PFOA	~100	[102]
Polylammonium chloride coagulation	PFOA	90 at optimal dose	[103]
Electro-Microfiltration	PFOX, PFHxA, PFOA, PFDA, PFHxS, PFOS	70–80	[104]
H_2O_2	PFOA	68	[105]
Mg-amino clay coated nanoscale zero valent iron	PFOA, PFNA, PFDA, PFOS	38–96	[106]
Chemical oxidation (ferrate)	PFOA and PFOS	23 and 34	[107]

1.5 Application of adsorption in PFAS removal

As indicated previously, biological treatment shows poor removals of PFAS, with some showing higher concentrations in the final effluent than influent. Many have observed that adsorption processes may be a more appropriate technique for PFAS in wastewater. Adsorption is a phenomenon where solute species (adsorbate) transport onto the surface of a solid phase (adsorbent) [108]. It is a separation process and has been employed in drinking and wastewater for the removal of organic substances [109]. The USEPA has further suggested that adsorption may be a more suitable wastewater treatment technique for PFAS removal compared to others [108]

because of its flexibility, high efficiency, ease of operation, stability to noxious substances, sustainability, low cost, and environmental sustainability [108], [110], [111], [112]. Additionally, a wide range of adsorbents could be derived from several different sources [113]. For example, activated carbon is processed from wood, coconut shells, coal, peat and biomass. Adsorption technology also sequesters pollutants from wastewater and was not found to produce any secondary pollution via by-product formation [110], [114]. Adsorption also allows for minimal waste, high recovery, and reuse [98]. Therefore, it is comparatively a practical approach to remove PFAS in wastewater treatment [115].

1.5.1 Adsorbents evaluated for PFAS removal

Because adsorption efficiency hugely depends on adsorbents [41], many conventional and novel adsorbents have been used in assessing PFAS removals from the water column at bench- and pilot-scales. One of the most commonly used adsorbents in water/wastewater treatment is activated carbon due to its high porosity and proven track record for removing organic substances (even at trace concentrations). The capacity of different activated carbon to remove PFAS is summarized in **Table 5**. The capacity varies among different types of activated carbon, ranging from a few ug/g to hundreds of mg/g. Also, since the specific surface area of powdered activated carbon (PAC) is much higher than that of granular activated carbon (GAC), the capacity and removal efficiency of PAC are better.

Although activated carbon could reach a relatively high adsorption capacity, its widespread application especially in wastewater is not practical because of its inefficient regeneration [109], [111], and activated carbon also showed to be inefficient for short-chain PFAS removal due to weak hydrophobic interaction [122]. Therefore, a variety of alternative adsorbents have been developed. Novel adsorbents extracted from natural materials, agricultural wastes, industrial wastes and biosorbents have been reported to have the potential for the removal of organic pollutants from the water column [109]. Metal-organic frame (MOF), biochar and ion exchange resin all have been shown (at the bench-scale) to have the potential to remove PFAS in water

(**Table 6**). The removal capacity of MOF is relatively stable, ~200 to ~600 mg/g while the capacity of biochar and ion exchange resin depends more on their pre-treatment and the source of their raw material. Most studies focus on the removal of two short-chain PFAS (PFBA, PFBS) and two long-chain ones (PFOA, PFOS). Almost all the adsorbents work well for the removal of long-chain PFAS than short-chain ones.

Table 5. *Adsorption capacity of activated carbon for PFAS removal from water. Adsorption Capacity was from the maximum adsorption capacity of fitting Langmuir isotherm model. GAC = granular activated carbon; PAC = powdered activated carbon. Please review* ***Table 9*** *for the PFAS full names.*

Adsorbate	Activated Carbon Type	Initial Concentration	Dosage	Adsorbent Capacity	Reference
PFOA, PFOS	PAC	20–250 mg/L	40 mg/L	1209, 520 mg/g	[116]
PFHpA, PFOA, PFOS	GAC	0.5–10 mg/L	0.2 g/L	41.3, 52.8, 72.3 mg/g	[117]
PFOA	PAC	500–1500 mg/L	-	484.46 mg/g	[118]
PFOA, PFOS	PAC	20–300 mg/L	66.67 mg/L	203, 535 mg/g	[119]
PFOA, PFBS, PFOS	GAC Calgon F400	15–150 mg/L	1 g/L	112.1, 98.7, 236.4 mg/g	[120]
PFHpA, PFHxA, PFOA, PFOS	GAC	0.15–2.5 mg/L	0.125 g/L	0.056, 0.22, 1.1, 5.3 mg/g	[121]

There are also limitations of these novel adsorbents to remove PFAS: (1) These studies focus on a few popular PFAS substances. However, in real wastewater, PFAS are in mixtures, and they will integrate and compete with each other as well as with other contaminates. (2) Most of these studies used a higher concentration of PFAS than the levels in WWTPs. Under different conditions, the adsorbent may show different performances in a pilot-scale experiment. (3) The materials need high cost of their production and regeneration, along with high time consuming and frequent replacement.

Table 6. *Adsorption capacity of metal-organic frame (MOF), biochar, and ion exchange resins for PFAS removal from water as reported in bench-scale laboratory experiments. MIL = Material Institute Lavoisier; BPDC = biphenyl-4,4'dicarboxylic acid; BTC = 1,3,5Benzenetricarboxylic; NU = Nusantara University; IRA = ion exchange resin adsorbent.*

Metal organic framework (MOF)			
Adsorbate	**Adsorbent**	**Capacity**	**Reference**
PFOS	MIL-53(Al)-BPDC	~180 mg/g	[24]
PFOS	MIL-53(Al)-BPDC	~220 mg/g	[24]
PFOA	Fe-BTC	418 mg/g	[41]
PFOA	MIL-100-Fe	349 mg/g	[41]
PFOA	MIL-101-Fe	370 mg/g	[41]
Three perfluoro sulfonic acids (PFSAs, C4−C8) and six perfluorinated carboxylic acids (PFCAs, C1−C9)	NU-1000	400−620 mg/g for PFSAs and 201−604 mg/g for PFCAs	[123]
Biochar			
Adsorbate	**Adsorbent**	**Capacity**	**Reference**
PFOS	Magnetic biochar	120.44±12.37 mg/g	[124]
Total 13 PFAS	Biochar	1.17 mg/g	[125]
PFOA	3D hierarchically microporous biochar (HMB)	1269 mg/g	[126]
PFOS	activated spent coffee grounds biochar	43.3 mg/g	[127]
PFOA	Karanja shell modified biochar	455.8 mg/g	[128]
Ion-exchange resins			
Adsorbate	**Adsorbent**	**Capacity**	**Reference**
PFOS	IRA67	2.75 g/g	[129]
PFOS	IRA67, IRA957	20–25 g/g	[130]
PFOS	IRA400	108.9 μg/g	[131]
PFBA, PFOA, PFBS, PFOS	A600E	19.1, 125.2, 34.6, 186.2 mg/g	[50]

1.6 Activated bauxite residue (ABR) as a potential adsorbent for PFAS removal

Bauxite Residue (BR, typical composition in **Table 7**), also known as red mud (RM) is a by-product from alumina extraction via Bayer's process [132], [133]. Bauxite is an aluminous rock containing hydrated aluminum oxide as well as iron, silica, sodium and titanium [134]. Approximately 1 to 2.5 tonne of BR is generated per tonne of alumina [132] with now a global generation of ~150 million tonnes per year [135]. The substantial amount of BR presents significant challenges in treatment, handling, and management [132]. Additionally, BR's high alkalinity (pH 10–13) complicates disposal efforts [136]. The potential presence and leaching of toxic materials further classify BR as hazardous waste posing serious environmental concerns [137], [138]. The current method for managing BR involves storing in specific constructed ponds or dams, often referred to as tailings [139]. According to the US Geological Survey, the estimated cumulative stock of BR is ~28 billion tonnes worldwide[132] [134]. This disposal method requires a large surface area and has a low utilization rate (<5% in the world) [140], owing to its high alkalinity.

The storage of BR poses potential leaching and contamination risks to the surrounding environment. In 2010, an accident occurring in Hungary resulted in nearly 1 million cubic meters of BR being released due to a dam collapse, covering approximately 800 ha of agricultural site, including 300 ha of grassland, 310 ha of tilled area, 150 ha of corn, 30 ha of alfalfa and 15 ha of sorghum (covered by 5–10 cm red mud) [141]. In 2016, around 2 million cubic meters of slurry tailing spilt to the nearby village over 1.5 km [133]. A similar accident happened in India in 2019, where a failure of BR disposal area resulted in leaching of contaminants into more than 35 acres of land [133].

Due to the urgent need to develop effective methods for reducing toxicity and enhancing the utilization of BR, much research has focused on exploiting its abundant metal elements composition (**Table 7**) as suitable for the construction industry. For instance, many studies have applied pre-treated BR in building and construction industries, including ceramics and clay

materials, stabilized bricks, geopolymers, cement and concrete application, fillers, landfill materials roads and pavements [132], [133], [142]. BR was also tested for use in pigment due to extremely fine particles and a characteristic red colour. Therefore, utilizing red mud as a secondary resource in these applications can significantly mitigate the environmental problems associated with its disposal.

Table 7. *Typical composition of red mud or bauxite residue [132], [134].*

Composition	Weight%
Fe_2O_3	30–62
Al_2O_3	10–23
SiO_2	3–50
TiO_2	Trace–25
Na_2O	2–10
CaO	0.5–8

1.6.1 Activated bauxite residue (ABR) in wastewater treatment

Due to its small particle size (diameter of 0.005–0.075 mm for about 90% of the particles), high specific surface area and high chemical reactivity [143], BR has been found to be efficient in removing different types of pollutants from water and wastewater, particularly metal ions [143], [144]. Utilizing BR as an adsorbent material not only mitigates hazardous environmental impacts but also promotes environmental restoration. BR has been widely tested (bench- and pilot-scale) as an adsorbent to remediate pollution in water or soil. **Figure 3** illustrates how BR has been applied to remove a wide variety of environmental pollutants via adsorption [145]. Notably, BR exhibits excellent performance in removing organic dyes and phenol from wastewater, suggesting its potential for adsorbing other organic contaminants such as PFAS in wastewater treatment [143], [144]. It is important to note that further modifying BR via activation (thermal or chemical) is almost always necessary to enhance its adsorption capacity and minimize potential secondary pollution via leaching. Once pre-treated, BR is referred to as activated bauxite residue (ABR).

ABR's utility as an adsorbent material for more complex wastewater is at its early stages, However, the global demand for aluminum will only grow, suggesting that alumina extraction from bauxite deposits will increase the waste associated with this process. As society moves towards more sustainable economic development, many have considered the potential for using ABR in additional applications, including PFAS removal.

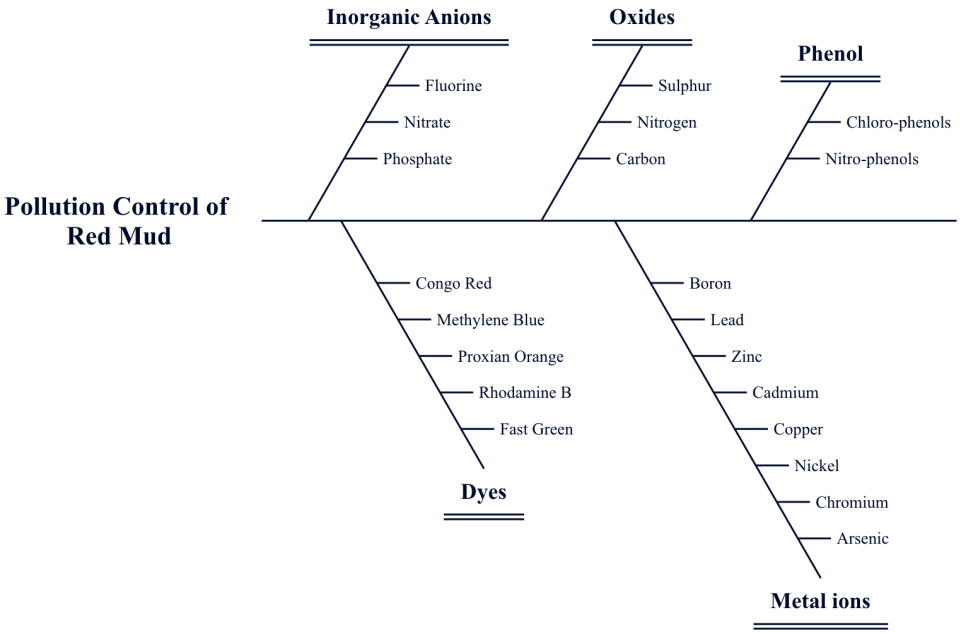

Figure 3. *Potential pollution control of Red Mud (or BR) in adsorption applications [134], created by using X Mind software.*

1.7 Problem statement

Although many studies have explored novel adsorbents to remove PFAS from wastewater, the removal efficiencies are not as promising, and the novel approaches have the drawbacks of high cost and energy consumption. The application of ABR material in wastewater treatment to remove PFAS shows potential.

1.8 Thesis objectives

The main purpose of this thesis is to evaluate the potential of the activated bauxite residue (ABR) as an adsorbent for removing PFAS from the water column. Specific objectives are described below:

(1) **Characterize ABR** based on its elemental composition, compositional mapping, bonds analysis, specific surface area, pore volume, pore size distribution, and zeta potential to understand the structure, properties and possible removal mechanisms as well as tell the differences before and after application of ABR as an adsorbent.

(2) **Determine adsorption kinetics and isotherm** for the removal of different PFAS substances in the mixing solution to understand the adsorption mechanism and evaluate optimal treatment conditions.

(3) **Assess the removal efficiency** of PFAS in the synthetic solution through adsorption by ABR and compare its removal with a commercially powdered activated carbon (PAC).

(4) Determine whether toxicity is introduced upon the addition of ABR in the solution via **Cell toxicity pathway evaluation** via cytotoxicity, estrogenicity, and mutagenicity in PFAS wastewater using *in-vitro* bioassays.

1.9 Research hypotheses

Based on the previous study conducted by Cheng [146], ABR has demonstrated effective performance in removing various contaminants and reducing toxicities in both synthetic and real wastewater (municipal and oil sands processed water). The potential for ABR to remove other organic compounds from water forms the basis of this study, with the assumption that organic substances exhibit affinity for ABR. The overall work performed is designed to test the following detailed set of hypotheses:

Hypothesis 1. ABR will exhibit comparable removal efficiencies for PFAS as demonstrated for other organic substances (e.g., methylene blue, cyclohexane carboxylic acid, and naphthenic acids).

Hypothesis 2. If PFAS were removed from wastewater by ABR, PFAS would attach to the surface of ABR, resulting in changes to surface properties (e.g., surface area, total ore volume, pore size distribution, element composes, and surface charge).

Hypothesis 3. With appropriate pre-treatment (pH adjustment to ~7), ABR will not introduce background toxicities (cytotoxicity, estrogenicity and mutagenicity) and potential toxic by-products will not be produced.

Hypothesis 4. ABR performs comparatively with a commercially available activated carbon, albeit will require a higher dosage due to differences in material characteristics. ABR still has the potential for being an alternative to conventional adsorbents now used in water/wastewater treatment.

1.10 Thesis scope

This thesis focusses on the assessment of ABR to remove PFAS from the water column. Chapter 2 discusses the overall experimental design, materials used, and all the methods employed in this study. More specifically, this study involves four aspects to evaluate the removal potential of PFAS from wastewater by ABR: (1) characterization of the adsorbent, (2) adsorption rate and capacity, (3) removal efficiency and comparison with a conventional adsorbent, (4) biological toxicity via acute toxicity (*Daphnia magna*) and cell toxicity pathways via *in-vitro* bioassays

Finally, Chapter 3 presents all the results obtained from experiments (material characterizations, adsorption kinetics, isotherms, removal efficiency, and toxicity evaluation) and a detailed discussion of the findings. Chapter 4 summarizes the conclusion, study limitations, and the recommendations.

2 Materials and Methods

2.1 General overview of the experimental design

The experiments and general methods utilized in this thesis are summarized in **Figure 4**. First, PFAS stock solution (1 g/L each substance, n=10 in ΣPFAS) was prepared and then mixed with ABR (0.1 to 100 g/L dosages) to achieve an initial concentration of 500 ng/L, 600 ng/L, 100 µg/L, 1 mg/L (depending on the experiment). The experiments were performed in a four-position jar tester (VELP FS 4S Flocculation Stirrer) or a tube roller (Globe Scientific GTR-AVS Tube Roller). Sets of experiments completed included: (1) material characterization (**Section 2.5**); (2) assessment of removal efficiency and comparison with powdered activated carbon (**Section 2.6.3**); (2) determination of adsorption kinetics (**Section 2.6.4**); (3) fitting to existing adsorption isotherm models (**Section 2.6.4**); (4) toxicity analyses (**Section 2.9**). Quality assurance/quality control (QA/QC) measures such as spiked samples (i.e., no ABR) were implemented to account for PFAS background levels. At the conclusion of each experiment (or at a specific sampling time point), the aqueous phase (water column) was separated from ABR via filtration or centrifugation. The ABR sludge was then dried at room temperature for material characterization (**Section 2.7**). Filtered water samples were sent to an accredited laboratory (Bureau Veritas North America [Edmonton, AB]) for chemical analysis. The *in-vitro* bioassay testing required additional sample cleanup via solid phase extraction (SPE) (**Section 2.8**) to concentrate the organic components.

2.2 Nomenclature

Two types of samples were assessed in this study: ABR sludge samples and aqueous phase samples. ABR sludge samples not used for treatment are referred to as "virgin" ABR, while ABR with PFAS is referred to as "spent" ABR. Since the experiments were conducted using a mixture of PFAS, the stated concentrations refer to **each individual** PFAS concentration in the mixture. For instance, a jar tester containing 100 µg/L PFAS meant 100 µg/L PFAS for each of the ten compounds, and therefore has a sum (Σ) concentration of 1000 µg/L or 1 mg/L PFAS. For the "spent" ABR treated with different concentrations of PFAS, the sample nomenclature of "ABR

dosage (g/L)" was adopted. For example, if 100 µg/L PFAS wastewater was treated with 2 g/L ABR, then the "spent" ABR sample was named 2g/L_100µg/L.

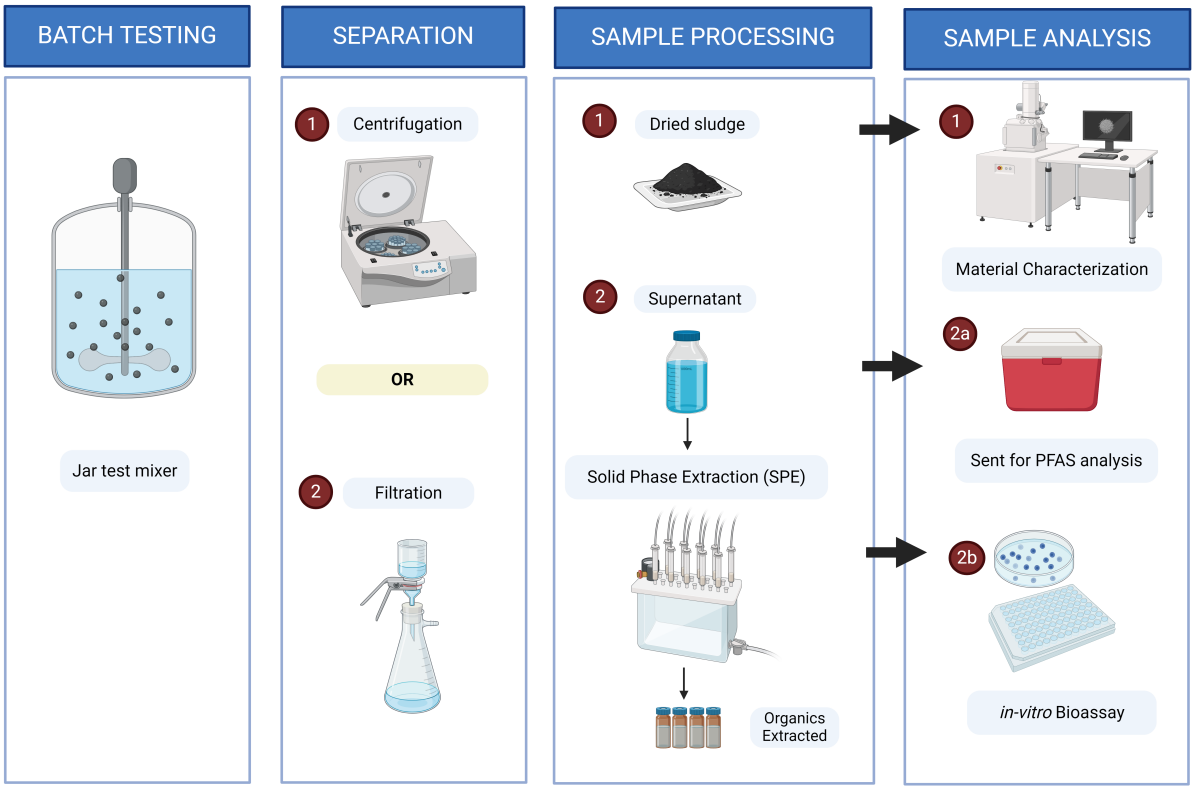

Figure 4. *The overall experiment flowchart, including characterization, analytical and bioanalytical methods employed in this thesis. ABR = activated bauxite residue. PFAS analysis was sent to an accredited lab (Bureau Veritas, North America) using the method LC-MS. Sample characterization and in-vitro bioassay testing were completed at the NanoFab facility and the Arlos Lab at the University of Alberta, respectively. The image is drawn with BioRender.*

2.3 Brief overview of analytical and bioanalytical methods

Table 8 summarizes all the analytical tools used in this study. Material characterization was completed at the nanoFAB Fabrication and Characterization Facility at the University of Alberta, Edmonton, Canada. Characterization was done for both "virgin" and "spent" ABR (i.e., clean ABR and ABR with PFAS). The elemental composition and mapping were obtained using the energy dispersive X-ray (EDX) analysis. The Brunauer-Emmett-Teller (BET) surface area, total pore

volume, and pore size distribution were estimated using the gas (N_2) adsorption method. The element concentration and bond types were determined by X-ray photoelectron spectroscopy (XPS). Samples of "virgin" and "spent" ABR were also sent to the University of Calgary (UofC), Department of Chemical and Petroleum Engineering, Research Instrumentation and Technical Support Lab for zeta potential measurements to determine surface charge.

Given that ABR can illicit toxicity, a battery of bioassays was used to determine whether any toxic by-product was produced during treatment or ABR itself contributes to toxicity. More specifically, whole organism acute toxicity was determined using *Daphnia magna*, cytotoxicity was determined based on the inhibition of the *Aliivibrio fischeri* bacteria; estrogenicity and mutagenicity were tested by using the Yeast Estrogen Screen (YES) assay and the UMU-Chromo Test, respectively.

Table 8. *Summary of analytical tools. SEM = scanning electron microscope; EDX = energy dispersive X-ray; XPS = X-ray photoelectron spectroscopy; YES = Yeast Estrogen Screen.*

Material Characterization	**Cell toxicity Pathway**	**PFAS Analysis Adsorption Removal Efficiency, Kinetics and Isotherm**
Elemental Analysis and mapping (EDX)	Cytotoxicity (BioTox - LumoPlate)	
BET Surface Area, Total pore Volume, and Pore Size Distribution (Adsorption of N_2)	Estrogenicity (YES)	Samples were sent to an accredited laboratory for analysis (Bureau Veritas - Edmonton) Method Number: CAM SOP-00894 RDL are provided in **Table 9**
Surface elemental properties (XPS)	Mutagenicity (Umu – Chromo (gene) Test)	
Surface Charge (Zeta potential measurement)		

2.4 Materials

The activated bauxite residue (ABR) used in this study was prepared via a reduction roasting process (provided by GRÖN Holding Corp. (Canada)) where raw bauxite residue was mixed with a stoichiometric amount of carbon and then thermally treated in a rotary calciner under an inert nitrogen atmosphere. The reduction roasting process was carried out at temperatures between 500 and 600 °C for a duration of 30 min (described in more detail in [147]). The commercially available powdered activated carbon was purchased from ClearTech, Canada. Hydrochloric acid (37%), sodium hydroxide (10 N), methanol (≥99.9%), 3,5-dichlorophenol (99%), and ethanol (70%) were purchased from Fisher Scientific, Canada. Ethyl acetate (≥99.5%), estradiol and all the PFAS substances were purchased from Sigma-Aldrich, Canada. Glass fibre filters (1.0 µm pore size, 47 mm) were purchased from Millipore Sigma. Ultrapure water was obtained from a MilliQ IQ 7000 purification system with a resistivity of 18.2 MΩ-cm (25°C) and total organic carbon (TOC) ≤ 5 ppb. Ten PFAS substances were used in this experiment, except for the BET analysis of "spent" ABR where only two PFAS substances at high concentrations were employed (PFNA and 6:2 FTSA). The PFAS physical-chemical properties are listed in **Table 9**. All PFAS stocks were stored in 10 mL amber bottles at -20℃ prior to use. All SPE extracts were stored in 2 mL amber vials at -20℃ prior to analysis. For cytotoxicity and mutagenicity testing, the BioTox-LumoPlate and the UMU-ChromoTest kits were purchased directly from Environmental Bio-detection Products Inc. (EBPI, Burlington, Ontario).

The yeast strain *Saccharomyces Cerevisiae* for the YES assay was provided by the Servos Lab at the University of Waterloo and the methods adapted from Barrow et al [148]. Reagents for YES including adenine hydrochloride hydrate, L-histidine-HCl, L-arginine-HCl, L-methionine, L-tyrosine, L-isoleucine, L-lysine-HCl, L-phenylalanine, L-glutamic acid, L-aspartic acid, L-valine, L-threonine, L-serine, L-leucine, L-tryptophan, uracil, glycerol, D-(+)-Glucose, copper sulfate pentahydrate, yeast nitrogen base (YNB) without amino acids were obtained from Sigma Aldrich, Canada. Bacto-agar and the yeast β-galactosidase assay kit (including 2X βgalactosidase assay

buffer and Y-PER yeast protein extraction reagent, and β-galactosidase assay stop solution) were purchased from ThermoFisher Scientific, Canada.

Table 9. *Names and properties of PFAS substances used in this study. The reported detection limits (RDLs) of all the compounds varied from 0.02–2 ug/L, depending on the concentration and volume of the submitted sample (tabulated in Appendix). Solubility was obtained from Chemicalize. Abb = abbreviation; MW = molecular weight; pKa = negative logarithm of the acid dissociation constant (Ka); NA = not available; GC = gas chromatography; T = Titration.*

Full Name – Short (S) or Long Chain (L)	Abb	Purity	Chemical Formula	MW (g/mol)	pKa (Strongest)	Solubility (pH=7) (g/L)
Perfluorobutanoic – S	PFBA	NA	$C_4HF_7O_2$	214.04	0.37	214.039
Perfluoropentanoic – S	PFPeA	≥98.0% (GC)	$C_5HF_9O_2$	264.05	0.34	264.047
Perfluorohexanoic – S	PFHxA	≥98.0% (GC)	$C_6HF_{11}O_2$	314.05	0.32	314.05
Perfluoroheptanoic – S	PFHpA	≥98.0% (GC)	$C_7HF_{13}O_2$	364.06	0.31	364.062
Perfluorooctanoic – L	PFOA	NA	$C_8HF_{15}O_2$	414.07	0.30	414.07
Perfluorononanoic – L	PFNA	97%	$C_9HF_{17}O_2$	464.08	0.29	262.6829
Perfluorodecanoic – L	PFDA	≥98.0% (GC)	$C_{10}HF_{19}O_2$	514.08	0.4	44.521
Perfluoroundecanoic – L	PFUnA	98.0–102.0% (T) ≥96.0% (GC)	$C_{11}HF_{21}O_2$	564.09	0.4	10.3686
Perfluorotetradecanoic – L	PFTEDA	96.0–104.0% (T) ≥96.0% (GC)	$C_{14}HF_{27}O_2$	714.11	0.4	0.2194
Perfluorobutanesulfonic – S	PFBS	96.0–104.0% (T) 97%	$C_4HF_9O_3S$	300.1	-3.31	300.09
6:2 Fluorotelomer Sulfonic – L	6:2 FTSA	NA	$C_8H_5F_{13}O_3S$	428.16	-2.72	428.16

2.5 Materials characterization

Energy dispersive X-ray spectroscopy (EDX) operates by emitting X-ray beams from an electron gun to remove the electrons with lower energy on the sample surface, known as excitation. Then, a detector identifies the element information by receiving the X-rays released by new electrons which fill the spot from a higher energy level [149]. The sample was affixed to stubs by carbon tapes prior to EDX analysis at 20 kV (Zeiss Sigma FeSEM). Elemental mapping option within EDX was employed to provide information on how well the elements or functional groups are distributed on the surface, and how the adsorbate is distributed after adsorption [149]. More specifically, ABR samples were oversaturated with PFAS for EDX analysis to (1) examine the changes of element concentrations compared with those obtained from XPS; (2) show the compositional mapping along the sample surface; (3) provide insight into possible interactions with the elements [150], [151].

X-ray photoelectron spectroscopy (XPS) is a surface-sensitive method which can identify atoms and functional groups on the surface of a solid adsorbent. There is a photon source that emits high energy X-rays toward the sample to excite the electrons from atoms on the sample surface. An analyzer then captures these electrons to measure their number and velocity [149]. In this study, XPS (Kratos Axis Ultra spectrometer) was performed with monochromatized Al Kα ($h\nu$ = 1486.71 eV). A hemispherical electron-energy analyzer working at a pass energy of 20 eV was used to collect core-level spectra while a survey spectrum covering binding energies from 0 to 1100 eV was collected at analyzer pass energy of 160 eV. Charge effects were corrected by using C 1s peak at 284.8 eV [152]. XPS was applied in this study to identify the chemical composition, and specific atomic structures present on the surface of both virgin and spent adsorbent (ABR).

Though EDX and XPS both provide information for chemical composition and element concentration on the surface of the adsorbent sample, they differ in the analysis depth. XPS is a much more surface-sensitive technology and provides an average assessment of the surface of the sample. It is minimally destructive and typically probes the top 1–10 nanometers (nm) of a sample

with elemental sensitivity in the order of 0.1 atomic percent [153], [154]. Therefore, XPS is ideal for the analysis of surface chemistry, thin films, and surface contamination. In contrast, EDX provides information from a larger volume compared to XPS. It can assess samples ranging from 1 μm to a few μms (up to 5000 nm) and can analyze bulk materials rather than just the surface. The analysis depth of EDX can reach 100–3000 nm [155], [156], [157], [158]. In this study, employing both XPS and EDX allowed the comparison between the element composition and concentration at different depths, and then provided insights into the adsorption process of PFAS on ABR.

Porosity is one of the most important features to evaluate an adsorbent's adsorption capacity. The Brunauer-Emmett-Teller (BET) surface area, total pore volume and pore size distribution were determined by AS-iQ-MP-XR (Anton-Paar GmbH) through the adsorption and desorption curves of N_2 gas. Before exposing the sample to N_2 (at a constant temperature of 77 K) [149], virgin ABR was outgassed at 200℃ for 4 hours while spent ABR was outgassed at 170℃ to avoid destroying PFAS on the surface.

Zeta potential was employed in this study to evaluate the surface charge of "virgin" and "spent" ABR and to investigate the interaction of negatively charged PFAS with the surface of the ABR. The samples were prepared by diluting "virgin" and "spent" ABR in ~150 mL of solution with a conductivity below 4.78 μs/cm. These processed samples were then sent to UofC for analysis. The point of zero charge was determined by identifying the pH at which the zeta potential measurements are at "zero" [149].

2.6 Batch test experiments

2.6.1 Preparation

Prior to use, all the glasswares were pre-washed with analytical-grade methanol followed by ultrapure water, then baked under 550°C for 2 h in a muffle furnace (wrapped in heavy-duty aluminum foil). Since adsorption on the containers may contribute significantly to the loss of PFAS in the samples, it is important to ensure that the containers are made of materials with minimal

adsorption. Although the drinking water PFAS analysis methods developed by the USEPA recommend the use of polypropylene containers and avoidance of contact between samples and glass surfaces [159], Lath et al. found that the lowest losses of PFOA occurred on glass containers (14–24%) compared to polypropylene (PP), polystyrene (PS), and polycarbonate (PC) (32–45%, 27–35%, 16–31%, respectively) [160]. Similar trends were observed by others when mixing PFAS solutions, with adsorption levels in containers (six PFAS) ranking as follows: polypropylene > High-Density Polyethylene (HDPE) > Polyethylene Terephthalate (PET) > glass > polystyrene [161]. Hence, in this study, glassware was employed for all the experiments except for the specific container (cartridges, amber bottles, sample bottles, and 96-well plates etc.) during specific routine laboratory procedures.

2.6.2 Preparation of stock solution

A PFAS stock solution at 1 g/L of each substance was prepared initially prepared. This stock solution was used to create all the synthetic PFAS wastewater. For powdered PFAS substances, 10 mg of each was weighed using an analytical balance and transferred into 10 mL volumetric flask immediately. Once all powders were transferred, a volumetric flask was filled with 10 mL methanol (up to the calibration line). For standards that came in liquid form, the volume equal to 10 mg (calculated using density) was pipetted and transferred into 10 mL volumetric flask. After transferring all the liquid substances, the volume was brought up to 10 mL with methanol as well. These two volumetric flasks were sonicated foiled with aluminum foil for 15 min to ensure complete dissolution of all particles. Finally, the entire stock was transferred into 2 × 20 mL amber vials with caps wrapped in parafilm (Millipore Sigma, Bemis). The concentrations of PFAS used for each experiment were summarized in **Table 10**. The differences in initial (nominal) concentrations were due to specific requirements of each experiment (e.g., environmentally relevant concentrations; amount necessary for detection during material characterization).

Table 10. *Types and concentrations of PFAS employed in each experiment. BET = Brunauer-Emmett-Teller; XPS = X-ray photoelectron spectroscopy; SEM = scanning electron microscopy; EDX = energy dispersive X-ray spectroscopy; PAC = powdered activated carbon.*

Experiment	Employed PFAS	Initial (Nominal) Concentration
BET	PFNA, 6:2 FTSA	100 mg/L
XPS	PFBA, PFPeA, PFHxA, PFHpA, PFOA, PFNA, PFDA, PFUnA, PFTEDA, PFBS	100 µg/L and 100 mg/L
SEM&EDX		100 mg/L
Zeta potential		100 µg/L
Removal Efficiency at different dosages and periods	PFBA, PFPeA, PFHxA, PFHpA, PFOA, PFNA, PFDA, PFUnA, PFTEDA, PFBS	600 ng/L
Removal Efficiency for PAC		500 ng/L
Adsorption kinetics		100 µg/L
Adsorption Isotherm		
Bioassays	PFBA, PFPeA, PFHxA, PFHpA, PFOA, PFNA, PFDA, PFUnA, PFTEDA, PFBS	500 ng/L and 100 µg/L

2.6.3 Adsorption removal efficiency and comparison to powdered activated carbon

Experiments were conducted under different conditions to inform adsorption kinetics and isotherm experiments. Then, the removal efficiency of ABR was compared with a commercially available powdered activated carbon (PAC, ClearTech, PACCL85003). In the first set of experiments, a mixture of 10 PFAS in ultrapure water (600 ng/L each PFAS) was combined with six different dosages of ABR (0, 10, 15, 25, 50, 100 g/L) in 2 L beakers at 120 rpm for 24 h using the jar tester. The second set of experiments explored the impact of short- (1 h) and long-term (24h) exposure on the adsorption of PFAS (n=10 in the mixture at C_o of 600 ng/L) using 2 different dosages of ABR (50 and 100 g/L), which were mixed in 2 L beakers at 120 rpm. Finally, the

removal of different concentrations of PFAS (500 ng/L and 100 µg/L each) using 0.1 g/L PAC was assessed and compared with a similar ABR dose (also mixed at 120 rpm for 24h).

At the end of each experiment, the solution was neutralized using hydrochloric acid to within the neutral pH range (6 to 8) and left to settle for 30 to 60 minutes. The supernatant was collected and filtered with 1 µm glass fibre filters (47 mm). The filtered samples were sent for chemical analysis directly. The removal efficiency equation is expressed as **(Equation 1)**.

$$Removal\ efficiency = \frac{C_0 - C_t}{C_0} \textbf{\textit{(Equation 1)}}$$

where, C_0 (µg/L) is the initial concentration of adsorbate, C_t (µg/L) is the concentration of the adsorbate at time t (min).

2.6.4 Adsorption kinetics and isotherm experiments

For the adsorption kinetic study, ABR was added into a 400 mL solution containing 100 µg/L PFAS in a 1L beaker. The ABR-PFAS solution was continuously mixed at 120 rpm using the jar tester. Samples were then collected at 0, 5, 10, 20, 30, 45, 60 and 120 minutes. QA/QC controls were also included consisting of a blank (ultrapure water only) and another control beaker containing only PFAS (i.e., 0 g/L ABR). All the water samples were filtered using glass fibre filters as before. The aqueous phase (supernatant) was then sent to Bureau Veritas (Edmonton) for analysis which provides the concentrations of PFAS remaining in the solution after treatment. The amount of PFAS adsorbed onto the ABR (q_t, µg/g) at different times was then calculated according to **(Equation 2**). Here, q_t experimental values were fitted with (1) Lagergren pseudo-first-order (**Equation 3**), (2) pseudo-second-order (**Equation 4**), (3) Weber's intraparticle diffusion (**Equation 5**), and (4) Elovich models (**Equation 6**) [162]. In this study, extrapolating the experimental data to estimate q_e is not applicable. So, the pseudo-first-order equation is expressed as **(Equation 7**).

$$q_t = \frac{(C_0 - C_t)V}{m}$$ ***(Equation 2)***

$$\frac{dq_t}{dt} = k_1(q_e - q_t)$$ ***(Equation 3)***

$$\frac{dq_t}{dt} = k_2(q_e - q_t)^2$$ ***(Equation 4)***

$$q_t = k_i t^{0.5} + C_i$$ ***(Equation 5)***

$$\frac{1}{q_t} = \frac{\frac{K_1}{Q_1}}{t} + \frac{1}{Q_1}$$ ***(Equation 6)***

$$q_t = \frac{1}{\beta}\ln(\alpha\beta) + \frac{1}{\beta} lnt$$ ***(Equation 7)***

where C_0 (μg/L) is the initial concentration of adsorbate, C_t (μg/L) is the concentration of the adsorbate at time t (min), V (L) is the sample volume, m (g) is the mass of adsorbent (ABR) added, q_e (μg/g) is the amount of adsorbate adsorbed at equilibrium, Q_1 is the equilibrium adsorption capacity (μg/g), C_i implies the effect of the boundary layer, K_1 (/min) is the equilibrium rate constant for the pseudo-first-order kinetic model, k_2 (g/μg/min) is the equilibrium rate constant for the pseudo-second-order kinetic model, k_i (μg/g/min$^{-1/2}$) is the equilibrium rate constant for the intraparticle diffusion, α is the initial adsorption rate for the Elovich kinetic model, and β is the desorption constant for the Elovich kinetic model.

For the adsorption isotherm study, different dosages of ABR (0, 0.1, 0.5, 1, 5, 10 g/L) were added into 200 mL 100 μg/L PFAS solution in 1 L beakers. The solutions were mixed continuously at 120 rpm using the jar tester for 24 hours to ensure the adsorption equilibrium was reached. After mixing, all the water samples were filtered to obtain the supernatant with glass fibre filters and then sent for analysis. The amount of PFAS adsorbed onto ABR at equilibrium was calculated as described previously. For isotherm models fitting, the data were fitted to four isotherm models: (1)

Langmuir (**Equation 8**), (2) Freundlich ((**Equation *9***), (3) Redlich Peterson and Langmuir-Freundlich (Sips) (**Equation 10**), and (4) Toth models (**Equation 11**).

$$q_e = \frac{K_L Q_m C_e}{1+K_L C_e} \textbf{\textit{(Equation 8)}}$$

$$q_e = K_F C_e^{1/n} \textbf{\textit{(Equation 9)}}$$

$$q_e = Q_m \frac{K_S C_e^b}{1+K_S C_e^b} \textbf{\textit{(Equation 10)}}$$

$$q_e = Q_m \frac{K_t C_e}{[1+(K_t C_e)^b]^{1/b}} \textbf{\textit{(Equation 11)}}$$

where K_L and Q_m are constants for the Langmuir isotherm model: Q_m (μg/g) is the maximum adsorption capacity and K_L is the adsorption affinity coefficient. K_F and n are Freundlich isotherm constants: K_F is the adsorption affinity coefficient and n is the nonlinear index. K_S and b are Sips isotherm constants: K_S is the adsorption affinity coefficient and b is the nonlinear index. K_t and b are Toth isotherm constants: K_t is the adsorption affinity coefficient and b is the nonlinear index.

Langmuir isotherm model is one of the widely used adsorption isotherm models to describe solid-liquid interface adsorption. The adsorption capacity depends on the adsorbate concentration and is based on four assumptions: (1) the surface of adsorbent is homogeneous; (2) each site can only adsorb one adsorbate, meaning the adsorption exists as a monolayer; (3) there is no lateral interaction between adsorbate molecules; and (4) the adsorption is reversible. By contrast, Freundlich isotherm model suggests a multilayer, irreversible adsorption process on a heterogeneous surface. Sips isotherm model is an empirical model that combines Langmuir and Freundlich approaches. Sips model can represent adsorption equilibrium in a wide range of adsorbate concentrations, no matter whether the surface is homogeneous or heterogeneous [162]. Toth isotherm model is an extension of Langmuir model to describe a heterogenous surface. Under

the same condition, the adsorption process following Toth model can uptake more adsorbate molecules. Toth model is more widely used as a supplement to Langmuir model when the latter does not yield satisfactory results [163].

2.6.5 Experiment to assess toxicity

The synthetic wastewater with 100 µg/L PFAS (n=10) and three different ABR dosages (0, 50, 100 g/L) were mixed in 2 L glass beakers at 120 rpm for 24 hours using a jar tester. Toward the end of mixing, the solution pH was lowered using hydrochloric acid to a neutral range (6 to 8). Then the solution was left to settle for 30–60 minutes. The supernatant was collected and filtered with 1µm glass fibre filters. The water samples were extracted following the SPE procedure described in **Section 2.8** and reconstituted with 1 mL methanol for *in-vitro* bioanalyses with extraction factors of 1000 or 2000. The analyses for cytotoxicity, estrogenicity, and mutagenicity followed the procedures described in **Section 2.9** below.

2.7 ABR sludge samples

ABR adsorbent samples for characterization were prepared as (1) "virgin" ABR (i.e., ABR without any treatment), (2) 2 g/L ABR treating ultrapure water, (3) 2, 5, 6, 10, 100 g/L ABR treating wastewater containing 100 µg/L PFAS, and (4) 3 g/L ABR treating wastewater with 100 mg/L PFAS. The solutions containing different concentrations of PFAS were mixed on a tube roller (Globe Scientific GTR-AVS Tube Roller) in 50 mL glass centrifuge tubes at 70 rpm for 3 hours. After mixing, they were centrifuged for 5 minutes at 300 rpm. Then, the supernatant was discarded and the spent ABR sludge was dried at room temperature in aluminum foil baking trays until completely dry. The dried sludge was collected into clear glass bottles and stored at room temperature for analysis.

2.8 Solid phase extraction (SPE)

The SPE procedure was adapted from Cheng (2023) [146] as illustrated in **Figure 5**. Briefly, all water samples were acidified to pH ~2 following separation (filtration) to improve retention of organics onto SPE cartridges. Then, the pre-cleaned 12-position vacuum manifold (Supelco,

Visiprep) was prepared to hold Oasis HLB SPE cartridges (6cc/500mg, Waters Corporation). The cartridges were then pre-conditioned with 5 mL of methanol followed by 10 mL ultrapure water. Samples were introduced into the cartridges under vacuum (GAST Model DOA-P704-AA, vacuum maintained within 20 mm Hg). After sample introduction, the cartridges were rinsed with 10 mL ultrapure water to remove attached impurities, then dried under vacuum for 45–60 minutes. Following vacuum drying, the cartridges were eluted with 5 mL methanol and then 5 mL 1:1 methanol:ethyl acetate by gravity. The eluates were collected in disposable glass culture tubes and then evaporated to complete dryness in a water bath at 35–40 °C with a gentle blow of nitrogen. The dried extracts were then reconstituted in methanol to reach target extraction factor (**Equation 12**) then transferred into 2 mL amber vials and stored with parafilm in the freezer (-40 °C) until analysis.

$$Extraction\ Factor\ (EF) = \frac{Sample\ Volume\ before\ SPE\ (mL)}{Sample\ Volume\ after\ Reconstituion\ (mL)} \textbf{\textit{(Equation 12)}}$$

2.9 Biological analysis

2.9.1 Overview of bioanalytical method selection

While chemical analysis and characterization technologies focus on the concentration of each known PFAS in the sample to assess water quality and the properties of adsorbent, chemicals may be present below the analytical detection limits. Hence, they may still contribute to the biological effects through individual or mixture effects [164]. Bioanalytical methods can assess the bioactivity of a mixture of interest, providing more accurate and straightforward evaluations of the toxic effects of raw/treated water, especially for technologies that may produce toxic by-products. More specifically, cell-based *in-vitro* bioassays work as an alternative to animal tests by applying molecular or cellular techniques operated in 96 or 384-well plate format[164], [165], [166]. They are more sensitive, cost-effective, less time-consuming, and have higher throughput [166].

Three *in-vitro* bioassays were employed in this thesis to represent non-specific, specific, and reactive toxicities covering three classes of modes of action (MOA). Barrow, Nelson et al., and

Huggett et al. have showed that these bioassays are representative in assessing the potential cell toxicity pathways elicited by municipal wastewater [166], [167], [168]. More specifically, cytotoxicity, estrogenicity, and mutagenicity were assessed whether they are introduced by PFAS in water samples or create additional by-products through interactions with ABR. ABR was specifically shown to have some cytotoxic effects [146], albeit is reduced when the finished/treated water is pH-adjusted (to neutral pH).

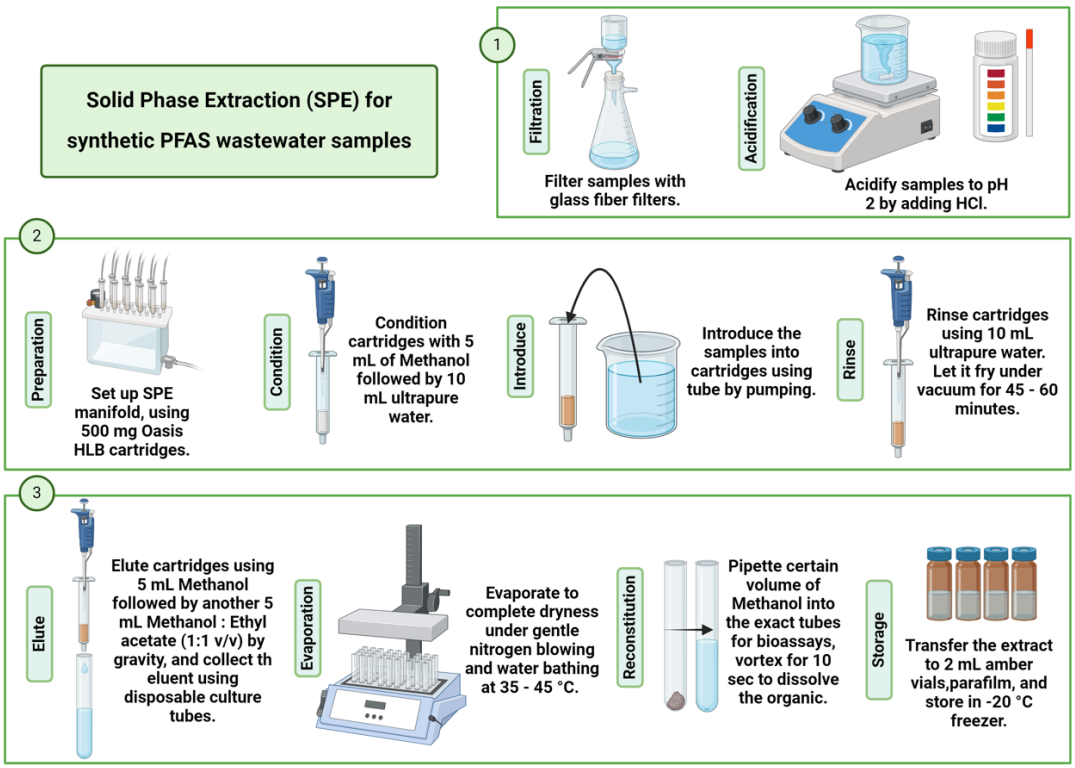

Figure 5. *The solid phase extraction (SPE) procedure for synthetic PFAS wastewater. The figure was taken and slightly modified from Cheng [146].*

2.9.2 *Daphnia magna* acute toxicity test

The *Daphnia magna* test was completed in the Blewett Lab at the Biological Sciences, University of Alberta. The ABR solutions were prepared with OECD water to determine if ABR would release acute toxicity into water. The water was collected from the supernatant without filtration. A gradient dilution series ranging from 100% to 0% in 10% increments (using pre-

prepared OECD water) of water samples was prepared. The pH of all samples was adjusted to 8±0.2, and the samples were allowed to stabilize for one day. Before exposure on the next day, pH of the samples was checked again.

One day before exposure, all the neonate *Daphnia* was removed from the colony to allow adults to produce new offspring. On the next day, neonates <24 h-old were collected for exposure. Here, 11 concentrations of each sample were analyzed with 3 replicates, with 20 mL of each sample transferred into uncapped transparent vials. Five neonates were then transferred into each vial for a 48-h exposure. All the vials were clearly labelled with concentration, number of replicates, start date and time. The test solutions were placed in random order to avoid subjective judgment. Temperature at 20±2°C and a 16 h light and 8 h dark cycle was adopted during the two-day exposure. The viability (alive, dead and immobile) of each neonate was observed and recorded under a microscope. The results were then analyzed using R code to calculate LC_{50} and EC_{50}.

2.9.3 Cytotoxicity

The *Aliivibrio fischeri* lyophilized bacteria was reconstituted with the reagent diluent (both provided by Environmental Bio-detection Product Inc [EBPI]) and stabilized at 4℃ for at least 30 minutes. The bacteria also had to be stabilized at 15 °C for another 30 minutes. A volume of 300 µL of SPE exact of PFAS wastewater was taken and evaporated to dryness by blowing under a gentle stream of nitrogen. Then, the dried extract was reconstituted with 600 µL ultrapure water containing 2% salinity (OAS solution provided by EPBI) in total [169]. The pH of all the samples was adjusted to a neutral condition (7±0.2) using 1N HCl and 1N NaOH. The samples were added to a 96-well plate for luminescence measurement and diluted two-fold serial by rows except for the first row with Sample Diluent so that 7 concentrations of each sample with duplicate were analyzed. Luminescence was measured using BioTek Synergy LX Multimode Reader equipped with Gen5 3.11 software. Here, 3,5-dichlorophenol (DCP) was employed as the positive control to validate the assay. Prior to exposure, the prepared plate was equilibrated on a cooling block (Torrey Pines Chilling/Heating Dry Bath) at 15 °C for 30 minutes. After exposing the cell solution

to the samples, luminescence was measured using the microplate reader at 0, 5, 10, 15 and 30 min [170]. The plate temperature was controlled at 15 °C again between each measurement. The concentration that could cause 10% light inhibition of exposure after 15 minutes ($IC_{10_{15min}}$) of samples was determined following the data analysis procedure analysis in **Table 11** [170].

2.9.4 Estrogenicity

All the stock solutions and agar plate for yeast culturing were prepared prior to the assay, following the process in **Appendix A.3**. The yeast cell stock solution was taken out from the -80 °C freezer and thawed at room temperature. Then, 50 µL of the cell solution was pipetted onto a corner of the agar plate and dried for approximately 5 minutes in the biosafety cabinet. Subsequently, plate streaking was performed to isolate colonies. The streaked plate was incubated at 30 °C upside down for 4–5 days for the colonies to develop and then stored in the 4 °C fridge and used within 2 weeks.

The YES assay was conducted over four days. On the first day, one colony-forming unit (CFU) of yeast from the agar plate was placed into 15 mL conical tubes with 1 mL gold media. Then, the tubes were incubated at 30°C at 300 rpm for 18–24 hours. On the second day, one cultured tube was used for checking cell growth condition, while the other one was refreshed for later use in the assay. The optical density was checked by measuring the absorbance of the mixture of 0.9 mL cell solution and 2.7 mL gold media at 660 nm after blanking the spectrophotometer with fresh gold media. If the reading was greater than 1, the assay could be continued. Then, 9 mL of minimal media and 1 mL of cell solution from another cultured tube were added into a flat bottom flask. Then the flask was incubated at 30 °C at 300 rpm for 18–24 hr again. The storage of yeast cells, preparation of the seeding solution, and exposure of cells to the sample are conducted on the next day. Here, 100 µL of cells were mixed with 100 µL of 30% glycerol in a microcentrifuge tube and stored at -80 °C freezer (vortexed) for future YES assays.

For the cell solution already incubated for 18–24 hours, another 10 mL minimal media was added into the flask and incubated at the same condition for another 4–6 hours. At the end of

incubation, 20 mL minimal media and 100 μL of 10 mM $CuSO_4$ pentahydrate were added into an autoclaved glass beaker then mixed. After blanking the spectrophotometer at 660 nm with this mixture, cells were added into the beaker as well. A small increment was required one time till the absorbance reading reached 0.03±0.002.

During the incubation period, sample extracts were dried before exposure to cells to avoid confounding issues related to the solvent carrier (methanol). For the PFAS samples, 200 μL of the extracts was pipetted into a 96-well plate then two-fold dilutions by row were performed. Overall, eight concentrations of each sample were analyzed, and the duplicates were conducted for each sample. Next, 10 μL 17β-Estradiol (E2) stock (eight samples with concentrations ranging from 17.0239 to 0.1330 μg/L through two-fold serial dilutions) was used as the positive control. The vials then were placed in the biosafety cabinet to evaporate all the methanol. Once the methanol had evaporated, 200 μL seeding media was added to all the sample vials, the vials were capped and incubated at 30 °C, 300 rpm for 18–24 hours. At the end of Day 3, the β-gal reagent (2× β-galactosidase assay buffer) was removed from -20°C freezer to 4 °C fridge for thawed. For the work on the final day, 25 μL of exposed cells were transferred from the amber vials into a new, clean, and transparent 96-well plate. Then 75 μL of minimal media was added for the cell growth. The absorbance at 600 nm of the plate was measured in the plate reader firstly for the quantification of the cell growth condition. After adding 100 μL 1:1 β-gal and Y-PER solution into every well, the absorbance at 420 nm was read to quantify the estrogenicity response. The concentration that could cause a 10% effect (EC_{10}) and the E2 equivalence (E2-EQ) were calculated for each sample following the data analysis procedure analysis in **Table 11**. Note that the E2 stock (positive control) was added into all the corresponding diluted PFAS extracts after being transferred into 2 mL amber vials in this thesis.

2.9.5 Mutagenicity

The mutagenicity assay implemented in this study followed the procedure provided in the UMU-ChromoTest kit from EBPI with minor modifications as outlined by [169]. Sixteen to 18

hours prior to running the assay, the freeze-dried bacteria were rehydrated in the growth media with nutrients added (all provided by EBPI), then incubated at 37 °C and 100 rpm. On the following day, SPE extract (200–400 µL) was transferred and evaporated to dryness under gentle N_2 then reconstituted in 10% dimethyl sulfoxide (DMSO) with 0.85% sterile saline water. The pH of the reconstituted sample was adjusted to neutralized (7±0.2) with 1 N NaOH. In the 96-well plate, the samples were diluted by two-fold five times and each one was in duplicates. For validation of the assay, 4-Nitroquinoline 1-oxide (4-NQO) was applied as the positive control. Glucose and growth media solution was added to the wells to provide nutrients for cells. This plate was named Plate A. The growth of the bacteria was assessed using the absorbance at 600 nm. Then the bacteria were mixed with fresh growth media again and incubated at the same condition for another 1.5 hours. The absorbance/optical density (OD) at 600 nm of the reinoculated bacteria was inspected again and compared with the prior one. Once the growth reached at least 80% of the overnight OD_{600}, the bacteria were added into plate A containing the prepared samples. After the plate A had been incubated for 2 hours, 30 µL all the samples were transferred to a second plate B containing growth media ano n g ded glucose. Then, the absorbance at 600 nm of plate B was read. After another 2 hours of incubation, plate B was read under 600 nm once again to evaluate the cell growth. Then, the samples were transferred into a third plate C again with a mixture of 2-mercaptoethanol and B-Buffer reagent followed by ONPG reagent to all the wells. After 30 minutes of incubation for colour development, the mutagenic response was measured by the absorbance at 420 nm. Finally, the sample concentration causing an induction ratio of 1.5, $EC_{IR_{1.5}}$ were determined using the data analysis method in **Table 11**.

Table 11. *Data analysis methods adapted from Barrow et al. [148]. RLU = relative light units; OD = optical density; IR = induction ratio; A = absorbance; QA/QC = quality assurance/quality control; BEQ = bioanalytical equivalents.*

Assay Type	QA/QC	Data Analysis
Aliivibrio fischeri toxicity assay	Positive control is 3,5-dichlorophenol. In this study, $IC_{10_{15min}}$ = 6.020±1.135 mg/L	1. Calculate %Inhibition from the raw RLU using the equation below: $$\%Inhibition = 1 - \frac{RLU_{sample,t\ min}}{RLU_{sample,0} \times \frac{RLU_{blank,t\ min}}{RLU_{blank,0}}}$$ 2. Normalize %Inhibition from 0–100% 3. Complete a Ligand Binding-Sigmoidal Dose response regression using log concentration and average normalized %Inhibition (on SigmaPlot) 4. Calculate IC_{10} using parameters obtained from regression fitting
YES assay	Positive control and reference compound to calculate BEQ is 17β-estradiol (E2). In this study, EC_{10} = 59.5±109.50 ng/L	1. Calculate the β-Galactosidase (β-Gal) response using the raw cell density (OD_{600}) and raw ß-Gal data (OD_{420}). Note that at OD_{420} only absorbance values between 0.2 to 1.0 were included in the analysis. $$\beta - Gal = \frac{1000 \times slope(raw\ \beta - Gal\ data)}{volume\ of\ cells\ plated\ (mL) \times average\ OD_{660}}$$ 2. Normalize β-Gal response from 0–100% 3. Remove cytotoxicity interferences at higher concentrations from the data set 4. Model the data using a 4-Parametric Logistic Equation using concentration and average normalized β-Gal response (on SigmaPlot) 5. Calculate EC_{10} using parameters obtained from regression fitting 6. Calculate the E2-EQ of each sample using the $EC_{10}$of E2

UMU-ChromoTest assay	Reference compound and positive control is 4-nitroquinoline 1-oxide (4-NQO). For validation, the IR of 4-NQO at 5.26 µM must be at least 2. In this study, IR5.26µM = 7.799 $EC_{IR_{1.5}}$= 79.11 µg/L	1. Determine the β-Galactosidase (β-Gal) activity using the following equation: $$\beta - Gal = \frac{A_{420}Sample - A_{420}blank}{A_{420}negative\ control - A_{420}blank}$$ 2. Determine the growth factor (G) using the following equation: $$Growth\ factor = \frac{A_{600}sample - A_{600}blank}{A_{600}negative\ control - A_{600}blank}$$ Note: G must be greater than 0.5 for results to be considered valid. 3. Find the IR by dividing the β-Gal by G. Note: For a sample to be considered mutagenic, IR must be > 1.5. 4. Find the slope by fitting the data to a linear trendline with a y-intercept of 1. 5. Find the $EC_{IR_{1.5}}$ for each sample using the following equation: $$EC_{IR_{1.5}} = \frac{0.5}{slope}$$ Calculate the 4-NQO-EQ using the $EC_{IR_{1.5}}$ of 4-NQO

3 Results and Discussions

3.1 Material characterization

Appropriate material characterization is recommended for new adsorbents to understand their properties, support their future application, relate their performance back to their characteristics, and enable comparison with currently existing (and commercially available) adsorbents [149]. As described subsequently below, this study employed the following ABR characterization methods: (1) surface area and porosity, (2) X-ray photoelectron spectroscopy (XPS), (3) scanning electron microscopy; (4) elemental analysis via energy dispersive X-ray spectroscopy (EDX); and (5) particle charge (zeta potential). These material characterization techniques were applied before (virgin) and after treatment (spent), or after over-saturation of the ABR material with PFAS.

3.1.1 Brunauer-Emmett-Teller (BET) for surface area analysis

Surface area and porosity (i.e., total pore volume and pore size distribution) influence the properties of many adsorbents and are often characterized using BET analysis (**Table 12**). BET test was conducted for both "virgin" (i.e., without any treatment) and "spent" ABR (here exposed to high concentration PFAS in ultrapure water (100 mg/L). The BET surface area of virgin ABR before treatment was 25.3 m^2/g and did not change substantially after exposure to a high concentration of PFAS (25.1 m^2/g). However, the total pore volume was reduced slightly from 0.137 mL/g to 0.116 mL/g, indicating that PFAS may have occupied the pores on the surface of ABR.

Table 12. *BET characterization results of ABR before and after over-saturation experiment (i.e., PFAS concentration of 100 mg/L).*

Sample	Surface Area (m^2/g)	Total Pore Volume (mL/g)	Pore Size Diameter (D) (nm)
"virgin" ABR (without treatment)	25.3	0.137	2–46
"spent" ABR (over-saturated)	25.1	0.116	2–76

The estimated pore size diameters (**Table 12**) and their distribution (**Figure 6**) indicate the heterogeneity of pore sizes for both virgin and spent ABR (over-saturated). The density functional theory (DFT) pore size distribution specifically suggests that the pores in ABR are mostly mesopores, i.e., pores with diameters between 2 and 50 nm. After treatment, more macropores (i.e., pores with diameters higher than 50 nm) appeared, indicating that some pores may have combined after the treatment. Furthermore, the presence of mesopores on ABR can promote the adsorption capacity and removal efficiency of PFAS. Punyapalakul et al. observed that PFOA and PFOS adsorbed more and faster on mesoporous than microporous adsorbents, and they also speculated that interparticle diffusion dominated the overall mechanism [171]. Gagliano et al. also reported meso- and macroporous adsorbents have higher adsorption capacity for long-chain PFAS because access to adsorption sites is easier for these substances (i.e., less blockage) [172]. Larger PFAS molecules can easily get in and aggregate in mesoporous and macroporous structures, leading to a higher removal [5]. Hence, these pore sizes may be an advantage of ABR when compared to other highly microporous materials (e.g., activated carbon), especially for long-chain PFAS.

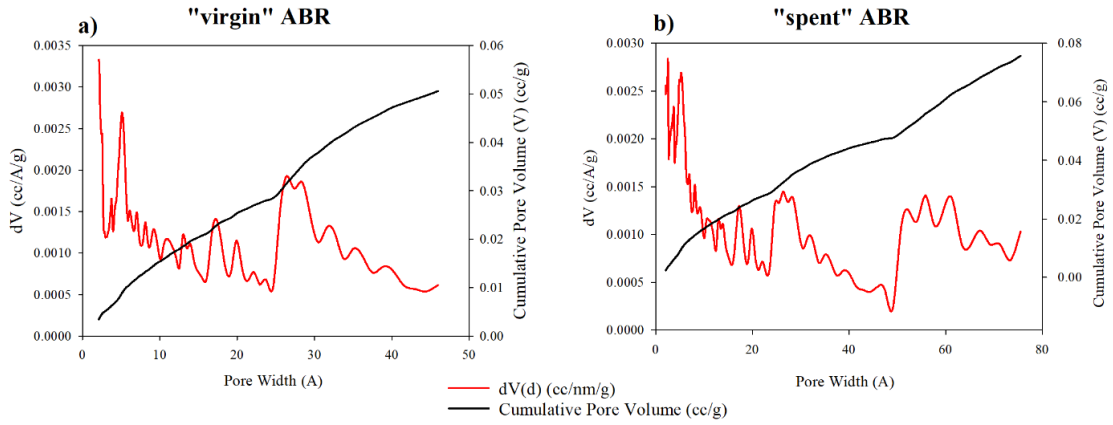

Figure 6. *Density Functional Theory (DFT) pore size distribution of ABR.* ***(a)*** *"virgin" ABR (without treatment);* ***(b)*** *"spent" ABR (oversaturated). Micro-, meso-, and macropores are described to have pore width/diameter of <2, 2–50, and >50 nm. The "virgin" and "spent" ABR are characterized to have heterogeneous pore sizes.*

The BET surface area of other bauxite residues that have been modified via heating and blending with additional substances are similar to ABR and are generally <100 m^2/g with the highest observed surface area of 77.94 m^2/g [173]. However, ABR has the highest total pore volume, approximately 3 times higher than others (i.e., 0.137 compared with 0.0317 mL/g) [174]. Adsorbents with high pore volume are more advantageous because they can enhance the adsorption capacity, especially for organic pollutants. For example, biochar with pore volumes between 0.2 and 0.9 cm^3/g has the best adsorption capacity of aromatics [175].

ABR has a much lower BET surface area (**Table 13**) when ABR was compared with activated carbon, a widely used (highly) porous adsorbent in water treatment. More specifically, activated carbon can have a surface area >1000 m^2/g. Of the emerging artificial adsorbents, the metal-organic framework (MOF) is the only one capable of potentially surpassing this benchmark. However, MOFs are expensive, and to date, they are still applied in bench-scales [176].

Although bauxite residues do not have the highest BET surface area or total pore volume, different adsorbents have diverse preferences for contaminants and may still be amenable to PFAS removal. Given that the ABR surface area and pore volume characteristics are more superior than other bauxite residues (**Table 13**), there is still a potential to determine its use as an alternative adsorbent material (described in detail in **Section 3.2**). With this limitation in mind (i.e., lower surface area than activated carbon), the optimal dosage can be assessed (**Section 3.3–3.4**), which can direct additional surface modification to improve its surface area.

Table 13. *BET surface area and total pore volume of some treated bauxite residue from the literature, as well as other common adsorbents that focused on the application of PFAS removal from the water column. GAC = granular activated carbon; ND = not determined.*

Type	Adsorbent	Surface area (m^2/g)	Total pore volume (mL/g)	Reference
Bauxite Residue	ABR	25.3	0.137	This study
	Bauxite residue A	7.96	0.0317	[177]
	Bauxite residue B	6.31	0.0318	[177]
	10% Bauxite Residue + 10% Clinoptilolite or 10 wt% Bentonite	61.35–77.94	0.0388–0.0729	[173]
	Raw bauxite Residue	20	ND	[178]
Activated Carbon	GAC	975	0.52	[179]
	PAC from GAC of Singi Chemical	1014	ND	[23]
	4 types of activated carbons	444–985	0.2435–0.5066	[180]
	GAC	895.5		[181]
	Raw Activated carbon	912	1.02	[182]
	4 bituminous coal-based activated carbons	755–788	0.31–0.41	[183]
Biochar	Granular biochar	152.3	ND	[181]
	Maize Tassel	2.52	ND	[184]
Metal-organic frame	Fe-BTC	1051	ND	[41]
	MIL-100-Fe	1237		[41]
	MIL-101-Fe	1811		[41]
	ZIF-7	14	ND	[185]
	ZIF-8	1291		[185]
	Uio-66-10/25/50/DF	687–1423	0.32–0.72	[186]
	Three MIL-101-(Cr)	433.16–6955	0.62–3.44	[187]

3.1.2 X-ray photoelectron spectroscopy (XPS) analysis

XPS was conducted to evaluate the composition of the surface element and the specific bonds on the surface of ABR. Na, Fe, Ti, Ca, Si, and Al (**Table 14**) were used for targeted scanning as the preliminary survey scan by XPS suggests they are the most abundant in ABR; C and F were added as they are the most abundant elements in PFAS. Overall, Al, Na, and Fe dominate the atom surface composition, which is expected since bauxite residues typically contain Fe_2O_3, Al_2O_3, and Na_2O (**Section 1.6**, Introduction). Their presence also suggested that these substances did not leach

out after PFAS exposure suggesting that the pH adjustment is important as what has been shown by Cheng [146]. The presence of metals on the ABR surface could also promote adsorption.

As the PFAS concentrations increased from 0.1 mg/L to 100 mg/L, F composition increased to ~58% of the relative atom concentration on the surface, suggesting that PFAS indeed adsorbed onto the surface. The F relative atom concentration was also lower at 6 and 10 g/L ABR dosage than 2 g/L likely due to an increased total surface area as the dosage increases. Note that the same concentration of PFAS was applied for 2, 6, and 10 g/L ABR dosage, but as the dosage increases, the relative density of PFAS adsorbed onto ABR material decreases. Hence, we observed the relative atom concentration to be ~50% lower in 6 and 10 than 2 g/L.

Table 14. *Relative atom concentrations of selected elements on the surface of ABR at different PFAS initial concentrations and ABR dosages. 0 g/L ABR dose = "virgin" ABR.*

Relative % atom concentration					
PFAS Conc	**0.1 mg/L**				**100 mg/L**
ABR Dose	**2 g/L**	**6 g/L**	**10 g/L**	**0 g/L**	**3 g/L**
F	**4.60**	**2.00**	**2.07**	**1.37**	**57.69**
Na	20.54	20.63	21.45	22.17	2.97
Fe	18.05	17.78	19.09	19.65	4.88
Ti	2.13	2.17	2.21	2.31	1.11
Ca	4.42	5.10	5.31	4.73	3.01
Si	15.41	16.86	15.50	16.18	7.88
Al	34.86	35.46	34.36	33.60	22.46

F-bond types were then qualitatively analyzed using the XPS spectra to identify whether C-F bonds were present or if F interacted with other surficial elements via metal bond. No specific peak of F-bonds in F spectra was observed for "virgin" ABR (i.e., 0 g/L) suggesting that F mainly comes from PFAS introduced into the solution. Although the F relative composition is low (4.6%) for 0.1 mg/L PFAS concentration (**Table 14**), the C-F and metal-F bonds can still be determined in the spectra, albeit the peak signals are quite low (**Figure B.1.1** and **Appendix B.1**). When the "spent" ABR (i.e., ABR used to adsorb PFAS) was baked at 550℃ for 2 h, C-F bond was not observed

(**Table 15**). This result suggests that the thermal treatment breaks C-F bonds, but F might still be present on the surface. Some studies have shown that a higher temperature (>1000°C) is needed to break down PFAS thoroughly and regenerate adsorbents [188]. Assessing regeneration and the re-use potential of spent ABR is outside of the scope of this study, but this is another avenue to explore.

The ABR was further oversaturated with PFAS (100 mg/L) to confirm whether C-F and metal-F bonds can still be observed at high pollutant concentrations. Indeed, when the PFAS concentration increased to 1000× times (100 mg/L), the C-F bond was more visible (**Table 15** and **Figure 7**), confirming the adsorption of PFAS on the surface.

Table 15. *Fluorine bond types tested from XPS spectra in different samples. ND = not determined.*

ABR Dose (g/L)	PFAS concentration (mg/L)	Fluorine bond energy position (eV)	Bond Type
0	0	ND	ND
100	0.1	685.0, 688.5	Metal bond, Carbon bond
	0.1 baked post-treatment	685.5	Metal bond
3	100mg	688.93	Carbon bond

The C-F bond could also be seen from the carbon spectra (**Figure 7 (a)**) as indicated by a peak at ~289 eV (first peak) which belongs to C-F bond energy ("~" as approximate only because the peak was fitted manually and automatically and there is no exact value except C-C bond). This peak was also only unique to higher concentrations of PFAS (100 mg/L). Hence, by adsorbing the low mass of PFAS, the C-F bond could be only tested and quantitated from the elemental F scan. However, it is important to note that metal-F bonds are also shown suggesting that F might be interacting with other metallic elements on the surface, albeit adsorption (C-F bonds present) is the most dominant mechanism. It is unclear how these surficial reactions occur (if any) but the diversity in elemental composition of ABR can be an advantage over other emerging adsorbents.

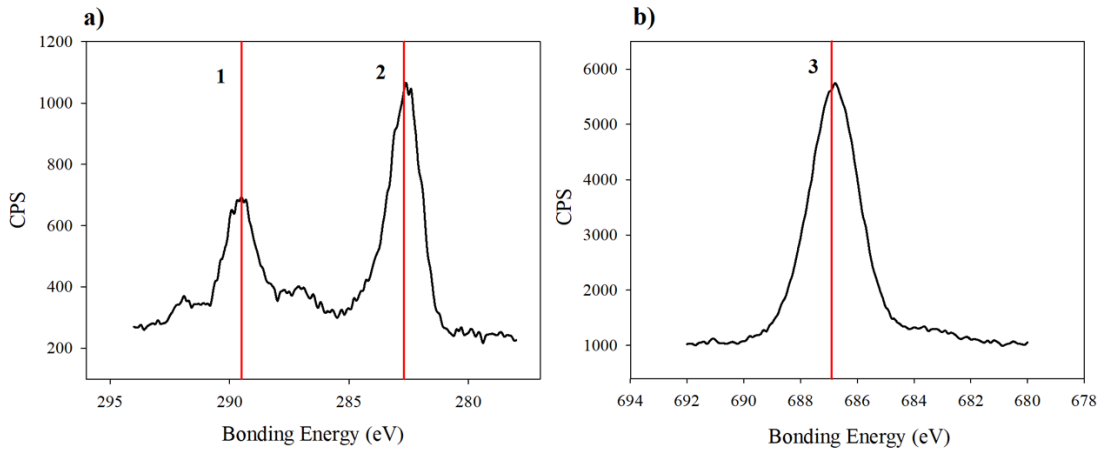

Figure 7. *Bond energy spectrum of* ***(a)*** *carbon and* ***(b)*** *fluorine from 3 g/L ABR exposed to 100 mg/L PFAS. Peak 1 = carbon-fluorine bond; Peak 2 = C-C bond; Peak 3 = fluorine peak.*

3.1.3 Scanning electron microscopy (SEM) and energy-dispersive X-ray spectroscopy (EDX) analysis

SEM and EDX analysis were conducted to detect the elemental composition change and map the element distribution of the "virgin" and "spent" ABR that was oversaturated with PFAS (100 mg/L). There was not a whole difference observed between "virgin" ABR and "spent" ABR based on the SEM images (**Figure B.2.1**), indicating that the porosity of ABR did not substantially change after being over-saturated. By comparing the elemental content before and after treatment (**Figure 8** (a)), the potential background carbon influence was eliminated (which could be from carbon tape or introduced during the activation of BR). After being oversaturated with 100 mg/L PFAS, both carbon and fluorine atom concentrations increased, again supporting that PFAS adsorbed on the surface of ABR.

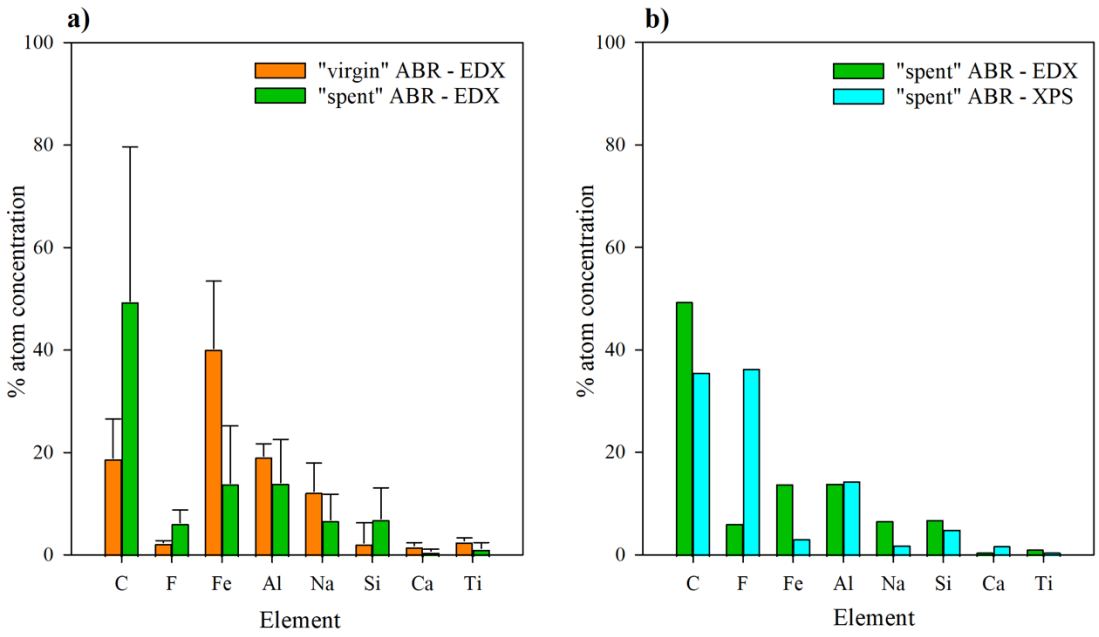

Figure 8. *Element relative mass by atom from ABR without treatment and over-saturated ABR.* ***(a)*** *comparison of EDX analysis for "virgin" and "spent" ABR (oversaturated at 100 mg/L PFAS), average from five different sites on the surface of ABR;* ***(b)*** *comparison of EDX analysis and XPS analysis for "spent" ABR.*

Note that the detection depths/accuracies are different between EDX and XPS (**Section 2.5**) analyses (more description in Methodology), although both provide information on overall elemental composition. EDX can complete the elemental scan in a better scan depth whereas XPS only provides an average/bulk surface scan (1–5 µm vs 0.1µm). As observed in **Figure 8 (b)**, F was only found at a lower percentage from EDX than XPS, but in combination, still provides multiple lines of evidence that PFAS adsorption by ABR happens on the surface.

Three different sites on the spent ABR (oversaturated at 100 mg/L PFAS) were tested for element distribution mapping (**Figure 9**). Different colours suggest different elemental distribution of target elements (green for fluorine and red for carbon). The more vivid the colour is, the higher the concentration of that element present on the surface. It appeared that F and C were not homogenously distributed throughout the surface of ABR, and this was also reflected in the large variability of C composition as seen in **Figure 8 (a)** (i.e., atom concentration was calculated as the average of five sites). Mapping of other elements are also shown in Appendix (**Figure B.2.2**),

though there are no clear relationships/similarities among their distribution on the surface relative to C and F.

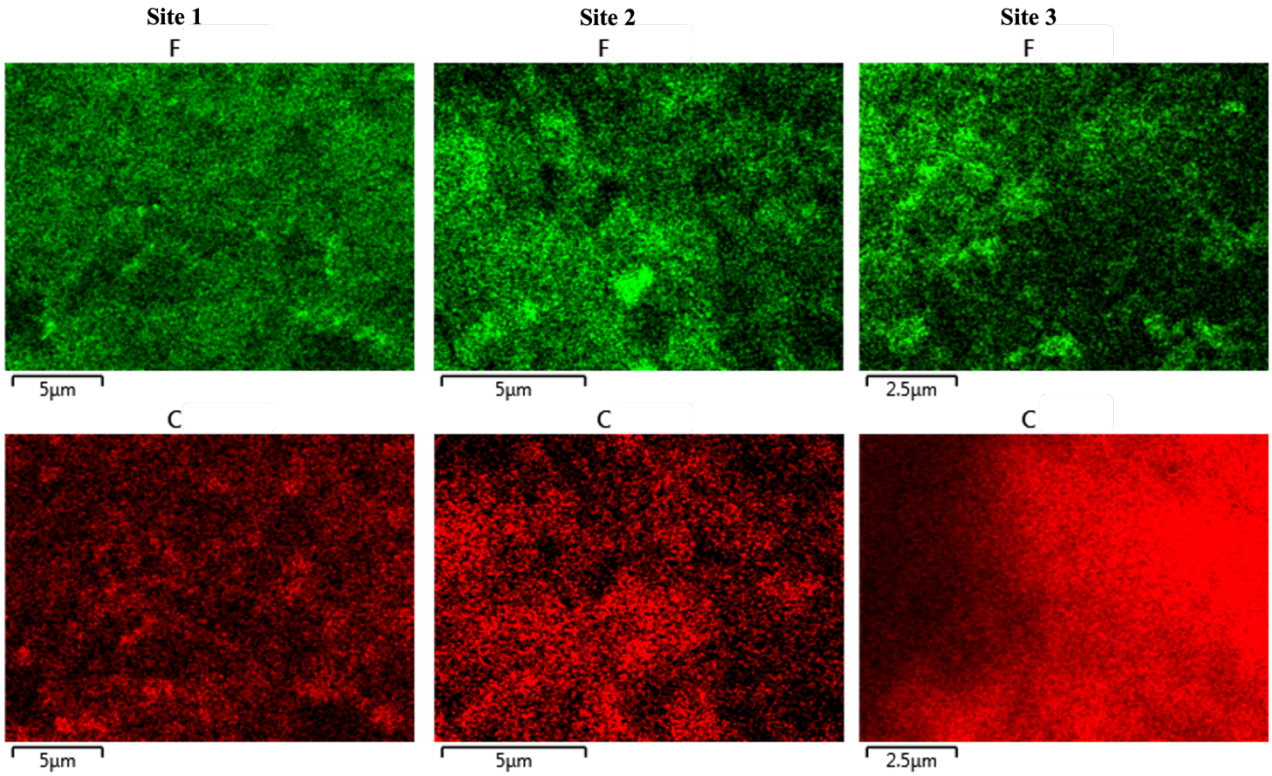

Figure 9. *Distribution mapping of fluorine and carbon on the ABR surface from three sites.*

3.1.4 Particle charge (zeta potential) of ABR

The zeta potential measurements of ABR at various pH conditions (**Figure 10**) describe the surface charge properties of ABR and evaluate whether PFAS has the potential to interact with ABR via electrostatic interactions. **Figure 10** showed that the surface charge of "virgin" ABR (i.e., without treatment) decreased with increasing pH (11.1 mV to -30 mV), suggesting that it is more negatively charged at alkaline pH conditions. This observation was similar to Wanninavake et al who further suggests that the solution pH can affect the surface charge on adsorbents [8].

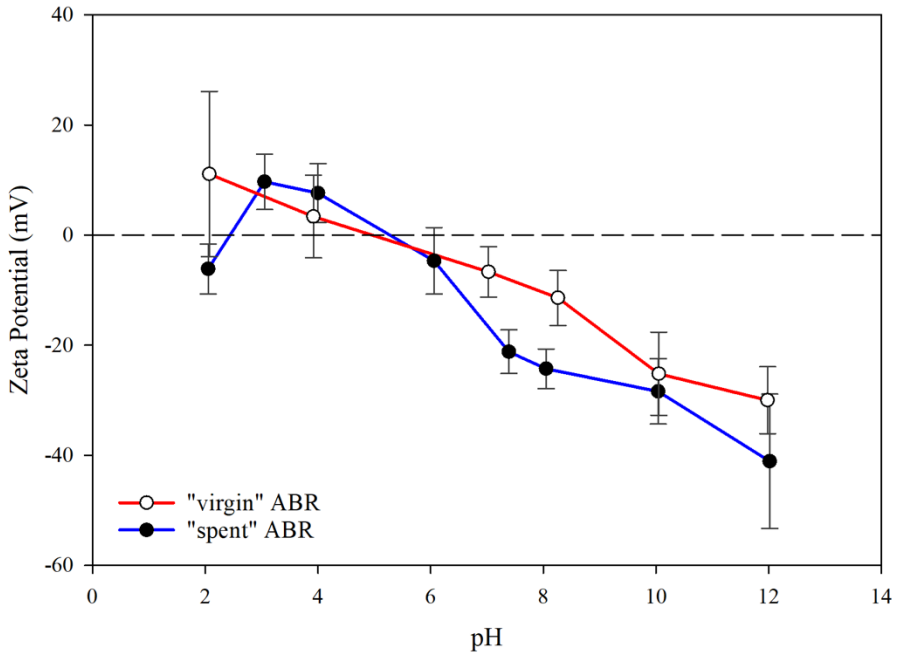

Figure 10. *Zeta potential of "virgin" and "spent" ABR under varying pH values. Concentration (n=10) is at 100 ug/L each PFAS.*

The charge of "spent" ABR (exposed to 100 µg/L PFAS) slightly showed different trend, such that its charge increased firstly, reaching a peak at pH=3.05 (9.69 mV). As the pH increased, the surface charge was more negative. Notably, when pH>6, the surface charge of spent ABR was evidently lower than that of the virgin sample. This result was expected since PFAS exist in the water column as anion (negatively charged), and its adsorption to ABR led to a change in its surface charge characteristic. Higher pH tends to change the adsorbent surface charge more negatively, enabling stronger electrostatic repulsion or weak attractions with anionic PFAS [5]. It is noteworthy that between pH 6 and 8, the surface charge between the virgin and spent ABR had the biggest difference, suggesting that for a PFAS to be adsorbed better, ABR should be close to its point-of-zero-charge so electrostatic interactions are more favourable (i.e., both are non-negative). This observation further supports the need to neutralize ABR to avoid leaching of metals. Of course, it may be more ideal for the pH to be lower as ABR is positive and electrostatic attraction may favour adsorption better. However, discharge guidelines for effluents are typically

not lower than pH 7 suggesting that acidic conditions of the treated effluent are unlikely. Therefore, the highest removal efficiency could be reached under neutral pH (7–8).

3.2 Removal efficiency of PFAS by ABR and powdered activated carbon

3.2.1 Preliminary investigation on dosage and batch adsorption period

Acceptable removal efficiencies of PFAS (C_o = 600 ng/L and 100 µg/L) were observed across varying ABR dosages (**Figure 11**), suggesting that ABR is a potential adsorbent for PFAS removals. While the sum removals (ΣPFAS) appeared very similar at all dosages, the highest removal efficiency (based on magnitude) was observed for 100 g/L ABR (~91% at 100 g/L) (**Figure 11 (a)**). This result was expected since the number of available adsorbable sites increases with higher dosages. However, the removal efficiency of PFBA did not show any trend with increasing dosage. Since there was no reduction in the initial concentration (**Table B.3.1**), additional experiments are required to assess the behaviour of PFAS substances under various conditions in the future. It is important to note that although higher dosages improve removals, they also lead to an increased rate of sludge production (assessment outside the scope of this study). Nonetheless, based on the results (**Figure 11 (a)**), it appears that dosages below 10 g/L may be appropriate for ΣPFAS removals and will be discussed further later in this section and the isotherm section (**Section 3.4**).

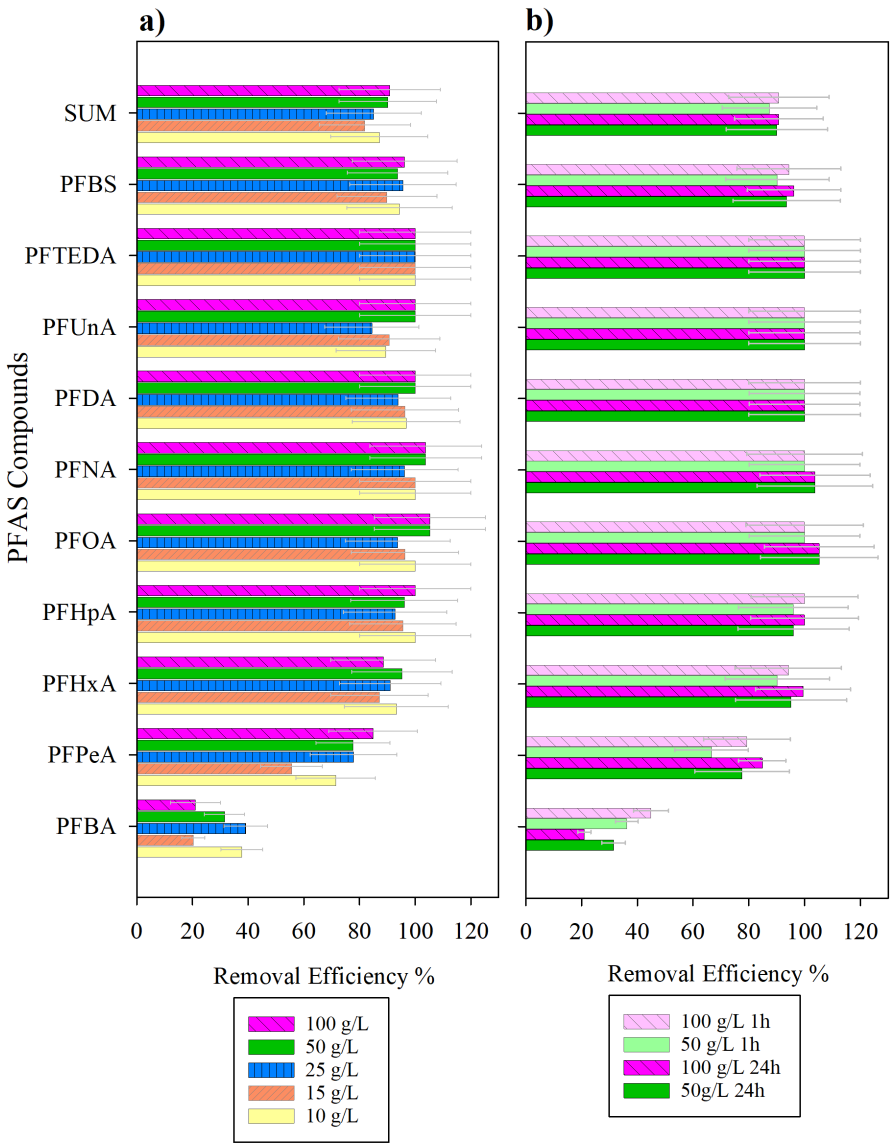

Figure 11. *Removal efficiency of PFAS treated by ABR at various* ***(a)*** *dosages (10–100 g/L) and* ***(b)*** *exposure/treatment periods (24 h vs 1 h). Complete substance names and other characteristics are found in* ***Table 9****. The "SUM" concentrations represent the total concentrations present in the aqueous phase after batch adsorption experiment. The error bars represent ±20% measurement uncertainty (typical for trace organic contaminant analysis).*

When assessing the adsorption of individual PFAS, it was found that removals were higher for long-chain PFAS compounds (#C ≥6 for PFSAs and ≥8 for PFCAs), each achieving nearly 100% removal (i.e., PFTEDA, PFUnA, PFDA, PFNA, PFOA, and PFHpA). The differences between short- and long-chain PFAS have been observed by others [23], [189] who attributed the

mechanisms to the electrostatic and hydrophobic interactions between PFAS and the adsorbents [23]. Electrostatic interactions stem from ionizable functional groups in PFAS (i.e., carboxylic [-COOH] and sulfonic groups [-SO_3H]) and the metallic oxides on the surface of the adsorbent, whereas hydrophobicity is related to the length of the C-F chain and the hydrophobic properties of the adsorbent. Interestingly, electrostatic negativity plays a more important role for short-chain PFAS adsorption while hydrophobic interactions dominate for longer-chain PFAS [190]. Long-chain PFAS also have a preference to form molecular/colloidal aggregates on the adsorbent surface [172].

In a system containing a mixture of PFAS, the hydrophobic interaction can outweigh the electrostatic interaction between PFAS and adsorbents [190]. Hydrophobic substances favour partitioning into adsorbent phases [183]. Park et al. specifically observed hydrophobicity as linearly related to the number of carbons [183], suggesting long-chain PFAS are more hydrophobic than shorter-chain ones [5]. The results of this current study (**Figure 11**) are supportive of this observation as higher removal efficiencies were observed for longer-chain PFAS when combined with ABR in the aqueous solution.

Some studies also suggest that molecular weight (MW) can have an impact on PFAS adsorption potential. For instance, Son et al. reported that MW is more linearly proportional (PFHxA, PFOA, PFDA, PFBS, PFHxS, PFOS) with the removal efficiency than the C-F chain length for PFAS (PFPeA, PFHxA, PFHpA, PFOA, PFNA, PFDA, PFBS, PFHxS, PFOS) [191]. Especially for ABR with abundant mesopores (see BET characterization results), long-chain PFAS can enable micelle/hemimicelle formation (i.e., colloidal aggregation) which may also block the intraparticle diffusion of short-chain ones [190], [192]. Notably, some studies suggested that the adsorbed short-chain PFAS can be replaced by long-chain competitors, eventually leading to their desorption from adsorbents and resulting in low removal efficiency of short-chain ones [172], [190], [192]. Although there was no obvious desorption of short-chain PFAS based on the kinetics experiments, it is likely that the PFAS replacement was negligible, or this process happened

relatively quickly and cannot be determined from the experiments. Shorter collection periods can be adopted for future experiments to investigate the adsorption process of PFAS on ABR further.

Based on the previous ABR experiments on oil sands processed water (OSPW) and municipal wastewater (primary, secondary, and tertiary treated) [146], the observed ABR dosages between 50 and 100 g/L provided optimal results [146]. However, these dosages are relatively high and will therefore produce large amounts of solid waste/sludge during operation (i.e., when coupled with rapid mixing and settling). Therefore, in this study, a preliminary dosage assessment suggests that 10 g/L (**Figure 11 (a)**) is an appropriate dose to begin experiments on adsorption isotherm (see **Section 3.4**). The batch exposure period was also assessed (**Figure 11 (b)**) to get an indication of when the equilibrium condition was achieved and to determine an appropriate timing for the adsorption kinetics experiment. Either short- (1h) or long-term (24h) exposure/mixing period was suitable for long-chain PFAS (all reached 100% removal). However, for the short-chain ones, a longer exposure period may be required to maximize removal, except for PFBA. PFBA is difficult to remove from the water column by adsorption, similar results have been observed with anion exchange resins [189]. As the exposure time went by, due to its short-chain nature, PFBA may desorb from ABR. Overall, the sum removal efficiency of all the PFAS compounds ranged between 80 and 90% for all dosages and exposure periods (i.e., 24 h vs 1 h), but this estimate is mostly dominated by the excellent removal of longer-chain PFAS. Therefore, depending on the target PFAS to remove, the dosage requirement must reflect this (more discussion in **Section 3.3 and 3.4**).

3.3 PFAS adsorption kinetics with ABR

Only 5 of 10 PFAS could be fitted to the adsorption kinetic models as the other substances (PFBA, PFHpA, PFDA, PFUnA, PFTEDA) were already found to be below the detection limits within the first few minutes of exposure period (<5 min) (**Table B.4.1**). To investigate if these five PFAS may have evaporated in the air (as indicated by the potential of PFAS to partition into the air column), the measured initial concentration was compared with the nominal (expected)

concentration (C_0 = 100 µg/L). For the short-chain PFAS (PFBA and PFHpA), the initial concentration was already below the detection limit (**Table B.4.1**). PFBA and PFHpA, with vapour pressures of 1443.11 and 301.69 Pa respectively (**Table B.5.1**), are considered highly volatile according to the World Health Organization's (WHO) definition of volatile organic compounds, which are substances with vapour pressures exceeding 133.32 Pa [193], [194]. This low measured initial concentration suggests that PFBA and PFHpA may have rapidly evaporated during the spiking process.

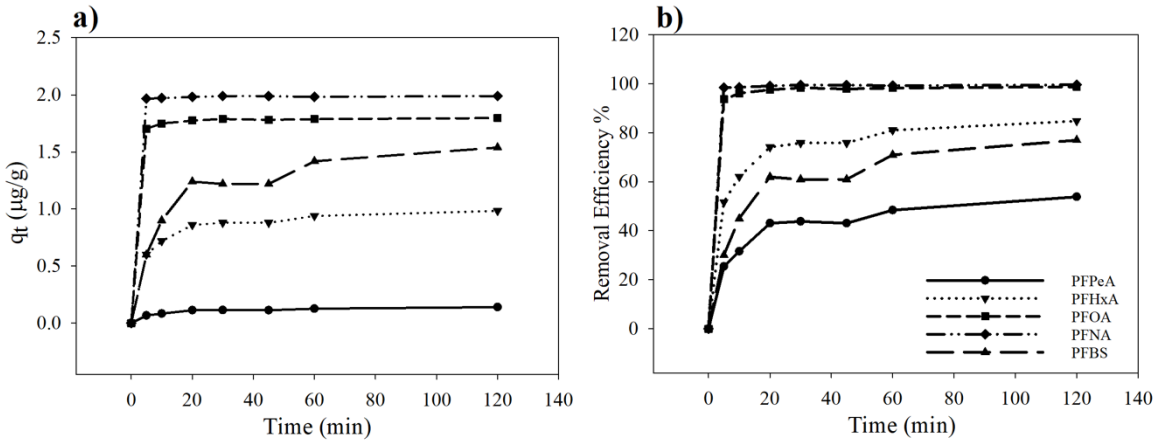

Figure 12. *Adsorption kinetics results for PFAS by 50 g/L ABR as described by* ***(a)*** *amount adsorbed (q_t) and* ***(b)*** *percent removal. Only 5 substances are shown here as the others remained undetected after 5 min of exposure.*

By contrast, PFDA and PFUnA had measured initial concentration close to the nominal concentration (i.e., 90 and 100 µg/L respectively) but was found to be below the detection limits after 5 min. This result may have been due to the fast adsorption of these two PFAS to adsorb onto ABR in a relatively short period (<5min). Interestingly, the longest-chain PFAS substance in this study, PFTEDA, had a relatively low initial concentration (25 µg/L) and is not considered volatile (vapour pressure is 0.52 Pa). PFTEDA may have adsorbed on the container or evaporated during the storage/transportation after spiking into the solution, creating an artifact in the experiment.

For the remaining substances (**Figure 12**), the kinetic experiments suggest that adsorption equilibrium could be reached between 5 and 60 min. The adsorption capacity, q(t), of ABR for these PFAS after 120 min of adsorption ranged from 0.1 to 2 μg/g after 2 h (**Figure 12**). As what was observed in the earlier experiments (**Figure 11**), the longer-chain PFAS reached 100% removal in a relatively short period. For the short-chain PFAS, the maximum removal efficiency at equilibrium was ~50–80% at a dosage of 50 g/L. Therefore, at lower dosages (<50 g/L), short-chain PFAS (PFPeA and PFHxA) will likely require a higher exposure period to achieve better removals. As mentioned before (**Section 3.2.1**), long-chain PFAS have higher hydrophobicity due to the longer carbon chain, leading to more affinity between them and the adsorbents. In other words, short-chain PFAS are more soluble in the water column. As more short-chain PFAS are applied in industry following the voluntary phasing out of long-chain ones, they attract more concern due to their high mobility and persistence in the aqueous phase. This could be the main reason why short-chain PFAS always have higher screening value in the health-based guidance (for example, the health-based guidance for PFAS in drinking water in Canada, **Table 2**).

The kinetic study results (**Table 16** and **Figure 13**) further indicate that the adsorption of PFAS by ABR can either be fitted to pseudo-first-order kinetic (PFO) or pseudo-second-order (PSO) models, though the PSO fits the experimental data slightly better (R^2 ranged from 0.995 to 1). The intraparticle diffusion model or Elovich model fitted relatively poorly compared to PFO and PSO (R^2 ranged from 0.634 to 0.944). A PSO model fit suggests that the rate-limiting step is chemisorption and specific bond formation likely happened on the surface (as what was originally hypothesized in [**Section 3.1.2**]). Recall that the spectra of F from XPS surface scan shows that metal-F bonds appeared on the ABR surface after adsorption (**Figure 7**) and supports the hypothesis that F (or PFAS molecules) may have interacted with metallic elements/oxides on the surface of ABR. Whether it is a chemical or physical bond (or both) is difficult to address but given the fitting of PSO kinetic model with the experimental data, the interactions may be dominated by chemisorption.

The results are also similar to other studies assessing the kinetics of PFAS removal by other adsorbents (i.e., PFAS adsorption onto other materials following PSO kinetics (**Table 17**)). PSO kinetic model is based on a few hypothetical conditions: (1) the initial concentration C_0 is low; (2) the adsorbent is abundant with active sites for the adsorbate; (3) adsorbates react with adsorbents irreversibly [195]. Again, previous analysis of the relationship between kinetics and adsorption mechanism indicate that chemisorption is expected to occur when PSO fits the experimental data [162]. Here, PFAS adsorption experiments showed that PFAS are more likely to sorb onto the adsorbent sites and form stronger chemical bonds. Chemisorption can enhance the binding between PFAS and adsorbents, increasing the removal efficiency of amphiphilic PFAS.

Table 16. *Adsorption kinetics parameters obtained for the removal of PFAS. q_e(μg/g) = the amount of adsorbate adsorbed at equilibrium; K_1(1/min) = equilibrium rate constant for the pseudo-first-order kinetic model; K_2(g/μg/min) = equilibrium rate constant for the pseudo-second-order kinetic model; K_i(μg/g min $^{-1/2}$) = the equilibrium rate constant for the intraparticle diffusion model; C_i(μg/g) = the intercept of the regression line; and b = Elovich model constants. The adsorption kinetics for PFBA, PFHpA, PFDA, PFUnA, and PFTEDA could not be determined due to their instantaneous/fast adsorption onto ABR. Visualization of these results is shown in* ***Figure 13****.*

PFAS compound	Pseudo First Order			Pseudo Second Order			Intraparticle Diffusion			Elovich		
	K_1 (/min)	q_e (μg/g)	R^2	K_2 (g/μg/min)	q_e (μg/g)	R^2	K_i (μg/g/min$^{-1/2}$)	C_i (μg/g)	R^2	a	b	R^2
PFPeA	5.484	0.136	0.965	0.807	0.147	0.995	0.008	0.062	0.847	0.096	44.053	0.944
PFHxA	3.239	0.979	0.983	0.228	1.012	0.999	0.040	0.605	0.792	5.167	8.425	0.934
PFOA	0.28	1.800	0.984	1.747	1.802	1	0.009	1.719	0.634	9.181×10^{9}	36.364	0.826
PFNA	0.063	1.990	0.838	5.691	1.992	1	0.003	1.968	0.646	5.498×10^{9}	131.579	0.803
PFBS	8.171	1.599	0.981	0.065	1.638	0.995	0.096	0.602	0.805	0.651	3.545	0.925

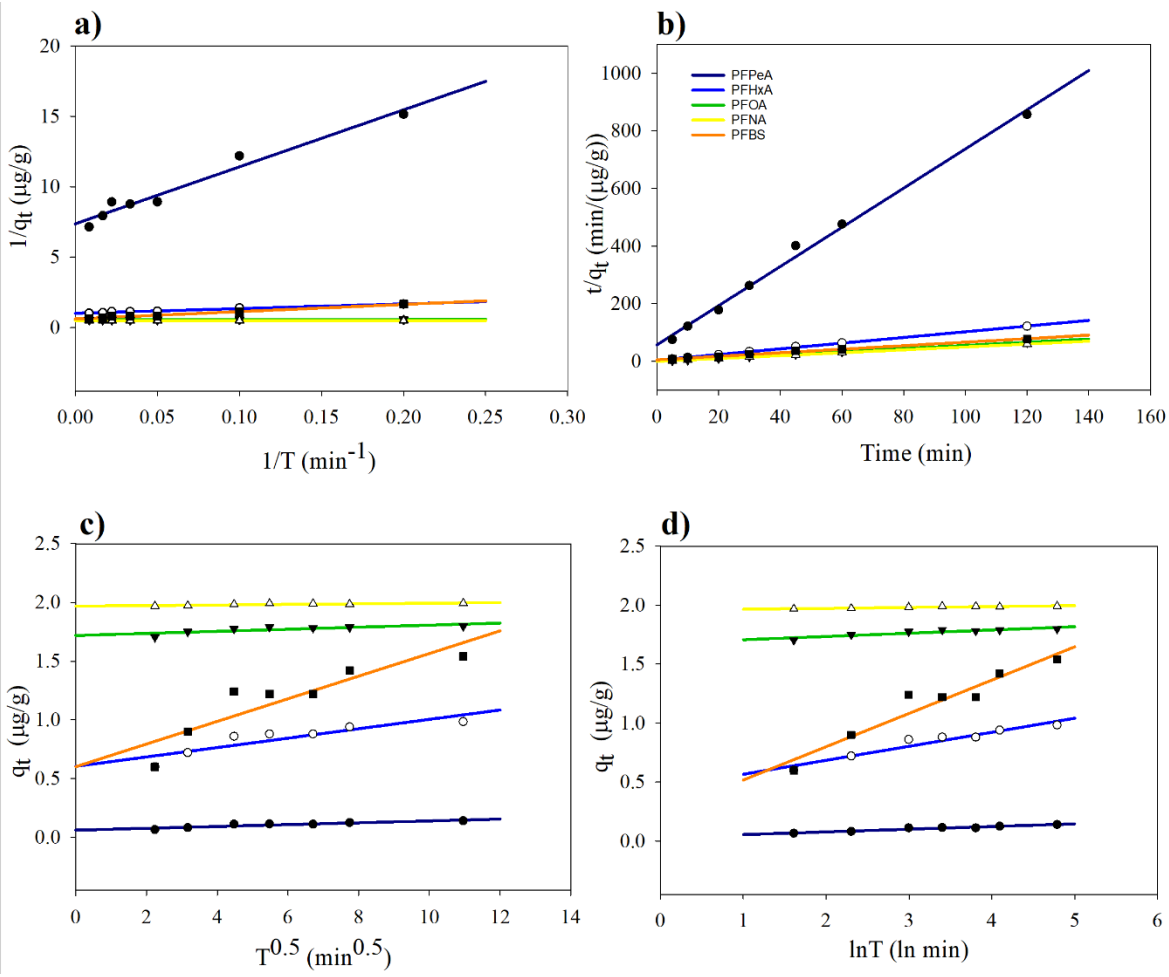

Figure 13. *The adsorption kinetics for PFAS by ABR. Fitting of the experimental data to* ***(a)*** *pseudo-first-order kinetic model;* ***(b)*** *pseudo-second-order kinetic model;* ***(c)*** *intraparticle diffusion kinetic model; and* ***(d)*** *Elovich kinetic model. Note that only 5 PFAS in the mixture can be assessed for kinetics as the other substances (PFPeA, PFHxA, PFDA, PFUnA, and PFTEDA) exhibited fast adsorption kinetics (i.e., below detection limits after 5 min of batch exposure study).*

In recent years, more studies [184], [196], [197] proposed that PSO model always outperforms PFO model (in terms of experimental data fit) because the equilibrium set is much longer, and the model is applied for the entire adsorption duration. For instance, PFO model tends to fit much better at the beginning of adsorption when C_0 is high [195], [198]. Fitting using PFO may require a piecewise approach to determine more precise adsorption mechanism at specific time points.

For PSO kinetics, it is also assumed that the adsorption rate of PFAS on ABR would depend on the ABR adsorption capacity, not PFAS initial concentration [162]. When comparing the PSO parameters, the rate of adsorption (K_2) and the amount adsorbed at equilibrium (q_e) varied with different PFAS (**Table 16**), suggesting differences in affinity among the 10 PFAS considered in this study. Generally speaking, as the carbon chain length and the molecule weight increase, ABR adsorbed PFAS faster at a higher equilibrium capacity (q_e). The q_e calculated from PSO was also consistent with the earlier experiment from **Figure 12**, suggesting consistency of results. When comparing the maximum adsorption capacity (q_e) for ABR with other adsorbents utilized for PFAS removal (bench-scale studies), ABR was observed to be much lower than other adsorbents. This was expected given ABR's relatively low porosity compared to other adsorbents.

Although it is difficult to compare the results with other published studies due to differences in experimental settings (i.e., higher initial concentration), PFAS adsorption onto ABR appeared to reach equilibrium relatively quickly (**Table 18**). It is apparent that the ABR dosage needed for good removals (>90%) was much higher than other adsorbents due to ABR's inherent low porosity. Therefore, it is worth considering the role of dosage when discussing time to reach equilibrium. For instance, Son et al. evaluated four dosages (0.01, 0.03, 0.05, 0.1 g/L) of powdered activated carbon (PAC) for removing 100 ng/L PFAS, and observed that the equilibrium time showed a decreasing trend of ~7 h, 4 h, ~0.5 h, and finally <0.5 h, respectively [23]. This confirms that adsorption equilibrium happens faster when a higher dosage of adsorbent is applied.

To enable better comparison with other adsorbents, a short-term experiment utilizing a commercially available powdered activated carbon was completed (**Figure 14**). Given the large difference in ABR surface compared to PAC, it was assumed that the ABR dose must be increased to make it more comparable to PAC. Here, dosages of 0.1 and 10 g/L ABR were employed based on the prior results (**Figure 11**) and a 0.1 g/L dose was selected for PAC based on published studies (**Table 18**). Individual PFAS concentration of 0.5 μg/L and 100 μg/L were also assessed to determine the relative differences between removals of PFAS at high and low concentrations.

Table 17. *Comparison of adsorption kinetic parameters obtained for this study and the removal of PFAS by different adsorbents. GAC = granular activated carbon; q_e = the amount of adsorbate adsorbed at equilibrium; K_1 = equilibrium rate constant for the pseudo-first-order kinetic model; K_2 = equilibrium rate constant for the pseudo-second-order kinetic model; K_i = the equilibrium rate constant for the intraparticle diffusion model; and C_i(μg/g) = the intercept of the regression line; DWT = drinking water treatment.*

PFAS	4PFCA + 2PFSA	7PFCA + 2PFSA	PFOS, PFOA	PFOS, PFOA	PFOS, PFOA	PFOA, PFOS, PFHpA
Adsorbents	ABR	PAC	Inactivated/activated maize tassel	Biochar	aluminum-based DWT residuals	GAC
Pseudo First Order						
K_1 **(/min)**	0.063–8.171	0.409–10.6	0.17–0.25	N/A	0.067–0.194	0.08–0.27
q_e **(μg/g)**	0.136–1.99	0.205–3.27	0.047–1.59		1–8	9900–15300
R^2	0.838–0.984	0.674–1	0.87–0.98		0.119–0.593	0.83–0.95
Pseudo Second Order						
K_2 **(g/μg/min)**	0.065–5.691	0.625–955	0.16–1.264	4×10^{-5}–1.57	0.641–2.842	0.35×10^{-3}–5.1×10^{-3}
q_e **(μg/g)**	0.147–1.992	0.345–6.73	12–13	0.7–908	84–99	N/A
R^2	0.995–1	0.962–1	0.99	0.90–0.99	1	0.99
Intraparticle diffusion						
K_i	0.003–0.096 g/μg/min$^{-1/2}$	N/A	N/A	N/A	N/A	3.12×10^{-3}–5.46×10^{-3} g/μg/h$^{-1/2}$
C_i	0.062–1.968 μg/g					
R^2	0.634–0.847					0.26–0.96
Reference	This study	[199]	[184]	[197]	[196]	[201]

Table 18. *Equilibrium time of removing PFAS from synthetic wastewater by different adsorbents. MOF = metal-organic frame; MAC = magnetic activated carbon; GAC =granular activated carbon; PAC = powdered activated carbon;* C_0 *= Initial concentration of adsorbate;* T_{equi} *= time to reach adsorption equilibrium; and NR = not reported.*

Adsorbate	Adsorbent	C_0	Dosage (g/L)	T_{equi}	Percent Removal %	Adsorption Capacity	Reference
10 PFAS	ABR	100 μg/L	50	< 5–20 min	54–100	0.14–2 µg/g	This study
PFOS	Ion exchange IRA67	189 mg/L	0.05	~20 h	NR	~250 mg/g	[129]
PFOS	MIL-53(Al)-NDC, MIL-53(Al)-BPDC	20–80 mg/L	NR	~200 min	~80	~120 mg/g	[24]
PFOA, PFOS	GAC, PAC, AI400	50 mg/L	0.1 for AC, 0.05 for MOF	>168 h for GAC and AI400, ~4 h for PAC	NR	PFOA: 166 mg/g for GAC, 331 mg/g for PAC, 1.12 g/g for AI400 PFOS: 225 mg/g for GAC, 325 mg/g for PAC, 100 mg/g for AI400	[116]
PFOA, PFOS	Bamboo-derived GAC	81, 100 mg/L	0.1	~24h	NR	248.5 mg/g PFOA, 700.2 mg/g PFOS	[201]
PFOA, PFOS, PFHpA	GAC	10 mg/L	0.2	24 h for PFOS, 120 h for PFOA and PFHpA	NR	10.3, 15.8, 7.5 mg/g	[200]
PFBS, PFOS, PFHxS, PFOA	MAC	~ 34.6 mg/L	0.14	≤2 h	NR	63, 815, 132, 373 mg/g	[202]
8 PFAS	Magnetic ion-exchange (MIEX) resin	300 ng/L	4.8	20 min	20–90	15–70 mg/L	[203]
9 PFAS	PAC	100 ng/L	0.01, 0.03, 0.05, 0.1	~6 h and < 1h	NR	1.2, 0.6, 0.8, .4 mg/g	[23]
13 PFAS	MPAC	10–50 µg/L	0.1	~2h	NR	2.5, 6, 18 mg/g Total	[204]

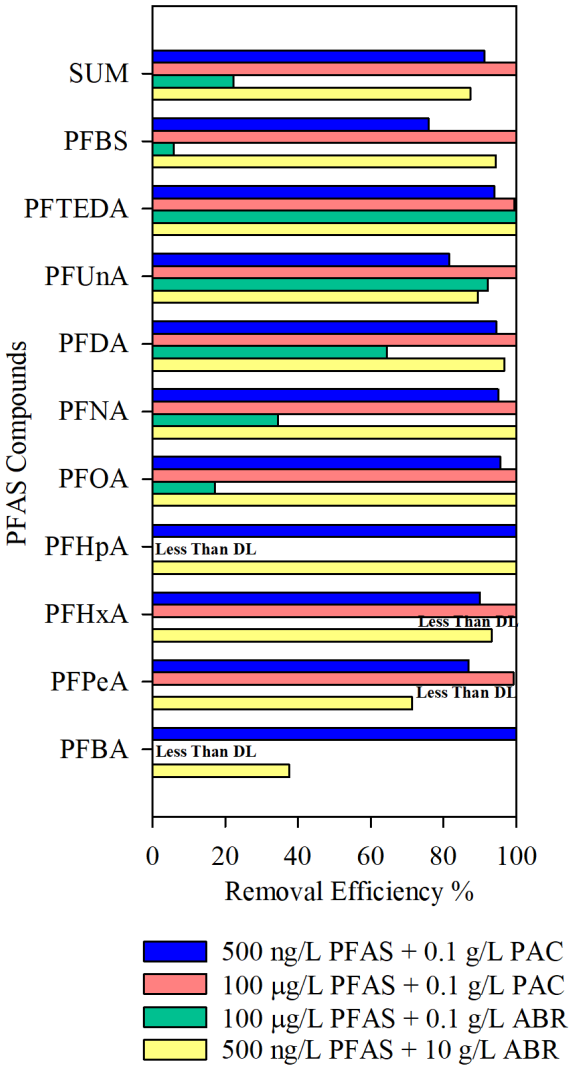

Figure 14. *Comparison of removal efficiency of PFAS treated by commercially available powdered activated carbon (PAC) and activated bauxite residue (ABR). DL = Detection Limit. Complete substance name and other characteristics are found in* ***Table 9****. The "SUM" concentrations represent the total concentrations present in the aqueous phase after batch adsorption experiment.*

Overall, it appears that the removal efficiency of 10 g/L ABR was comparable to PAC (at 500 ng/L individual PFAS concentration, ΣPFAS= 5 µg/L respectively) (**Figure 14**). Although the removal efficiency of PAC for short-chain PFAS (4–6 carbon atoms, PFBA, PFPeA, and PFHxA) was higher than that of ABR, ABR worked better for PFAS with ≥6 carbons. When the concentration of PFAS was increased by 200 times (100 µg/L), both adsorbents behaved similarly for the long-chain PFAS compounds (**Figure 14**). However, the performance of 0.1 g/L ABR was the worst regardless of the individual substance or ΣPFAS removal. This result

suggests that indeed the dosage of ABR cannot be lowered to the same levels as conventional adsorbents. Hence, the amount of sludge produced from ABR needs to be considered.

Finally, the adsorption was enhanced for PAC at higher PFAS concentration (100 vs 0.5 µg/L), which was also observed in another study [205]. More specifically, Niarchos et al. associate this observation with the formation of layers and colloid aggregation (hemi-micelles) between PFAS molecules. Though no similar experiments were conducted for ABR (i.e., same dosage, different PFAS concentration), the theory may be applied here as well. Overall, it suggests the potential of ABR to exhibit higher adsorption capacity when containing higher concentration PFAS in the mixture.

Table 19. *Comparison of removal efficiency of short-chain PFAS treated by commercially available powdered activated carbon (PAC) and activated bauxite residue (ABR). <DL= the initial concentration was lower than the detection limit.*

PFAS substance	500 ng/L + 0.1 g/L PAC	100 µg/L+ 0.1 g/L PAC	100 µg/L + 0.1 g/L ABR	500 ng/L + 10 g/L ABR
PFBA	100.00	<DL	< DL	37.68
PFPeA	87.00	99.39	0	71.43
PFHxA	90.00	99.91	0	93.28

3.4 PFAS adsorption isotherm

The equilibrium performance of ABR was obtained from the adsorption isotherm study, with experimental data fitted to Langmuir, Freundlich, Sips, and Toth isotherm models (**Table 20** and **Figure 15**).

Similar to the result of adsorption kinetics, only 6 of 10 PFAS could be fitted to the adsorption isotherm models. For the other 4 ones (PFBA, PFPeA, PFUnA, and PFTEDA), the initial concentrations were only slightly higher than the detection limit (similar to the results obtained in the kinetics experiment). Therefore, there were not enough data under different dosage conditions to fit the models. However, unlike the kinetics study where all of the substances followed a pseudo-second-order model, the individual PFAS (in mixture) fits different isotherm models. For instance, PFNA fit the Langmuir model (R^2 of 0.977) well whereas PFHxA and PFHpA followed the Freundlich model (R^2 of 0.966 and 0.998

respectively). Finally, PFOA and PFBS can be represented by the Sips model (R^2 of 0.982 and 0.973 respectively), although Langmuir and Freundlich also apply (R^2 of 0.963 and 0.950 for PFOA as well as 0.802 and 0.915 for PFBS respectively). None of them followed the Toth model.

Langmuir model assumes the surface of the adsorbent is homogeneous and the adsorption is a monolayer process, i.e., each site can adsorb only one adsorbate molecule [162]. Because there is no lateral interaction between each adsorbed molecule, the adsorption is reversible for Langmuir adsorption. Freundlich isotherm often describes nonideal, multilayer, and irreversible adsorption at a heterogeneous surface [162]. Since 1/n parameters for PFHxA and PFHpA were found to be >1, this suggests that cooperative adsorption (chemisorption and physisorption) may have existed [162] and the adsorption process is unfavourable [206]. Nonetheless, the process may be dominated mostly by chemisorption given their fit to a pseudo-second-order kinetics model.

The experimental data of PFOA and PFBS fit Langmuir, Freundlich, and Sips model well, but Sips model may be more appropriate as the underlying mechanisms behind the Langmuir and Freundlich formulation may not apply. For instance, Langmuir applies more homogenous surface, but this is not the case for ABR based on SEM/EDX results (i.e., ABR is heterogenous). Also, Langmuir is for monolayer sorption, but it has been observed that long-chain PFAS can form micelle/hemimicelle (i.e., multilayer) during adsorption [207], [192]. Though Freundlich isotherm describes adsorption on heterogeneous surfaces with multilayers, the adsorption process is considered irreversible [206]. Again, given the chemisorption potential for PFOA (based on PSO kinetics), desorption may not be possible. Sips model is a hybrid of Langmuir and Freundlich (mathematically) and can represent adsorption equilibrium in a wide range of adsorbate concentrations, whether the surface is homogeneous or heterogeneous [162]. The good fit of experimental data to Sips model also indicates PFOA adsorption on ABR can reduce to the Freundlich isotherm as the concentration decreases [207].

Finally, among the longer-chain PFAS compounds, PFDA (#C=10) fitted every isotherm model poorly (R^2 = 0.523 for Langmuir and 0.641 for Freundlich), suggesting that the two- (Langmuir and Freundlich) and three-parameter (Sips, Toth) models do not represent the equilibrium adsorption of PFDA in mixture.

Table 20. *Adsorption isotherm parameters obtained for the removal of PFAS. Q_m (μg/g) =adsorption capacity for each model; K_L (L/g) = the isotherm constant for the Langmuir model; K_F = the isotherm constant for the Freundlich model; 1/n = the constant for the Freundlich model; K_s = the isotherm constant for the Sips model; b = intercept for Sips model. None of the PFAS followed Toth model.*

PFAS	Langmuir			Freundlich			Sips			
	K_L (L/μg)	Q_m (μg/g)	R^2	K_F	1/n	R^2	K_s	b	Q_m (μg/g)	R^2
PFHxA	0	4.11E11	0.515	0.009	2.050	**0.966**		-		
PFHpA		-		1.523	1.416	**0.998**		-		
PFOA	0.029	188.679	0.963	5.958	0.834	0.950	0.001	2.433	198.793	**0.982**
PFNA	0.005	3333.333	**0.977**	20.469	0.791	0.881		-		
PFDA	0	5.380×10^{9}	0.523	60.632	0.693	0.641		-		
PFBS	0	2.288×10^{12}	0.802	0.009	1.887	0.915	1.24×10^{-12}	6.123	106.729	**0.973**

In general, Langmuir and Freundlich isotherms are commonly applied models to describe equilibrium sorption and have been considered as best-fit models for organic substances in aqueous system (e.g., pesticides, herbicides, and pharmaceuticals). Sips have been found to work well with dyes and metals [206]. Toth is mostly used for adsorbents with surfaces that are not homogenous such as ABR and was modified from Langmuir model to reduce fitting errors between experimental and predicted values [206]. In addition to Langmuir and Freundlich, Sips and Toth have also been employed in adsorption studies of organic contaminants including PFAS [204].

The choice of the most appropriate isotherm model typically lies on the equilibrium data (i.e., maximum adsorption observed), isotherm model fit (i.e., R^2 value), and whether the model is thermodynamically realistic (e.g., positive slope for all concentration). Regardless of the which model fits well, it appears that PFAS equilibrium performance differ among each other when present as mixtures. These differences can be contributed by three potential mechanisms: (1) the pore filling of longer-chain PFAS hinder access of subsequent PFAS to available sites [208]; (2) the interactions between PFAS molecules [208], [209], [210], for example, micelle/hemimicelle formation; and (3) the varying numbers of layers with different

hydrophobicities and adsorbent heterogeneity [210], [211]. In terms of ABR, the latter two mechanisms may exert a greater influence as ABR largely contains mesopores (BET results, **Section 3.1.1**), which can mitigate pore clogging to a certain degree. Additionally, as the surface of ABR is not homogenous (from SEM) and most PFAS employed are long-chain ones, more interactions can happen during the adsorption process.

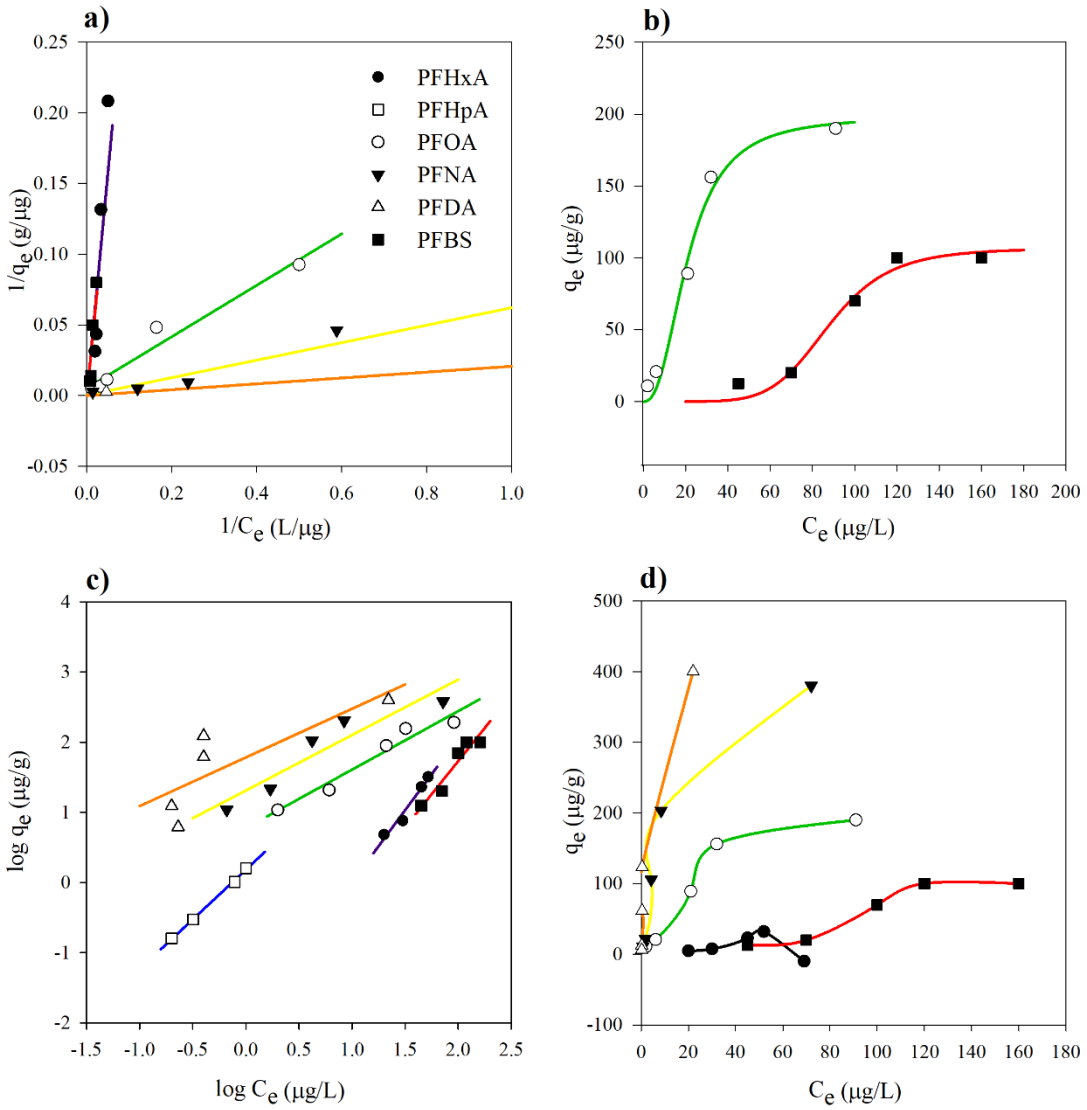

Figure 15. *The adsorption isotherm for PFAS by ABR. Fitting of experiment data to* ***(a)*** *Langmuir adsorption isotherm model;* ***(b)*** *Freundlich model; and* ***(c)*** *SIPs model.* ***(d)*** *amount adsorbed (q_t) vs remaining concentration (C_e). Note that the x- and y-axis vary depending on the isotherm model explored.*

The results of this study also support many findings reported in the literature (**Table 21**). For instance, Umeh et al [212] assessed the adsorption isotherm for nine PFAS compounds

(mixture) treated with PAC, none of them fitted the Sips model but fitted both Langmuir and Freundlich better (**Table 21**). However, in binary mixtures containing PFOS and PFOA, the isotherm fitting depends on the adsorbents used. For instance, Podrigo et al [197] found a good fit with Sips when applying biochar with Fe_3O_4 onto PFOS and PFOA. Sips follows the monolayer adsorption from Langmuir, and operating conditions such as concentration, pH, and temperature are the parameters governing the adsorption [206].

An important information derived from isotherm experiments is the maximum adsorption capacity (Q_m) of the material (Langmuir and Sips), and the opportunity to determine the desired dosage of adsorbent when operated in a completely mixed flow reactor system (CMFR) (Freundlich isotherm) **(Equation 9**). The fitted results showed that the adsorption capacity of ABR to adsorb PFAS ranged from 107 to 3333 μg/g (**Table 20**) which is comparable to other novel adsorbents (e.g., aluminum-based drinking water treatment residuals). Note that a low dosage of 10 g/L is capable of removing most PFAS (**Figure 11**). Depending on the target removal requirements, the ABR dose to reach the target efficiency could be estimated. For instance, to remove 50–95% of PFHpA via ABR, doses ranging from 0.1 to 6.4 g/L are required (**Table B.6.1**). Furthermore, it appears that a concentration of up to 10 g/L is suitable to remove most of the substances (ΣPFAS removal of >85%), with some shorter chains remaining in the aqueous phase. However, when the removal efficiency of short-chain PFAS treated with other adsorbents (conventional or emerging) was compared with ABR, ABR was observed to have a better performance (**Table 22**). Except for PFBA, ABR could remove at least 70% short-chain PFAS from wastewater (even at 10 g/L) while other adsorbents remained <50%. More specifically, short-chain PFAS removal in other studies treated by GAC or PAC could only reach a maximum of 70% removal, far lower than ABR.

Table 21. *Adsorption isotherm parameters obtained for the removal of PFAS by different adsorbents in literatures.* Q_m *=adsorption capacity for each model;* K_L *= the isotherm constant for the Langmuir model;* K_F *= the isotherm constant for the Freundlich model; 1/n = the constant for the Freundlich model;* K_s *= the isotherm constant for the Sips mode;and. b = intercept for Sips model.*

PFAS compounds	4PFCA + 2PFSA	7PFCA + 2PFSA	PFOS, PFOA	PFOS, PFOA	PFOS, PFOA
Adsorbents	ABR	PAC	Inactivated/activated maize tassel	Biochar w/o Fe_3O_4	aluminum-based drinking water treatment residuals
			Langmuir		
K_L	0–0.005 L/µg	166–2012 L/mg	~0 L/mg		0.0048–0.029 L/µg
Q_m	188.679–2.288×10^{-12} µg/g	0.97–3 mg/g	103.19–666.67×10^{3} mg/g	N/A	139–316 mg/g
R^2	0.515–0.977	0.93–0.98	0.83–0.95		0.943–0.995
			Freundlich		
K_F	0.009–60.632	$2.83–5.33\times10^{5}$	36.99–1552.5		0.452–10.693
1/n	0.693–2.05	1.69–4.76	1.12–2.01	N/A	0.893–1.062
R^2	0.641–0.998	0.93–0.96	0.96–0.99		0.921–0.995
			SIPS		
K_S	1.24×10^{-12}–0.001	N/A	N/A	5.9×10^{-5}–2.1×10^{-4}	N/A
b	2.433–6.123			1–4.5	
Q_m	106.729–198.793 µg/g			3256.5–33007 µg/g	
R^2	0.973–0.982			0.99	
Reference	This study	[212]	[185], [200]	[197]	[196]

Table 22. *Comparison of short-chain PFAS removal efficiency by ABR with other adsorbents. BAC= biological activated carbon; GAC = granular activated carbon; PAC = powdered activated carbon.*

PFAS compound	Adsorbent	Concentration (PFAS)	Dosage (g/L)	Removal Efficiency	Reference
PFBA, PFPeA, PFHxA, PFHpA, PFBS	ABR	500 ng/L	10	38%, 71%, 93%, 100%, 94%	This study
PFBA, PFPeA, PFHxA, PFHpA, PFBS	ABR	100 µg/L	50	31%, 77%, 95%, 96%, 94%	This study
PFHxA, PFHpA	BAC	30 mg/L	0.2	<10%, 10–30%	[213]
PFBA, PFHxA, PFBS	GAC	1 and 100 µg/L	0.2	50% (10%), 68% (30%), 70% (40%)	[214]
PFPeA, PFHxA, PFHpA, PFBS	GAC, PAC	100 ng/L	0.01 and 0.05 g/L	(GAC) 20%, 30%, 50%, 45%, (PAC) 10% for all	[191]
PFBA, PFHxA, PFBS	IRA910 (ion-exchange resin)	30 mg/L	0.05	<10%, <10%, 15%	[189]
PFHxA	Different ionic fluorogels with amine	1 µg/L	0.01	20 %–80 %	[215]
PFBA, PFPeA, PFHxA, PFHpA, PFBS	PEI-F-CMC (Poly ethylenimine -functionalized cellulose microcrystals)	1 µg/L	0.025	2%, 2%, 12%, 37%, 5%	[216]
PFBA, PFPeA, PFHxA, PFHpA, PFBS	cationic quaternized nanocellulose	∑11.7 µg/L	0.032	10%, 10%, 20%, 60%, 10%	[217]
PFBA, PFHxA, PFHpA, PFBS	CDP1, CDP2 (cyclodextrin Polymers)	1 µg/L	0.01	40% (5%), 90% (15%), 100% (30%), 95% (20%)	[218]

3.5 Additional insights into PFAS adsorption by ABR

A main disadvantage of ABR against commercially available adsorbents (PAC or GAC) is its relatively low porosity and therefore requires a higher dosage to achieve the same removal. Also, the removal capacity of PFAS by ABR was restricted to synthetic wastewater where PFAS mixture was spiked into an ultrapure or OECD water. Though the result of the isotherm study suggested 10 g/L of ABR is enough to remove most PFAS in a "PFAS-only" system when other organic matter (natural and synthetic ones) and inorganic anions are not present, low dosage of ABR may not be applicable. Also, more stable sorption bonds (i.e., chemisorption) post challenges to the regeneration of the adsorbent, but this is not expected to be a primary drawback of ABR. ABR material is envisioned to be prepared for extraction of magnetite (Fe_2O_3) after wastewater treatment, which can then be further processed for other metal extraction and use as construction material. The use of ABR in large amounts (i.e., high ABR sludge material) therefore benefits the subsequent processes as it can be done in bulk and creates a more efficient recovery of valuable metals/metal oxides in the ABR (i.e., higher input material, higher throughput).

Additionally, when the assessment is moving forward from bench-scale to pilot-scale or full-scale, the large amount of sludge produced needs to be evaluated alongside existing unit processes at the treatment plant facilities. More experiments and analyses are necessary to optimize the sedimentation/settling/separation approach of ABR. Nonetheless, the source material for ABR is found in large amounts (4.6 billion global storage) and can be easily accessed and utilized. The global demand for aluminum will only grow, suggesting that alumina extraction from bauxite deposits will increase the waste associated with this process. As society moves towards more sustainable economic development, considered the potential for using bauxite residue in other applications is promising.

3.6 Toxicity analysis

As a waste by-product, bauxite residue has been noted for its environmental concern due to its high alkalinity and presence of trace metals [136], [137], [138]. Given that ABR is derived from bauxite residue, it is important to assess the toxicity impacts before and after treatment (i.e., whether it releases toxicity). PFAS has also been linked to several environmental and human health effects (see **Section 1**), so it is important to assess the combined toxicities once

mixed with ABR treatment. A prior study has reduced ABR toxicity and leaching of trace metals simply by adjusting pH (pH to ~7) [146]. Following the pH adjustment recommendation, a battery of toxicity assays was completed to assess any residual toxicity derived from ABR exposure and/or complexation with PFAS.

3.6.1 *Daphnia magna* acute toxicity

Acute toxicity was evaluated on *Daphnia magna* and the LC_{50} (50% lethality) for OECD water treated with 50 g/L ABR (n = 3) could not be determined, as all observed mortality rates were below 25%, which is considered background mortality (**Figure B.7.1**). Given that the optimal dosage determined from this study is likely to be below 10 g/L, it is suspected that ABR will not introduce acute toxicity into treated water at practical levels. Notably, some observed immobility in *D. magna* was due to entrapment in residue rather than actual toxicity. When scaling up to pilot- or full-scale applications, the impact of ABR residue on acute toxicity should be thoroughly evaluated to ensure it contributes little to no acute toxicity. To further create more lines of evidence related to ABR environmental safety, additional toxicity analyses were completed via *in-vitro* bioassays as discussed subsequently below.

3.6.2 Cytotoxicity analysis

Cytotoxicity assessment via the *Aliivibrio fisheri* assay shows that toxicity varied under different concentrations and dosages (**Figure 16**). More specifically, cytotoxicity decreased from 0 to 10 g/L ABR, increased at 50 g/L and dropped to background levels at 100 g/L dosage, which is similar to a prior toxicity assessment of ABR [146]. While it was observed here that PFAS removals were improved at higher ABR dosages, the result further suggests that there is a potential for increased toxicity at higher dosages. Nonetheless, the toxicities did not significantly differ (ANOVA, $\alpha = 0.05$, $p = 0.249$) from each other, indicating that the cytotoxicities are similar. Therefore, no substantial cytotoxicity was introduced into the aqueous phase as the dosage increased (100 g/L), supporting the results of *D. magna* acute toxicity testing.

The results further support the use of <10g/L ABR dosage (**Section 3.4**) as both removal efficiency is maximized, and the potential toxicity is minimized. The average $1/IC_{10}$ (1/10% inhibition of *Aliivibrio fisheri* growth) of 50 g/L was approximately two times higher than that of 100 g/L for all the samples. Although it is unclear why this is the case, it was hypothesized

that as the higher dosage of ABR was applied, more hydrochloric acid is needed for post-neutralization which could lead to more metal ions leaching from ABR, contributing to overall cytotoxicity. Moving forward with environmentally realistic samples (e.g., actual wastewater samples containing other organic and inorganic matters), cytotoxicity assessment via *in-vitro* bioassays can be used to continuously monitor cytotoxicity changes before, during, and after ABR treatment.

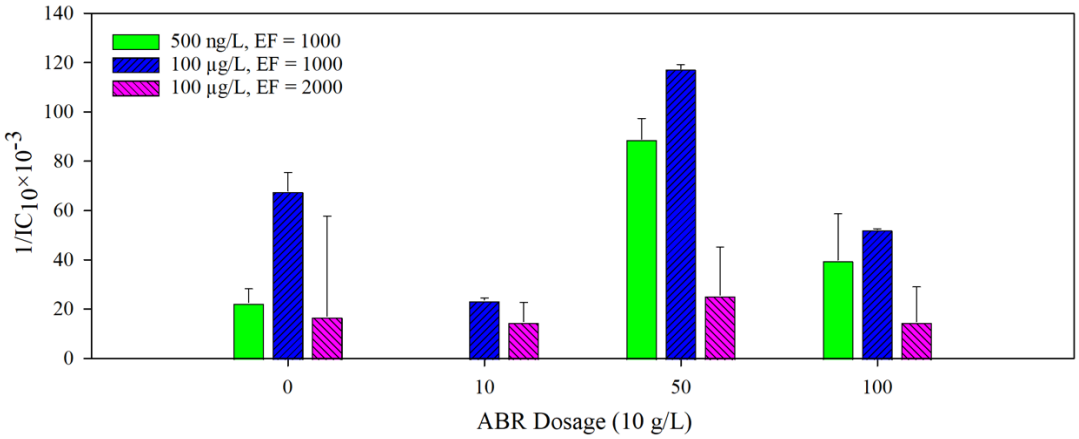

Figure 16. *1/IC_{10} of samples after treatment with different dosages of ABR. EF = extraction factors utilized during sample preparation to assess differences in toxicity results. The 500 ng/L PFAS was not tested for 10 g/L ABR dosage.*

Note that although ABR was observed to have cytotoxicity at high dosages, PFAS has been reported to lack cytotoxic effects via *Aliivibrio fischeri* bacteria [219], [220]. Additionally, Spyrou et al. [220] observed no inhibition of *Aliivibrio fischeri* after exposure to 0.5–200 µg/L PFOA and PFOS. Although these observations are promising, note that PFAS human health impacts lie within the immune and thyroid function, liver disease, lipid and insulin dysregulation, kidney disease, adverse reproductive and developmental outcomes, and cancer [221]. The use of cytotoxicity here was mainly to assess the impacts of dosages and to see if there were any synergistic or additive effects when a toxicant (i.e., PFAS) was added to the ABR mixture simultaneously. *Vibrio fischeri* bioluminescence inhibition assay such as the one completed here is preferred over conventional bioassays due to its reliability, reproducibility and high sensitivity. *A. fischeri* was also reported to be much more sensitive than *Daphnia magna*, especially for wastewater toxicity tests [222].

3.6.3 Estrogenicity analysis

Weilsoe et al. [223] found that PFAS extracted from human placenta homogenates activated estrogen receptors using a mammalian cell-based *in vitro* bioassay (E-SCREEN). Additionally, others have predicted that PFAS (i.e., PFHxS) can potentially dock on estrogen and androgen receptors in fish, potentially disrupting endocrine function. Given that PFAS can concentrate largely in the bile and other tissues, high concentrations of PFAS are required to activate the assays. Hence, 17β-estradiol standard (E2) was added in every extract as a baseline (i.e., after sample preparation) tested for estrogenicity to compare the removal efficacy under varying dosages of ABR (i.e., whether estrogenicity was removed or added after the ABR treatment) (**Figure 17**).

The baseline estrogenicity of the synthetic wastewater sample (i.e., 0 g/L ABR) containing 100 µg/L PFAS+E2 was 0.9±0.2 E2-BEQ. A BEQ<1 means the sample contained estrogenicity higher than what is being imposed by the E2 standard and vice versa. Thus, the response observed in the 0 g/L ABR treatment was expected as the 10% estrogenic activity in the mixture can be attributed to the PFAS mixture (**Figure 17**). After 50 g/L ABR treatment, BEQ was determined to be 1.0±0.4 E2-BEQ suggesting that the treatment brought down the estrogenicity close to the levels that E2 would only be responsible (BEQ~1). Hence, the application of 50 g/L ABR did not only remove PFAS (see **Section 3.2.1**), but also their estrogenic activity. Finally, when the mixture was treated with 100 g/L ABR, the BEQ increased to 1.3, indicating that as the dosage of ABR is higher, the estrogenicity level in the sample is lower. However, when statistical analysis (One-Way ANOVA, $\alpha = 0.05$, $p = 0.226$) showed no significant differences among treatments suggesting that estrogenicity is not impacted by the ABR treatment overall.

In summary, the results suggest that ABR is effective in removing estrogenicity at the PFAS mixture concentrations tested (ΣPFAS = 1 mg/L). Note that the work completed here involved high concentrations of PFAS which may not be environmentally realistic in wastewater/riverine environments but could be in other areas such as industrial sites and landfill leachates that are known to have high PFAS concentrations.

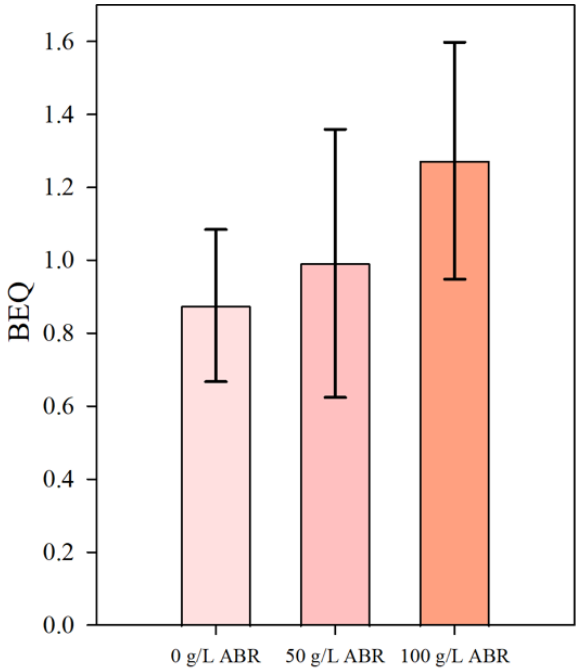

Figure 17. *BEQ of samples after treatment with different dosages of ABR. E2 standard as positive control was added into every exact sample. BEQ = bioanalytical equivalents in terms of 17β-estradiol (i.e., E2 equivalents).*

3.6.4 Mutagenicity analysis

There was no detectable DNA damage via umuC assay suggesting that the PFAS mixture with ABR can cause no mutagenicity via the genotoxicity pathway. This result is supported by the literature where studies reported PFAS having no genotoxic tendencies *in-vivo* and *in-vitro* bioassays. However, most studies focus on the genotoxicity of PFAS only tested PFOA and PFOS [220], [224] with contradicting results. For example, genotoxicity was observed for a mixture of PFOS and PFOA in human lymphocyte cells at a high concentration (1 mg/L) [220], but Crebelli et al. did not find any genotoxicity related to PFAS after injection into mice [225]. Given that genotoxicity via umuC assay has been observed in wastewater influent/effluent, it is still a useful assay that indicates that genotoxicity in these complex mixtures is due to other substances and not PFAS.

4 Conclusions

This study assessed the potential application of ABR to remove PFAS in the aqueous phase through material characterizations and chemical analysis of water samples. Both "virgin" and "spent" ABR (before and after PFAS treatment) are heterogeneous materials with mesopores dominating the porosity of the material. Comparison with other bauxite residues from the literature shows that ABR exhibits superior surface area and pore volume characteristics. This result indicates that the pre-treatment process of ABR can significantly enhance the adsorption capacity for organic pollutants including PFAS.

The target surface scan of ABR through XPS analysis revealed no metal leaching during PFAS exposure, and the presence of metals also appeared to facilitate adsorption. After over-saturation with 100 mg/L PFAS, the relative atom concentration of fluorine on ABR reached 58%, further suggesting surface adsorption of PFAS onto ABR. Both metal-F and C-F bonds were observed from XPS spectra. As the concentration of PFAS increased, C-F bonds became more dominant and visible, indicating that F might be interacting with other metallic elements on the surface. When comparing the element composition obtained from SEM and XPS at different depths, F was present at a higher percentage in XPS results, providing further evidence of adsorption occurring on the surface. Also, F and C were both not homogenously distributed throughout the surface and no clear relationships between them were observed.

Both "virgin" and "spent" ABR were more negatively charged under more alkaline pH conditions. When pH >6, the surface charge of the "spent" ABR was evidently lower than that of the "virgin" one. The most significant difference between pH 6 and 8 was observed, highlighting the importance of neutralizing the ABR solution to enhance removal efficiency. However, discharge guidelines for effluent have a specified pH range. Therefore, the removal efficiency under various pH conditions is expected to be investigated in the future to determine the optimal and most practical pH.

Preliminary results showed that the removal efficiency of ∑PFAS appeared consistent (between 85–90%) across all dosages (from 10 to 100 g/L). Long-chain PAS showed a higher affinity for ABR with ~100% removal, which is similar to other adsorbents from the literature. This behavior is likely due to electrostatic interactions and hydrophobic properties of both ABR and PFAS. For exposure periods of 1 h at a dosage of 50g/L, the removal efficiency of ∑PFAS

can reach at least 80%. This result suggests the potential to reduce the exposure time when applying ABR in wastewater treatment. In comparison with 0.1 g/L of a commercial powdered activated carbon (PAC), the same dosage of ABR was less effective (22.37% and 91.23% for ∑PFAS removal), which was due to the inherent limitation of ABR (fewer micropores than PAC). Hence, the amount of sludge produced from ABR treatment should be considered when scaling up the process. In the next phase, optimizing the settling process could be beneficial.

The adsorption of PFAS by ABR happened rapidly. Five out of ten PFAS were already below detection limits within the first 5 min, the remaining PFAS reached equilibrium between 5 (PFNA, and PFOA) and 60 min (PFPeA, PFHxA, and PFBS). This result demonstrates that short-chain PFAS may require a longer exposure period to achieve better removals. The adsorption of all the PFAS followed both the pseudo-first-order (PFO) and the pseudo-second-order (PSO) kinetic model, with a better fit with the latter (R^2 ranging from 0.995 to 1). Therefore, the interactions may be dominated by chemisorption and the adsorption rate appears to depend on the ABR adsorption capacity. As a next step, a more precise approach needs to be conducted to investigate the adsorption mechanism. Materials synthesis and further enhancement of the ABR material can be considered to increase the available sites but they were not addressed in this thesis.

The adsorption isotherm experiments show that individual PFAS (in the mixture) fits different isotherm models (Langmuir, Freundlich, and Sips model). Three factors may account for these differences: (1) blockage of pores due to the longer-chain PFAS filling; (2) interactions between PFAS molecules; (3) various numbers of adsorption layers. It might be worthwhile to explore the relationships between the fit of different isotherm models and the presence of various PFAS substances.

The maximum adsorption capacity (Q_m) of the material can be determined from the isotherm experiments. A dosage of up to 10 g/L is sufficient to remove most of the substances (∑PFAS removal >80%). This dosage can remove at least 70% short-chain PFAS from the aqueous phase except for PFBA, which is significantly higher than that of other adsorbents (<50%). Due to the complexity of ABR and PFAS adsorption process, it may be beneficial to optimize the dosage of ABR through direct experimentation with actual wastewater, rather than using the predictions from isotherm models.

No acute toxicity was observed in OECD water treated with 50 g/L ABR through 48-h *Daphnia magna* test, supporting the subsequent hypothesis that the optimal dosage of ABR at <10 g/L is unlikely to introduce acute toxicity into the treated water. The potential impact of ABR residue on acute toxicity should be thoroughly evaluated to confirm toxicity issues especially when scaling up to pilot- or full-scale applications. The cytotoxicity assessment via the *Aliivibrio fisheri* assay did not show significant differences (One-Way ANOVA, $\alpha = 0.05$, $p = 0.249$) across different dosages (0, 10, 50, and 100 g/L). Notably, cytotoxicity was the lowest at 10 g/L ABR (IC_{10} of 19.27×10^{-3} compared to 35.93×10^{-3} at 0 g/L, 77.35×10^{-3} at 50 g/L, and 35.69×10^{-3} at 100 g/L). Again, this supports the use of <10 g/L ABR, where the removal efficiency is maximized, and the potential toxicity is minimized. *Aliivibrio fisheri* is more sensitive to wastewater toxicity testing than *Daphnia magna*. Consequently, the absence of toxicity as a result of ABR components leaching during treatment was also confirmed.

The Yeast Estrogenicity Screen (YES) analysis shows that the baseline estrogenicity for 100 µg/L PFAS + 17β-estradiol standard (E2) was 0.9 ± stdev 0.2 E2-BEQ. After 50 and 100 g/L ABR treatment, the BEQ was determined to be 1.0 and 1.3 respectively, indicating that a higher dosage of ABR can lower estrogenicity more effectively. Note that there were no significant differences (One-Way ANOVA, $\alpha = 0.05$, $p = 0.226$) were observed, suggesting that ABR treatment will not impact estrogenicity in general. There was also no detectable DNA damage via umuC assay, suggesting PFAS would not induce mutagenicity. Given that ABR has been assessed to remove mutagenicity caused by complex mixtures including PFAS from wastewater influent/effluent, there is potential for using ABR to reduce overall genotoxicity in wastewater.

Overall, the use of ABR to remove PFAS substances from the water column is a promising solution. It offers sustainable potential, and environmental and economic benefits, as well as provides a practical approach to addressing the emerging PFAS issue. Although there are aspects of ABR treatment that can be optimized (e.g., ABR dosage, exposure period and the removal of short-chain PFAS), this thesis suggests that ABR can be explored at a larger-scale experiment (e.g., pilot-scale) to elucidate addition benefits and improvements for removal and degradation of PFAS.

5 Study Limitations and Recommendations

Although the results from this study suggest that ABR is a potential adsorbent material for removing PFAS from the water column, the findings presented in this thesis have several limitations as detailed below:

(1) Most of the treatment experiments and the chemical analyses of the water samples before and after ABR treatment were conducted only once due to limited sample volume. Although positive control and blank samples were included for validation, the repeatability of the variations caused by the overall experimental design and background was not assessed.

(2) Due to the limited ABR sludge sample mass, only 2 PFAS substances were used to saturate ABR in the BET analysis. For future studies, it is recommended to characterize the surface area and porosity of ABR saturated with a wider range of PFAS and other organic compounds to better understand the surface interactions.

(3) All the experiments were performed with synthetic PFAS wastewater by spiking PFAS stock into ultrapure water. Organic matter (OM) and natural organic matter (NOM) present in actual wastewater would likely influence the removal efficacy of ABR, either positively or negatively, depending on the concentration and water matrix. The performance of ABR treatment needs to be assessed before it can be applied to any real-life wastewater scenarios.

(4) The concentrations of PFAS (∑PFAS ranging from 500 ng/L to 100 mg/L) used in this thesis were much higher than typical levels in actual wastewater, although might be representative of sites with high PFAS contamination (e.g., US industrial sites). Note that ∑PFAS 500 ng/L was considered environmentally relevant, but this working concentration is low to effectively assess adsorption mechanisms. The performance of ABR under lower concentration conditions and in the presence of other soluble pollutants may also vary. To better assess the practical potential of ABR, it would be beneficial to introduce additional organic substances (e.g., pharmaceuticals, personal care products, pesticides) for evaluation.

(5) Although the short exposure periods and kinetic experiments were carried out, most of the removal experiments were completed within a contact time of 24 h to achieve

maximum adsorption. The removal efficacy, especially for short-chain PFAS, and the associated toxicities (maybe introduced by PFAS or ABR) would likely change depending on different treatment conditions.

(6) After PFAS were removed efficiently from the aqueous phase via adsorption by ABR, fluorine still attaches to the surface of ABR as indicated in the material characterization. Due to the strong stability of fluorine-carbon bonds, more advanced oxidative methods or catalytic degradation are required to remove or decompose PFAS in the environment. Subsequently, ABR can be further regenerated, and this aspect was not considered in this thesis.

(7) Only *in-vitro* bioassays were employed to assess the toxicity of PFAS. According to reported studies, PFAS can affect humans and animals through multiple pathways. Although the bacteria and cell lines employed in this study are effective at the screening stage, this study requires additional follow-up to prove toxicity is not an issue for future ABR applications.

References

[1] R. E. Banks, B. E. Smart, and J. C. Tatlow, *Organofluorine Chemistry: Principles and Commercial Applications*. Springer Science & Business Media, 2013.

[2] R. C. Buck *et al.*, "Perfluoroalkyl and polyfluoroalkyl substances in the environment: Terminology, classification, and origins," *Integr. Environ. Assess. Manag.*, vol. 7, no. 4, pp. 513–541, 2011, doi: 10.1002/ieam.258.

[3] OECD, *Reconciling Terminology of the Universe of Per- and Polyfluoroalkyl Substances: Recommendations and Practical Guidance*. Paris: Organisation for Economic Co-operation and Development, 2021. Accessed: Aug. 15, 2024. [Online]. Available: https://www.oecd-ilibrary.org/environment/reconciling-terminology-of-the-universe-of-per-and-polyfluoroalkyl-substances_e458e796-en

[4] J. Zhang, H. Pang, S. Gray, S. Ma, Z. Xie, and L. Gao, "PFAS removal from wastewater by in-situ formed ferric nanoparticles: Solid phase loading and removal efficiency," *J. Environ. Chem. Eng.*, vol. 9, no. 4, p. 105452, Aug. 2021, doi: 10.1016/j.jece.2021.105452.

[5] Z. Du *et al.*, "Adsorption behavior and mechanism of perfluorinated compounds on various adsorbents—A review," *J. Hazard. Mater.*, vol. 274, pp. 443–454, Jun. 2014, doi: 10.1016/j.jhazmat.2014.04.038.

[6] C. Gallen, G. Eaglesham, D. Drage, T. H. Nguyen, and J. F. Mueller, "A mass estimate of perfluoroalkyl substance (PFAS) release from Australian wastewater treatment plants," *Chemosphere*, vol. 208, pp. 975–983, Oct. 2018, doi: 10.1016/j.chemosphere.2018.06.024.

[7] S. P. Lenka, M. Kah, and L. P. Padhye, "A review of the occurrence, transformation, and removal of poly- and perfluoroalkyl substances (PFAS) in wastewater treatment plants," *Water Res.*, vol. 199, p. 117187, Jul. 2021, doi: 10.1016/j.watres.2021.117187.

[8] D. M. Wanninayake, "Comparison of currently available PFAS remediation technologies in water: A review," *J. Environ. Manage.*, vol. 283, p. 111977, Apr. 2021, doi: 10.1016/j.jenvman.2021.111977.

[9] P. Ssebugere *et al.*, "Environmental levels and human body burdens of per- and polyfluoroalkyl substances in Africa: A critical review," *Sci. Total Environ.*, vol. 739, p. 139913, Oct. 2020, doi: 10.1016/j.scitotenv.2020.139913.

[10] I. Ross *et al.*, "A review of emerging technologies for remediation of PFASs," *Remediat. J.*, vol. 28, no. 2, pp. 101–126, 2018, doi: 10.1002/rem.21553.

[11] Z. Abunada, M. Y. D. Alazaiza, and M. J. K. Bashir, "An Overview of Per- and Polyfluoroalkyl Substances (PFAS) in the Environment: Source, Fate, Risk and Regulations," *Water*, vol. 12, no. 12, Art. no. 12, Dec. 2020, doi: 10.3390/w12123590.

[12] H. Brunn, G. Arnold, W. Körner, G. Rippen, K. G. Steinhäuser, and I. Valentin, "PFAS: forever chemicals—persistent, bioaccumulative and mobile. Reviewing the status and the need for their phase out and remediation of contaminated sites," *Environ. Sci. Eur.*, vol. 35, no. 1, p. 20, Mar. 2023, doi: 10.1186/s12302-023-00721-8.

[13] S. Verma, R. S. Varma, and M. N. Nadagouda, "Remediation and mineralization processes for *per*- and polyfluoroalkyl substances (PFAS) in water: A review," *Sci. Total Environ.*, vol. 794, p. 148987, Nov. 2021, doi: 10.1016/j.scitotenv.2021.148987.

[14] O. S. Arvaniti, Y. Hwang, H. R. Andersen, A. S. Stasinakis, N. S. Thomaidis, and M. Aloupi, "Reductive degradation of perfluorinated compounds in water using Mg-aminoclay coated nanoscale zero valent iron," *Chem. Eng. J.*, vol. 262, pp. 133–139, Feb. 2015, doi:

10.1016/j.cej.2014.09.079.
[15] D. Cui, X. Li, and N. Quinete, “Occurrence, fate, sources and toxicity of PFAS: What we know so far in Florida and major gaps,” *TrAC Trends Anal. Chem.*, vol. 130, p. 115976, Sep. 2020, doi: 10.1016/j.trac.2020.115976.
[16] D. Szabo, T. L. Coggan, T. C. Robson, M. Currell, and B. O. Clarke, “Investigating recycled water use as a diffuse source of per- and polyfluoroalkyl substances (PFASs) to groundwater in Melbourne, Australia,” *Sci. Total Environ.*, vol. 644, pp. 1409–1417, Dec. 2018, doi: 10.1016/j.scitotenv.2018.07.048.
[17] S. P. Lenka, M. Kah, and L. P. Padhye, “A review of the occurrence, transformation, and removal of poly- and perfluoroalkyl substances (PFAS) in wastewater treatment plants,” *Water Res.*, vol. 199, p. 117187, Jul. 2021, doi: 10.1016/j.watres.2021.117187.
[18] Y. Yu, C. Zhao, L. Yu, P. Li, T. Wang, and Y. Xu, “Removal of perfluorooctane sulfonates from water by a hybrid coagulation–nanofiltration process,” *Chem. Eng. J.*, vol. 289, pp. 7–16, Apr. 2016, doi: 10.1016/j.cej.2015.12.048.
[19] D. Zhou *et al.*, “Simulating PFAS adsorption kinetics, adsorption isotherms, and nonideal transport in saturated soil with tempered one-sided stable density (TOSD) based models,” *J. Hazard. Mater.*, vol. 411, p. 125169, Jun. 2021, doi: 10.1016/j.jhazmat.2021.125169.
[20] J. Glüge *et al.*, “An overview of the uses of per- and polyfluoroalkyl substances (PFAS),” *Environ. Sci. Process. Impacts*, vol. 22, no. 12, pp. 2345–2373, 2020, doi: 10.1039/D0EM00291G.
[21] R. Lohmann *et al.*, “Are Fluoropolymers Really of Low Concern for Human and Environmental Health and Separate from Other PFAS?,” *Environ. Sci. Technol.*, vol. 54, no. 20, pp. 12820–12828, Oct. 2020, doi: 10.1021/acs.est.0c03244.
[22] Y. Wang *et al.*, “A review of sources, multimedia distribution and health risks of novel fluorinated alternatives,” *Ecotoxicol. Environ. Saf.*, vol. 182, p. 109402, Oct. 2019, doi: 10.1016/j.ecoenv.2019.109402.
[23] H. Son and B. An, “Investigation of Adsorption Kinetics for Per- and Poly-fluoroalkyl substances (PFAS) Adsorption onto Powder Activated Carbon (PAC) in the Competing Systems,” *Water. Air. Soil Pollut.*, vol. 233, no. 4, p. 129, Apr. 2022, doi: 10.1007/s11270-022-05599-5.
[24] C. Zhao, Y. Xu, F. Xiao, J. Ma, Y. Zou, and W. Tang, “Perfluorooctane sulfonate removal by metal-organic frameworks (MOFs): Insights into the effect and mechanism of metal nodes and organic ligands,” *Chem. Eng. J.*, vol. 406, p. 126852, Feb. 2021, doi: 10.1016/j.cej.2020.126852.
[25] N. H. Lam, C.-R. Cho, K. Kannan, and H.-S. Cho, “A nationwide survey of perfluorinated alkyl substances in waters, sediment and biota collected from aquatic environment in Vietnam: Distributions and bioconcentration profiles,” *J. Hazard. Mater.*, vol. 323, pp. 116–127, Feb. 2017, doi: 10.1016/j.jhazmat.2016.04.010.
[26] K. Y. Kwok *et al.*, “Transport of Perfluoroalkyl substances (PFAS) from an arctic glacier to downstream locations: Implications for sources,” *Sci. Total Environ.*, vol. 447, pp. 46–55, Mar. 2013, doi: 10.1016/j.scitotenv.2012.10.091.
[27] F. Orata, N. Quinete, F. Werres, and R.-D. Wilken, “Determination of Perfluorooctanoic Acid and Perfluorooctane Sulfonate in Lake Victoria Gulf Water,” *Bull. Environ. Contam.*

Toxicol., vol. 82, no. 2, pp. 218–222, Feb. 2009, doi: 10.1007/s00128-008-9543-1.
[28] Y. Zhou *et al.*, "Ecological effect and risk towards aquatic plants induced by perfluoroalkyl substances: Bridging natural to culturing flora," *Chemosphere*, vol. 167, pp. 98–106, Jan. 2017, doi: 10.1016/j.chemosphere.2016.09.146.
[29] S. Chen *et al.*, "Perfluorinated compounds in soil, surface water, and groundwater from rural areas in eastern China," *Environ. Pollut.*, vol. 211, pp. 124–131, Apr. 2016, doi: 10.1016/j.envpol.2015.12.024.
[30] K. Y. Kwok *et al.*, "Occurrence and distribution of conventional and new classes of per- and polyfluoroalkyl substances (PFASs) in the South China Sea," *J. Hazard. Mater.*, vol. 285, pp. 389–397, Mar. 2015, doi: 10.1016/j.jhazmat.2014.10.065.
[31] M. Brumovský, P. Karásková, M. Borghini, and L. Nizzetto, "Per- and polyfluoroalkyl substances in the Western Mediterranean Sea waters," *Chemosphere*, vol. 159, pp. 308–316, Sep. 2016, doi: 10.1016/j.chemosphere.2016.06.015.
[32] G. Codling, H. Yuan, P. D. Jones, J. P. Giesy, and M. Hecker, "Metals and PFAS in stormwater and surface runoff in a semi-arid Canadian city subject to large variations in temperature among seasons," *Environ. Sci. Pollut. Res.*, vol. 27, no. 15, pp. 18232–18241, May 2020, doi: 10.1007/s11356-020-08070-2.
[33] S. Kleywegt, M. Raby, S. McGill, and P. Helm, "The impact of risk management measures on the concentrations of per- and polyfluoroalkyl substances in source and treated drinking waters in Ontario, Canada," *Sci. Total Environ.*, vol. 748, p. 141195, Dec. 2020, doi: 10.1016/j.scitotenv.2020.141195.
[34] B. Lalonde and C. Garron, "Perfluoroalkyl Substances (PFASs) in the Canadian Freshwater Environment," *Arch. Environ. Contam. Toxicol.*, vol. 82, no. 4, pp. 581–591, May 2022, doi: 10.1007/s00244-022-00922-x.
[35] S. L. Domazet, T. K. Jensen, N. Wedderkopp, F. Nielsen, L. B. Andersen, and A. Grøntved, "Exposure to perfluoroalkylated substances (PFAS) in relation to fitness, physical activity, and adipokine levels in childhood: The european youth heart study," *Environ. Res.*, vol. 191, p. 110110, Dec. 2020, doi: 10.1016/j.envres.2020.110110.
[36] S. Poothong, E. Papadopoulou, J. A. Padilla-Sánchez, C. Thomsen, and L. S. Haug, "Multiple pathways of human exposure to poly- and perfluoroalkyl substances (PFASs): From external exposure to human blood," *Environ. Int.*, vol. 134, p. 105244, Jan. 2020, doi: 10.1016/j.envint.2019.105244.
[37] G. Munoz, L. Mercier, S. V. Duy, J. Liu, S. Sauvé, and M. Houde, "Bioaccumulation and trophic magnification of emerging and legacy per- and polyfluoroalkyl substances (PFAS) in a St. Lawrence River food web," *Environ. Pollut.*, vol. 309, p. 119739, Sep. 2022, doi: 10.1016/j.envpol.2022.119739.
[38] E. Panieri, K. Baralic, D. Djukic-Cosic, A. Buha Djordjevic, and L. Saso, "PFAS Molecules: A Major Concern for the Human Health and the Environment," *Toxics*, vol. 10, no. 2, Art. no. 2, Feb. 2022, doi: 10.3390/toxics10020044.
[39] C. Liu, V. W. C. Chang, K. Y. H. Gin, and V. T. Nguyen, "Genotoxicity of perfluorinated chemicals (PFCs) to the green mussel (*Perna viridis*)," *Sci. Total Environ.*, vol. 487, pp. 117–122, Jul. 2014, doi: 10.1016/j.scitotenv.2014.04.017.
[40] L. Mhadhbi, D. Rial, S. Pérez, and R. Beiras, "Ecological risk assessment of perfluorooctanoic acid (PFOA) and perfluorooctanesulfonic acid (PFOS) in marine

environment using Isochrysis galbana, Paracentrotus lividus, Siriella armata and Psetta maxima," *J. Environ. Monit.*, vol. 14, no. 5, pp. 1375–1382, May 2012, doi: 10.1039/C2EM30037K.
[41] Y. Yang, Z. Zheng, W. Ji, J. Xu, and X. Zhang, "Insights to perfluorooctanoic acid adsorption micro-mechanism over Fe-based metal organic frameworks: Combining computational calculation with response surface methodology," *J. Hazard. Mater.*, vol. 395, p. 122686, Aug. 2020, doi: 10.1016/j.jhazmat.2020.122686.
[42] M. Mastrantonio, E. Bai, R. Uccelli, V. Cordiano, A. Screpanti, and P. Crosignani, "Drinking water contamination from perfluoroalkyl substances (PFAS): an ecological mortality study in the Veneto Region, Italy," *Eur. J. Public Health*, vol. 28, no. 1, pp. 180–185, Feb. 2018, doi: 10.1093/eurpub/ckx066.
[43] I. T. Cousins *et al.*, "The concept of essential use for determining when uses of PFASs can be phased out," *Environ. Sci. Process. Impacts*, vol. 21, no. 11, pp. 1803–1815, 2019, doi: 10.1039/C9EM00163H.
[44] A. Cordner, V. Y. De La Rosa, L. A. Schaider, R. A. Rudel, L. Richter, and P. Brown, "Guideline levels for PFOA and PFOS in drinking water: the role of scientific uncertainty, risk assessment decisions, and social factors," *J. Expo. Sci. Environ. Epidemiol.*, vol. 29, no. 2, pp. 157–171, Mar. 2019, doi: 10.1038/s41370-018-0099-9.
[45] M. Wilhelm, S. Bergmann, and H. H. Dieter, "Occurrence of perfluorinated compounds (PFCs) in drinking water of North Rhine-Westphalia, Germany and new approach to assess drinking water contamination by shorter-chained C4–C7 PFCs," *Int. J. Hyg. Environ. Health*, vol. 213, no. 3, pp. 224–232, Jun. 2010, doi: 10.1016/j.ijheh.2010.05.004.
[46] C. Gallen, G. Eaglesham, D. Drage, T. H. Nguyen, and J. F. Mueller, "A mass estimate of perfluoroalkyl substance (PFAS) release from Australian wastewater treatment plants," *Chemosphere*, vol. 208, pp. 975–983, Oct. 2018, doi: 10.1016/j.chemosphere.2018.06.024.
[47] Z. Abunada, M. Y. D. Alazaiza, and M. J. K. Bashir, "An Overview of Per- and Polyfluoroalkyl Substances (PFAS) in the Environment: Source, Fate, Risk and Regulations," *Water*, vol. 12, no. 12, Art. no. 12, Dec. 2020, doi: 10.3390/w12123590.
[48] State Water Resources Control Board Division of Water Quality GAMA Program, "GROUNDWATER INFORMATION SHEET Perfluorooctanoic Acid (PFOA) & Perfluorooctanesulfonic Acid (PFOS)," 2019.
[49] J. Martin, "Environmental Health Program," Jun. 2019.
[50] A. Zaggia, L. Conte, L. Falletti, M. Fant, and A. Chiorboli, "Use of strong anion exchange resins for the removal of perfluoroalkylated substances from contaminated drinking water in batch and continuous pilot plants," *Water Res.*, vol. 91, pp. 137–146, Mar. 2016, doi: 10.1016/j.watres.2015.12.039.
[51] M. Clara, O. Gans, S. Weiss, D. Sanz-Escribano, S. Scharf, and C. Scheffknecht, "Perfluorinated alkylated substances in the aquatic environment: An Austrian case study," *Water Res.*, vol. 43, no. 18, pp. 4760–4768, Oct. 2009, doi: 10.1016/j.watres.2009.08.004.
[52] Z. Wang, I. T. Cousins, M. Scheringer, and K. Hungerbuehler, "Hazard assessment of fluorinated alternatives to long-chain perfluoroalkyl acids (PFAAs) and their precursors: Status quo, ongoing challenges and possible solutions," *Environ. Int.*, vol. 75, pp. 172–179, Feb. 2015, doi: 10.1016/j.envint.2014.11.013.
[53] F. Li *et al.*, "Short-chain per- and polyfluoroalkyl substances in aquatic systems:

Occurrence, impacts and treatment," *Chem. Eng. J.*, vol. 380, p. 122506, Jan. 2020, doi: 10.1016/j.cej.2019.122506.
[54] J. Zhou, Z. Li, X. Guo, Y. Li, Z. Wu, and L. Zhu, "Evidences for replacing legacy per- and polyfluoroalkyl substances with emerging ones in Fen and Wei River basins in central and western China," *J. Hazard. Mater.*, vol. 377, pp. 78–87, Sep. 2019, doi: 10.1016/j.jhazmat.2019.05.050.
[55] S. Brendel, É. Fetter, C. Staude, L. Vierke, and A. Biegel-Engler, "Short-chain perfluoroalkyl acids: environmental concerns and a regulatory strategy under REACH," *Environ. Sci. Eur.*, vol. 30, no. 1, p. 9, Feb. 2018, doi: 10.1186/s12302-018-0134-4.
[56] S. B. Gewurtz, A. S. Auyeung, A. O. De Silva, S. Teslic, and S. A. Smyth, "Per- and polyfluoroalkyl substances (PFAS) in Canadian municipal wastewater and biosolids: Recent patterns and time trends 2009 to 2021," *Sci. Total Environ.*, vol. 912, p. 168638, Feb. 2024, doi: 10.1016/j.scitotenv.2023.168638.
[57] J. Li, J. He, Z. Niu, and Y. Zhang, "Legacy per- and polyfluoroalkyl substances (PFASs) and alternatives (short-chain analogues, F-53B, GenX and FC-98) in residential soils of China: Present implications of replacing legacy PFASs," *Environ. Int.*, vol. 135, p. 105419, Feb. 2020, doi: 10.1016/j.envint.2019.105419.
[58] K. Dasu, X. Xia, D. Siriwardena, T. P. Klupinski, and B. Seay, "Concentration profiles of per- and polyfluoroalkyl substances in major sources to the environment," *J. Environ. Manage.*, vol. 301, p. 113879, Jan. 2022, doi: 10.1016/j.jenvman.2021.113879.
[59] M. M. Schultz, D. F. Barofsky, and J. A. Field, "Quantitative Determination of Fluorotelomer Sulfonates in Groundwater by LC MS/MS," *Environ. Sci. Technol.*, vol. 38, no. 6, pp. 1828–1835, Mar. 2004, doi: 10.1021/es035031j.
[60] E. F. Houtz, C. P. Higgins, J. A. Field, and D. L. Sedlak, "Persistence of Perfluoroalkyl Acid Precursors in AFFF-Impacted Groundwater and Soil," *Environ. Sci. Technol.*, vol. 47, no. 15, pp. 8187–8195, Aug. 2013, doi: 10.1021/es4018877.
[61] X. C. Hu *et al.*, "Detection of Poly- and Perfluoroalkyl Substances (PFASs) in U.S. Drinking Water Linked to Industrial Sites, Military Fire Training Areas, and Wastewater Treatment Plants," *Environ. Sci. Technol. Lett.*, vol. 3, no. 10, pp. 344–350, Oct. 2016, doi: 10.1021/acs.estlett.6b00260.
[62] J. R. Lang, B. M. Allred, J. A. Field, J. W. Levis, and M. A. Barlaz, "National Estimate of Per- and Polyfluoroalkyl Substance (PFAS) Release to U.S. Municipal Landfill Leachate," *Environ. Sci. Technol.*, vol. 51, no. 4, pp. 2197–2205, Feb. 2017, doi: 10.1021/acs.est.6b05005.
[63] H. Hamid, L. Y. Li, and J. R. Grace, "Review of the fate and transformation of per- and polyfluoroalkyl substances (PFASs) in landfills," *Environ. Pollut.*, vol. 235, pp. 74–84, Apr. 2018, doi: 10.1016/j.envpol.2017.12.030.
[64] S. L. Capozzi, A. L. Leang, L. A. Rodenburg, B. Chandramouli, D. A. Delistraty, and C. H. Carter, "PFAS in municipal landfill leachate: Occurrence, transformation, and sources," *Chemosphere*, vol. 334, p. 138924, Sep. 2023, doi: 10.1016/j.chemosphere.2023.138924.
[65] J. Busch, L. Ahrens, R. Sturm, and R. Ebinghaus, "Polyfluoroalkyl compounds in landfill leachates," *Environ. Pollut.*, vol. 158, no. 5, pp. 1467–1471, May 2010, doi: 10.1016/j.envpol.2009.12.031.
[66] H. Yan, I. T. Cousins, C. Zhang, and Q. Zhou, "Perfluoroalkyl acids in municipal landfill leachates from China: Occurrence, fate during leachate treatment and potential impact

on groundwater," *Sci. Total Environ.*, vol. 524–525, pp. 23–31, Aug. 2015, doi: 10.1016/j.scitotenv.2015.03.111.
[67] H. Hamid and L. Li, "Role of wastewater treatment plant in environmental cycling of poly- and perfluoroalkyl substances," *Ecocycles*, vol. 2, no. 2, Art. no. 2, Nov. 2016, doi: 10.19040/ecocycles.v2i2.62.
[68] C. V. Furl, C. A. Meredith, M. J. Strynar, and S. F. Nakayama, "Relative importance of wastewater treatment plants and non-point sources of perfluorinated compounds to Washington State rivers," *Sci. Total Environ.*, vol. 409, no. 15, pp. 2902–2907, Jul. 2011, doi: 10.1016/j.scitotenv.2011.04.035.
[69] J. Elmoznino, P. Vlahos, and M. Whitney, "Occurrence and partitioning behavior of perfluoroalkyl acids in wastewater effluent discharging into the Long Island Sound," *Environ. Pollut.*, vol. 243, pp. 453–461, Dec. 2018, doi: 10.1016/j.envpol.2018.07.076.
[70] K. M. Stroski, K. H. Luong, J. K. Challis, L. G. Chaves-Barquero, M. L. Hanson, and C. S. Wong, "Wastewater sources of per- and polyfluorinated alkyl substances (PFAS) and pharmaceuticals in four Canadian Arctic communities," *Sci. Total Environ.*, vol. 708, p. 134494, Mar. 2020, doi: 10.1016/j.scitotenv.2019.134494.
[71] B. Lebeau and P. Eng, "23-013 — Sewage Biosolids – Managing Urban Nutrients Responsibly for Crop Production." Jan. 2023.
[72] Canadian Council of Ministers of the Environment, "Canada-wide Approach for the Management of Wastewater Biosolids." Oct. 11, 2012.
[73] M. Lewis, M.-H. Kim, N. Wang, and K.-H. Chu, "Engineering artificial communities for enhanced FTOH degradation," *Sci. Total Environ.*, vol. 572, pp. 935–942, Dec. 2016, doi: 10.1016/j.scitotenv.2016.07.223.
[74] Y. Shi *et al.*, "Characterizing direct emissions of perfluoroalkyl substances from ongoing fluoropolymer production sources: A spatial trend study of Xiaoqing River, China," *Environ. Pollut.*, vol. 206, pp. 104–112, Nov. 2015, doi: 10.1016/j.envpol.2015.06.035.
[75] X. Liu, Z. Guo, E. E. Folk, and N. F. Roache, "Determination of fluorotelomer alcohols in selected consumer products and preliminary investigation of their fate in the indoor environment," *Chemosphere*, vol. 129, pp. 81–86, Jun. 2015, doi: 10.1016/j.chemosphere.2014.06.012.
[76] S. B. Gewurtz, A. S. Auyeung, A. O. De Silva, S. Teslic, and S. A. Smyth, "Per- and polyfluoroalkyl substances (PFAS) in Canadian municipal wastewater and biosolids: Recent patterns and time trends 2009 to 2021," *Sci. Total Environ.*, p. 168638, Nov. 2023, doi: 10.1016/j.scitotenv.2023.168638.
[77] O. S. Arvaniti and A. S. Stasinakis, "Review on the occurrence, fate and removal of perfluorinated compounds during wastewater treatment," *Sci. Total Environ.*, vol. 524–525, pp. 81–92, Aug. 2015, doi: 10.1016/j.scitotenv.2015.04.023.
[78] M. M. Schultz, D. F. Barofsky, and J. A. Field, "Quantitative Determination of Fluorinated Alkyl Substances by Large-Volume-Injection Liquid Chromatography Tandem Mass SpectrometryCharacterization of Municipal Wastewaters," *Environ. Sci. Technol.*, vol. 40, no. 1, pp. 289–295, Jan. 2006, doi: 10.1021/es051381p.
[79] R. Guo, W.-J. Sim, E.-S. Lee, J.-H. Lee, and J.-E. Oh, "Evaluation of the fate of perfluoroalkyl compounds in wastewater treatment plants," *Water Res.*, vol. 44, no. 11, pp. 3476–3486, Jun. 2010, doi: 10.1016/j.watres.2010.03.028.

[80] O. S. Arvaniti, E. I. Ventouri, A. S. Stasinakis, and N. S. Thomaidis, "Occurrence of different classes of perfluorinated compounds in Greek wastewater treatment plants and determination of their solid–water distribution coefficients," *J. Hazard. Mater.*, vol. 239–240, pp. 24–31, Nov. 2012, doi: 10.1016/j.jhazmat.2012.02.015.
[81] E. Houtz, M. Wang, and J.-S. Park, "Identification and Fate of Aqueous Film Forming Foam Derived Per- and Polyfluoroalkyl Substances in a Wastewater Treatment Plant," *Environ. Sci. Technol.*, vol. 52, no. 22, pp. 13212–13221, Nov. 2018, doi: 10.1021/acs.est.8b04028.
[82] X. Dauchy *et al.*, "Mass flows and fate of per- and polyfluoroalkyl substances (PFASs) in the wastewater treatment plant of a fluorochemical manufacturing facility," *Sci. Total Environ.*, vol. 576, pp. 549–558, Jan. 2017, doi: 10.1016/j.scitotenv.2016.10.130.
[83] J. Yu, J. Hu, S. Tanaka, and S. Fujii, "Perfluorooctane sulfonate (PFOS) and perfluorooctanoic acid (PFOA) in sewage treatment plants," *Water Res.*, vol. 43, no. 9, pp. 2399–2408, May 2009, doi: 10.1016/j.watres.2009.03.009.
[84] H. Chen, H. Peng, M. Yang, J. Hu, and Y. Zhang, "Detection, Occurrence, and Fate of Fluorotelomer Alcohols in Municipal Wastewater Treatment Plants," *Environ. Sci. Technol.*, vol. 51, no. 16, pp. 8953–8961, Aug. 2017, doi: 10.1021/acs.est.7b00315.
[85] A. S. Stasinakis *et al.*, "Contribution of primary and secondary treatment on the removal of benzothiazoles, benzotriazoles, endocrine disruptors, pharmaceuticals and perfluorinated compounds in a sewage treatment plant," *Sci. Total Environ.*, vol. 463–464, pp. 1067–1075, Oct. 2013, doi: 10.1016/j.scitotenv.2013.06.087.
[86] B. G. Loganathan, K. S. Sajwan, E. Sinclair, K. Senthil Kumar, and K. Kannan, "Perfluoroalkyl sulfonates and perfluorocarboxylates in two wastewater treatment facilities in Kentucky and Georgia," *Water Res.*, vol. 41, no. 20, pp. 4611–4620, Dec. 2007, doi: 10.1016/j.watres.2007.06.045.
[87] E. Tavasoli, J. L. Luek, J. P. Malley, and P. J. Mouser, "Distribution and fate of per- and polyfluoroalkyl substances (PFAS) in wastewater treatment facilities," *Environ. Sci. Process. Impacts*, vol. 23, no. 6, pp. 903–913, 2021, doi: 10.1039/D1EM00032B.
[88] C. Kunacheva *et al.*, "Mass flows of perfluorinated compounds (PFCs) in central wastewater treatment plants of industrial zones in Thailand," *Chemosphere*, vol. 83, no. 6, pp. 737–744, Apr. 2011, doi: 10.1016/j.chemosphere.2011.02.059.
[89] U. Eriksson, P. Haglund, and A. Kärrman, "Contribution of precursor compounds to the release of per- and polyfluoroalkyl substances (PFASs) from waste water treatment plants (WWTPs)," *J. Environ. Sci.*, vol. 61, pp. 80–90, Nov. 2017, doi: 10.1016/j.jes.2017.05.004.
[90] P. Guerra, M. Kim, L. Kinsman, T. Ng, M. Alaee, and S. A. Smyth, "Parameters affecting the formation of perfluoroalkyl acids during wastewater treatment," *J. Hazard. Mater.*, vol. 272, pp. 148–154, May 2014, doi: 10.1016/j.jhazmat.2014.03.016.
[91] C. Gallen, G. Eaglesham, D. Drage, T. H. Nguyen, and J. F. Mueller, "A mass estimate of perfluoroalkyl substance (PFAS) release from Australian wastewater treatment plants," *Chemosphere*, vol. 208, pp. 975–983, Oct. 2018, doi: 10.1016/j.chemosphere.2018.06.024.
[92] M. Filipovic and U. Berger, "Are perfluoroalkyl acids in waste water treatment plant effluents the result of primary emissions from the technosphere or of environmental recirculation?," *Chemosphere*, vol. 129, pp. 74–80, Jun. 2015, doi: 10.1016/j.chemosphere.2014.07.082.
[93] W. Zhang *et al.*, "Distribution and fate of perfluoroalkyl substances in municipal

wastewater treatment plants in economically developed areas of China," *Environ. Pollut.*, vol. 176, pp. 10–17, May 2013, doi: 10.1016/j.envpol.2012.12.019.
[94] E. Houtz, M. Wang, and J.-S. Park, "Identification and Fate of Aqueous Film Forming Foam Derived Per- and Polyfluoroalkyl Substances in a Wastewater Treatment Plant," *Environ. Sci. Technol.*, vol. 52, no. 22, pp. 13212–13221, Nov. 2018, doi: 10.1021/acs.est.8b04028.
[95] M. Shigei, L. Ahrens, A. Hazaymeh, and S. S. Dalahmeh, "Per- and polyfluoroalkyl substances in water and soil in wastewater-irrigated farmland in Jordan," *Sci. Total Environ.*, vol. 716, p. 137057, May 2020, doi: 10.1016/j.scitotenv.2020.137057.
[96] M. Lorenzo, J. Campo, M. Morales Suárez-Varela, and Y. Picó, "Occurrence, distribution and behavior of emerging persistent organic pollutants (POPs) in a Mediterranean wetland protected area," *Sci. Total Environ.*, vol. 646, pp. 1009–1020, Jan. 2019, doi: 10.1016/j.scitotenv.2018.07.304.
[97] O. S. Arvaniti, E. I. Ventouri, A. S. Stasinakis, and N. S. Thomaidis, "Occurrence of different classes of perfluorinated compounds in Greek wastewater treatment plants and determination of their solid–water distribution coefficients," *J. Hazard. Mater.*, vol. 239–240, pp. 24–31, Nov. 2012, doi: 10.1016/j.jhazmat.2012.02.015.
[98] S. De Gisi, G. Lofrano, M. Grassi, and M. Notarnicola, "Characteristics and adsorption capacities of low-cost sorbents for wastewater treatment: A review," *Sustain. Mater. Technol.*, vol. 9, pp. 10–40, Sep. 2016, doi: 10.1016/j.susmat.2016.06.002.
[99] S. Yin and D. Villagrán, "Design of nanomaterials for the removal of per- and poly-fluoroalkyl substances (PFAS) in water: Strategies, mechanisms, challenges, and opportunities," *Sci. Total Environ.*, vol. 831, p. 154939, Jul. 2022, doi: 10.1016/j.scitotenv.2022.154939.
[100] N. B. Singh, G. Nagpal, S. Agrawal, and Rachna, "Water purification by using Adsorbents: A Review," *Environ. Technol. Innov.*, vol. 11, pp. 187–240, Aug. 2018, doi: 10.1016/j.eti.2018.05.006.
[101] H. Hori *et al.*, "Efficient Decomposition of Environmentally Persistent Perfluorocarboxylic Acids by Use of Persulfate as a Photochemical Oxidant," *Environ. Sci. Technol.*, vol. 39, no. 7, pp. 2383–2388, Apr. 2005, doi: 10.1021/es0484754.
[102] X. Hang, X. Chen, J. Luo, W. Cao, and Y. Wan, "Removal and recovery of perfluorooctanoate from wastewater by nanofiltration," *Sep. Purif. Technol.*, vol. 145, pp. 120–129, May 2015, doi: 10.1016/j.seppur.2015.03.013.
[103] S. Deng, Q. Zhou, G. Yu, J. Huang, and Q. Fan, "Removal of perfluorooctanoate from surface water by polyaluminium chloride coagulation," *Water Res.*, vol. 45, no. 4, pp. 1774–1780, Feb. 2011, doi: 10.1016/j.watres.2010.11.029.
[104] Y.-T. Tsai, A. Yu-Chen Lin, Y.-H. Weng, and K.-C. Li, "Treatment of Perfluorinated Chemicals by Electro-Microfiltration," *Environ. Sci. Technol.*, vol. 44, no. 20, pp. 7914–7920, Oct. 2010, doi: 10.1021/es101964y.
[105] S. M. Mitchell, M. Ahmad, A. L. Teel, and R. J. Watts, "Degradation of Perfluorooctanoic Acid by Reactive Species Generated through Catalyzed H2O2 Propagation Reactions," *Environ. Sci. Technol. Lett.*, vol. 1, no. 1, pp. 117–121, Jan. 2014, doi: 10.1021/ez4000862.
[106] O. S. Arvaniti, Y. Hwang, H. R. Andersen, A. S. Stasinakis, N. S. Thomaidis, and M. Aloupi, "Reductive degradation of perfluorinated compounds in water using Mg-aminoclay coated nanoscale zero valent iron," *Chem. Eng. J.*, vol. 262, pp. 133–139, Feb. 2015, doi:

10.1016/j.cej.2014.09.079.
[107] B. J. Yates, R. Darlington, R. Zboril, and V. K. Sharma, “High-valent iron-based oxidants to treat perfluorooctanesulfonate and perfluorooctanoic acid in water,” *Environ. Chem. Lett.*, vol. 12, no. 3, pp. 413–417, Sep. 2014, doi: 10.1007/s10311-014-0463-5.
[108] R. Rashid, I. Shafiq, P. Akhter, M. J. Iqbal, and M. Hussain, “A state-of-the-art review on wastewater treatment techniques: the effectiveness of adsorption method,” *Environ. Sci. Pollut. Res.*, vol. 28, no. 8, pp. 9050–9066, Feb. 2021, doi: 10.1007/s11356-021-12395-x.
[109] P. Senthil Kumar *et al.*, “A critical review on recent developments in the low-cost adsorption of dyes from wastewater,” *DESALINATION WATER Treat.*, vol. 172, pp. 395–416, 2019, doi: 10.5004/dwt.2019.24613.
[110] M. Faysal Hossain, N. Akther, and Y. Zhou, “Recent advancements in graphene adsorbents for wastewater treatment: Current status and challenges,” *Chin. Chem. Lett.*, vol. 31, no. 10, pp. 2525–2538, Oct. 2020, doi: 10.1016/j.cclet.2020.05.011.
[111] A. A. Siyal, M. R. Shamsuddin, A. Low, and N. E. Rabat, “A review on recent developments in the adsorption of surfactants from wastewater,” *J. Environ. Manage.*, vol. 254, p. 109797, Jan. 2020, doi: 10.1016/j.jenvman.2019.109797.
[112] M. Ince and O. Kaplan Ince, “An Overview of Adsorption Technique for Heavy Metal Removal from Water/Wastewater: A Critical Review,” *Int. J. Pure Appl. Sci.*, pp. 10–19, Dec. 2017, doi: 10.29132/ijpas.372335.
[113] S. Rajendran *et al.*, “A critical and recent developments on adsorption technique for removal of heavy metals from wastewater-A review,” *Chemosphere*, vol. 303, p. 135146, Sep. 2022, doi: 10.1016/j.chemosphere.2022.135146.
[114] F. Younas *et al.*, “Current and Emerging Adsorbent Technologies for Wastewater Treatment: Trends, Limitations, and Environmental Implications,” *Water*, vol. 13, no. 2, Art. no. 2, Jan. 2021, doi: 10.3390/w13020215.
[115] H. Sukmana, N. Bellahsen, F. Pantoja, and C. Hodur, “Adsorption and coagulation in wastewater treatment – Review,” *Prog. Agric. Eng. Sci.*, vol. 17, no. 1, pp. 49–68, Nov. 2021, doi: 10.1556/446.2021.00029.
[116] Q. Yu, R. Zhang, S. Deng, J. Huang, and G. Yu, “Sorption of perfluorooctane sulfonate and perfluorooctanoate on activated carbons and resin: Kinetic and isotherm study,” *Water Res.*, vol. 43, no. 4, pp. 1150–1158, Mar. 2009, doi: 10.1016/j.watres.2008.12.001.
[117] D. Zhang, Q. Luo, B. Gao, S.-Y. D. Chiang, D. Woodward, and Q. Huang, “Sorption of perfluorooctanoic acid, perfluorooctane sulfonate and perfluoroheptanoic acid on granular activated carbon,” *Chemosphere*, vol. 144, pp. 2336–2342, Feb. 2016, doi: 10.1016/j.chemosphere.2015.10.124.
[118] J. Li, Q. Li, L. Li, and L. Xu, “Removal of perfluorooctanoic acid from water with economical mesoporous melamine-formaldehyde resin microsphere,” *Chem. Eng. J.*, vol. 320, pp. 501–509, Jul. 2017, doi: 10.1016/j.cej.2017.03.073.
[119] W. Chen, X. Zhang, M. Mamadiev, and Z. Wang, “Sorption of perfluorooctane sulfonate and perfluorooctanoate on polyacrylonitrile fiber-derived activated carbon fibers: in comparison with activated carbon,” *RSC Adv.*, vol. 7, no. 2, pp. 927–938, Jan. 2017, doi: 10.1039/C6RA25230C.
[120] V. Ochoa-Herrera and R. Sierra-Alvarez, “Removal of perfluorinated surfactants by sorption onto granular activated carbon, zeolite and sludge,” *Chemosphere*, vol. 72, no. 10, pp.

1588–1593, Aug. 2008, doi: 10.1016/j.chemosphere.2008.04.029.
[121] M. C. Hansen, M. H. Børresen, M. Schlabach, and G. Cornelissen, "Sorption of perfluorinated compounds from contaminated water to activated carbon," *J. Soils Sediments*, vol. 10, no. 2, pp. 179–185, Mar. 2010, doi: 10.1007/s11368-009-0172-z.
[122] S. Das and A. Ronen, "A Review on Removal and Destruction of Per- and Polyfluoroalkyl Substances (PFAS) by Novel Membranes," *Membranes*, vol. 12, no. 7, Art. no. 7, Jul. 2022, doi: 10.3390/membranes12070662.
[123] R. Li *et al.*, "Efficient Removal of Per- and Polyfluoroalkyl Substances from Water with Zirconium-Based Metal–Organic Frameworks," *Chem. Mater.*, vol. 33, no. 9, pp. 3276–3285, May 2021, doi: 10.1021/acs.chemmater.1c00324.
[124] M. Hassan *et al.*, "Magnetic biochar for removal of perfluorooctane sulphonate (PFOS): Interfacial interaction and adsorption mechanism," *Environ. Technol. Innov.*, vol. 28, p. 102593, Nov. 2022, doi: 10.1016/j.eti.2022.102593.
[125] S. S. Dalahmeh, N. Alziq, and L. Ahrens, "Potential of biochar filters for onsite wastewater treatment: Effects of active and inactive biofilms on adsorption of per- and polyfluoroalkyl substances in laboratory column experiments," *Environ. Pollut.*, vol. 247, pp. 155–164, Apr. 2019, doi: 10.1016/j.envpol.2019.01.032.
[126] Y. Zhou *et al.*, "Modulating hierarchically microporous biochar via molten alkali treatment for efficient adsorption removal of perfluorinated carboxylic acids from wastewater," *Sci. Total Environ.*, vol. 757, p. 143719, Feb. 2021, doi: 10.1016/j.scitotenv.2020.143719.
[127] J. M. Steigerwald and J. R. Ray, "Adsorption behavior of perfluorooctanesulfonate (PFOS) onto activated spent coffee grounds biochar in synthetic wastewater effluent," *J. Hazard. Mater. Lett.*, vol. 2, p. 100025, Nov. 2021, doi: 10.1016/j.hazl.2021.100025.
[128] M. A. N. Shaikh, P. Sarkar, and T. Nawaz, "PFOA remediation from aqueous media using CTAB impregnated activated carbon: A closed-loop sustainable study with comprehensive selectivity analysis," *J. Water Process Eng.*, vol. 54, p. 103965, Aug. 2023, doi: 10.1016/j.jwpe.2023.103965.
[129] Y. Gao, S. Deng, Z. Du, K. Liu, and G. Yu, "Adsorptive removal of emerging polyfluoroalky substances F-53B and PFOS by anion-exchange resin: A comparative study," *J. Hazard. Mater.*, vol. 323, pp. 550–557, Feb. 2017, doi: 10.1016/j.jhazmat.2016.04.069.
[130] S. Deng, Q. Yu, J. Huang, and G. Yu, "Removal of perfluorooctane sulfonate from wastewater by anion exchange resins: Effects of resin properties and solution chemistry," *Water Res.*, vol. 44, no. 18, pp. 5188–5195, Oct. 2010, doi: 10.1016/j.watres.2010.06.038.
[131] S. T. M. L. D. Senevirathna *et al.*, "A comparative study of adsorption of perfluorooctane sulfonate (PFOS) onto granular activated carbon, ion-exchange polymers and non-ion-exchange polymers," *Chemosphere*, vol. 80, no. 6, pp. 647–651, Jul. 2010, doi: 10.1016/j.chemosphere.2010.04.053.
[132] S. Rai, S. Bahadure, M. J. Chaddha, and A. Agnihotri, "A Way Forward in Waste Management of Red Mud/Bauxite Residue in Building and Construction Industry," *Trans. Indian Natl. Acad. Eng.*, vol. 5, no. 3, pp. 437–448, Sep. 2020, doi: 10.1007/s41403-020-00100-2.
[133] S. Alam, S. Jain, and S. K. Das, "Characterization and an Overview of Utilization and Neutralization for Efficient Management of Bauxite Residue for Sustainable Environment," in *Building Materials for Sustainable and Ecological Environment*, V. Achal and C. S. Chin, Eds.,

Singapore: Springer, 2021, pp. 25–47. doi: 10.1007/978-981-16-1706-5_3.
[134] S. Rai, S. Bahadure, M. J. Chaddha, and A. Agnihotri, "Utilization of Aluminium Industry Solid Waste (Red Mud/Bauxite Residue) in Pollution Control," in *Innovations in Sustainable Mining: Balancing Environment, Ecology and Economy*, K. Randive, S. Pingle, and A. Agnihotri, Eds., Cham: Springer International Publishing, 2021, pp. 21–43. doi: 10.1007/978-3-030-73796-2_2.
[135] K. Evans, "The History, Challenges, and New Developments in the Management and Use of Bauxite Residue," *J. Sustain. Metall.*, vol. 2, no. 4, pp. 316–331, Dec. 2016, doi: 10.1007/s40831-016-0060-x.
[136] S. Rai, S. Bahadure, M. J. Chaddha, and A. Agnihotri, "Disposal Practices and Utilization of Red Mud (Bauxite Residue): A Review in Indian Context and Abroad," *J. Sustain. Metall.*, vol. 6, no. 1, pp. 1–8, Mar. 2020, doi: 10.1007/s40831-019-00247-5.
[137] A. Vidya, A. S. Poojitha, N. G. Reddy, and K. Samal, "Utilization of Red Mud (Bauxite Residue) in Environmental and Geotechnical Engineering Applications—An Overview," in *Transportation and Environmental Geotechnics*, K. Muthukkumaran, D. Rathod, E. R. Sujatha, and M. Muthukumar, Eds., Singapore: Springer Nature, 2023, pp. 243–251. doi: 10.1007/978-981-19-6774-0_23.
[138] M. C. Mishra, N. Gangadhara Reddy, B. Hanumantha Rao, and S. Kumar Das, "A Study on Evaluating the Usefulness and Applicability of Additives for Neutralizing Extremely Alkaline Red Mud Waste," in *Sustainable Environmental Geotechnics*, K. R. Reddy, A. K. Agnihotri, Y. Yukselen-Aksoy, B. K. Dubey, and A. Bansal, Eds., Cham: Springer International Publishing, 2020, pp. 139–149. doi: 10.1007/978-3-030-51350-4_16.
[139] W. Tang, M. Khavarian, and A. Yousefi, "14 - Red Mud," in *Sustainable Concrete Made with Ashes and Dust from Different Sources*, R. Siddique and R. Belarbi, Eds., in Woodhead Publishing Series in Civil and Structural Engineering. , Woodhead Publishing, 2022, pp. 577–606. doi: 10.1016/B978-0-12-824050-2.00013-9.
[140] I. Panda, S. Jain, S. K. Das, and R. Jayabalan, "Characterization of red mud as a structural fill and embankment material using bioremediation," *Int. Biodeterior. Biodegrad.*, vol. 119, pp. 368–376, Apr. 2017, doi: 10.1016/j.ibiod.2016.11.026.
[141] S. Ruyters, J. Mertens, E. Vassilieva, B. Dehandschutter, A. Poffijn, and E. Smolders, "The Red Mud Accident in Ajka (Hungary): Plant Toxicity and Trace Metal Bioavailability in Red Mud Contaminated Soil," *Environ. Sci. Technol.*, vol. 45, no. 4, pp. 1616–1622, Feb. 2011, doi: 10.1021/es104000m.
[142] J. Zhang *et al.*, "Sustainable utilization of bauxite residue (Red Mud) as a road material in pavements: A critical review," *Constr. Build. Mater.*, vol. 270, p. 121419, Feb. 2021, doi: 10.1016/j.conbuildmat.2020.121419.
[143] L. Wang *et al.*, "Application of Red Mud in Wastewater Treatment," *Minerals*, vol. 9, no. 5, Art. no. 5, May 2019, doi: 10.3390/min9050281.
[144] A. Bhatnagar, V. J. P. Vilar, C. M. S. Botelho, and R. A. R. Boaventura, "A review of the use of red mud as adsorbent for the removal of toxic pollutants from water and wastewater," *Environ. Technol.*, vol. 32, no. 3, pp. 231–249, Feb. 2011, doi: 10.1080/09593330.2011.560615.
[145] M. Habuda-Stanić, M. E. Ravančić, and A. Flanagan, "A Review on Adsorption of Fluoride from Aqueous Solution," *Materials*, vol. 7, no. 9, Art. no. 9, Sep. 2014, doi: 10.3390/ma7096317.

[146] F. Cheng, “Treating Waste with Waste – Calcined Bauxite Residue (CBR) as a Potential Wastewater Treatment Option for Oil Sands Process-affected Water (OSPW) and Municipal Wastewater,” ERA. Accessed: Aug. 15, 2024. [Online]. Available: https://era.library.ualberta.ca/items/17f1bf62-3fbb-4918-9599-6140896122a6
[147] S. Gostu, “Investigation of carbon-based reductant, low-temperature process for conversion of hematite in red-mud to magnetite - ProQuest.” Accessed: Aug. 06, 2024. [Online]. Available: https://www.proquest.com/docview/1766582114?pq-origsite=gscholar&fromopenview=true&sourcetype=Dissertations%20&%20Theses
[148] K. Barrow, B. I. Escher, K. A. Hicks, M. König, R. Schlichting, and M. J. Arlos, “Water quality monitoring with in vitro bioassays to compare untreated oil sands process-affected water with unimpacted rivers,” *Environ. Sci. Water Res. Technol.*, vol. 9, no. 8, pp. 2008–2020, 2023, doi: 10.1039/D2EW00988A.
[149] L. Pellenz *et al.*, “A comprehensive guide for characterization of adsorbent materials,” *Sep. Purif. Technol.*, vol. 305, p. 122435, Jan. 2023, doi: 10.1016/j.seppur.2022.122435.
[150] S. Bao, W. Yang, Y. Wang, Y. Yu, Y. Sun, and K. Li, “PEI grafted amino-functionalized graphene oxide nanosheets for ultrafast and high selectivity removal of Cr(VI) from aqueous solutions by adsorption combined with reduction: Behaviors and mechanisms,” *Chem. Eng. J.*, vol. 399, p. 125762, Nov. 2020, doi: 10.1016/j.cej.2020.125762.
[151] Y. Liu *et al.*, “Highly efficient and rapid removal of non-steroidal anti-inflammatory drugs from environmental samples based on an eco-friendly ZIF-67-molecularly imprinted composite,” *Chem. Eng. J.*, vol. 443, p. 136396, Sep. 2022, doi: 10.1016/j.cej.2022.136396.
[152] “Krotos Axis Ultra XPS description - nanoFAB Knowledge Base - nanoFAB Confluence.” Accessed: Aug. 15, 2024. [Online]. Available: https://confluence.nanofab.ualberta.ca/display/NFCORE/Krotos+Axis+Ultra+XPS+description
[153] P. Kingshott, G. Andersson, S. L. McArthur, and H. J. Griesser, “Surface modification and chemical surface analysis of biomaterials,” *Curr. Opin. Chem. Biol.*, vol. 15, no. 5, pp. 667–676, Oct. 2011, doi: 10.1016/j.cbpa.2011.07.012.
[154] J. Lefebvre, F. Galli, C. L. Bianchi, G. S. Patience, and D. C. Boffito, “Experimental methods in chemical engineering: X-ray photoelectron spectroscopy-XPS,” *Can. J. Chem. Eng.*, vol. 97, no. 10, pp. 2588–2593, 2019, doi: 10.1002/cjce.23530.
[155] V. Presser, C. Berthold, R. Wirth, and K. G. Nickel, “Structural characterisation of tribologically influenced silicon carbide ceramic surfaces,” *Curr. Opin. Solid State Mater. Sci.*, vol. 12, no. 5, pp. 73–80, Oct. 2008, doi: 10.1016/j.cossms.2009.02.001.
[156] rmladmin, “Difference between EDS and XPS Analysis,” Rocky Mountain Labs. Accessed: May 17, 2024. [Online]. Available: https://rockymountainlabs.com/eds-and-xps-analysis/
[157] B. V. Crist, “SEM-EDS Information Depth,” The XPS Library of XPS Technology and Science for Self-Training. Accessed: May 17, 2024. [Online]. Available: https://xpslibrary.com/sem-eds-information-depth/
[158] I. Murrieta-Pazos, C. Gaiani, L. Galet, B. Cuq, S. Desobry, and J. Scher, “Comparative study of particle structure evolution during water sorption: Skim and whole milk powders,” *Colloids Surf. B Biointerfaces*, vol. 87, no. 1, pp. 1–10, Oct. 2011, doi: 10.1016/j.colsurfb.2011.05.001.

[159] O. US EPA, “Method 533: Determination of Per- and Polyfluoroalkyl Substances in Drinking Water by Isotope Dilution Anion Exchange Solid Phase Extraction and Liquid Chromatography/Tandem Mass Spectrometry.” Accessed: Aug. 15, 2024. [Online]. Available: https://www.epa.gov/dwanalyticalmethods/method-533-determination-and-polyfluoroalkyl-substances-drinking-water-isotope
[160] S. Lath, E. R. Knight, D. A. Navarro, R. S. Kookana, and M. J. McLaughlin, “Sorption of PFOA onto different laboratory materials: Filter membranes and centrifuge tubes,” *Chemosphere*, vol. 222, pp. 671–678, May 2019, doi: 10.1016/j.chemosphere.2019.01.096.
[161] J. E. Zenobio, O. A. Salawu, Z. Han, and A. S. Adeleye, “Adsorption of per- and polyfluoroalkyl substances (PFAS) to containers,” *J. Hazard. Mater. Adv.*, vol. 7, p. 100130, Aug. 2022, doi: 10.1016/j.hazadv.2022.100130.
[162] J. Plazas-Tuttle, F. M. Giraldo, and A. Avila, *Nanomaterials for the Detection and Removal of Wastewater Pollutants*. Elsevier, 2020. doi: 10.1016/B978-0-12-818489-9.00001-3.
[163] A. Ladshaw, S. Yiacoumi, C. Tsouris, and D. DePaoli, “Generalized gas–solid adsorption modeling: Single-component equilibria,” *Fluid Phase Equilibria*, vol. 388, pp. 169–181, Feb. 2015, doi: 10.1016/j.fluid.2015.01.003.
[164] P. Neale, F. Leusch, and B. Escher, *Bioanalytical Tools in Water Quality Assessment: Second Edition*. IWA Publishing, 2021. doi: 10.2166/9781789061987.
[165] P. A. Neale *et al.*, “Application of Effect-Based Methods to Water Quality Monitoring: Answering Frequently Asked Questions by Water Quality Managers, Regulators, and Policy Makers,” *Environ. Sci. Technol.*, vol. 57, no. 15, pp. 6023–6032, Apr. 2023, doi: 10.1021/acs.est.2c06365.
[166] L. Zhang, Y. Zhang, M. Zhu, L. Chen, and B. Wu, “A critical review on quantitative evaluation of aqueous toxicity in water quality assessment,” *Chemosphere*, vol. 342, p. 140159, Nov. 2023, doi: 10.1016/j.chemosphere.2023.140159.
[167] J. Nelson, F. Bishay, A. van Roodselaar, M. Ikonomou, and F. C. P. Law, “The use of *in vitro* bioassays to quantify endocrine disrupting chemicals in municipal wastewater treatment plant effluents,” *Sci. Total Environ.*, vol. 374, no. 1, pp. 80–90, Mar. 2007, doi: 10.1016/j.scitotenv.2006.11.031.
[168] D. B. Huggett *et al.*, “Comparison of in Vitro and in Vivo Bioassays for Estrogenicity in Effluent from North American Municipal Wastewater Facilities,” *Toxicol. Sci.*, vol. 72, no. 1, pp. 77–83, Mar. 2003, doi: 10.1093/toxsci/kfg017.
[169] “BioTox™ LumoPlate™ Ultimate Matrix Kit.” Accessed: May 20, 2024. [Online]. Available: https://www.biotoxicity.com/index.php/ebpi-toxicity-tests/sediment-toxicity-tests/seditox-biotox-lumoplate-ultimate-matrix-kit-2
[170] K. Barrow, “In vitro bioassay monitoring to assess baseline conditions prior to potential discharge of treated oil sands process water in receiving aquatic environments,” ERA. Accessed: Dec. 02, 2023. [Online]. Available: https://era.library.ualberta.ca/items/b88edd72-d319-4b58-bd5f-f41c20e46d02
[171] P. Punyapalakul, K. Suksomboon, P. Prarat, and S. Khaodhiar, “Effects of Surface Functional Groups and Porous Structures on Adsorption and Recovery of Perfluorinated Compounds by Inorganic Porous Silicas,” *Sep. Sci. Technol.*, vol. 48, no. 5, pp. 775–788, Jan. 2013, doi: 10.1080/01496395.2012.710888.

[172] E. Gagliano, M. Sgroi, P. P. Falciglia, F. G. A. Vagliasindi, and P. Roccaro, "Removal of poly- and perfluoroalkyl substances (PFAS) from water by adsorption: Role of PFAS chain length, effect of organic matter and challenges in adsorbent regeneration," *Water Res.*, vol. 171, p. 115381, Mar. 2020, doi: 10.1016/j.watres.2019.115381.
[173] B. A. Mohamed, X. Bi, L. Y. Li, L. Leng, E.-S. Salama, and H. Zhou, "Bauxite residue as a catalyst for microwave-assisted pyrolysis of switchgrass to high quality bio-oil and biochar," *Chem. Eng. J.*, vol. 426, p. 131294, Dec. 2021, doi: 10.1016/j.cej.2021.131294.
[174] X. Qi *et al.*, "Analysis of bauxite residue components responsible for copper removal and related reaction products," *Chemosphere*, vol. 207, pp. 209–217, Sep. 2018, doi: 10.1016/j.chemosphere.2018.05.041.
[175] X.-F. Tan *et al.*, "Role of biochar surface characteristics in the adsorption of aromatic compounds: Pore structure and functional groups," *Chin. Chem. Lett.*, vol. 32, no. 10, pp. 2939–2946, Oct. 2021, doi: 10.1016/j.cclet.2021.04.059.
[176] J. Ren, X. Dyosiba, N. M. Musyoka, H. W. Langmi, M. Mathe, and S. Liao, "Review on the current practices and efforts towards pilot-scale production of metal-organic frameworks (MOFs)," *Coord. Chem. Rev.*, vol. 352, pp. 187–219, Dec. 2017, doi: 10.1016/j.ccr.2017.09.005.
[177] X. Qi *et al.*, "Analysis of bauxite residue components responsible for copper removal and related reaction products," *Chemosphere*, vol. 207, pp. 209–217, Sep. 2018, doi: 10.1016/j.chemosphere.2018.05.041.
[178] P. A. Mangrulkar, M. V. Joshi, S. P. Kamble, N. K. Labhsetwar, and S. S. Rayalu, "Hydrogen evolution by a low cost photocatalyst: Bauxite residue," *Int. J. Hydrog. Energy*, vol. 35, no. 20, pp. 10859–10866, Oct. 2010, doi: 10.1016/j.ijhydene.2009.10.075.
[179] E. K. Stebel *et al.*, "Absorption of short-chain to long-chain perfluoroalkyl substances using swellable organically modified silica," *Environ. Sci. Water Res. Technol.*, vol. 5, no. 11, pp. 1854–1866, 2019, doi: 10.1039/C9EW00364A.
[180] R. Mailler *et al.*, "Removal of emerging micropollutants from wastewater by activated carbon adsorption: Experimental study of different activated carbons and factors influencing the adsorption of micropollutants in wastewater," *J. Environ. Chem. Eng.*, vol. 4, no. 1, pp. 1102–1109, Mar. 2016, doi: 10.1016/j.jece.2016.01.018.
[181] T. M. Huggins, A. Haeger, J. C. Biffinger, and Z. J. Ren, "Granular biochar compared with activated carbon for wastewater treatment and resource recovery," *Water Res.*, vol. 94, pp. 225–232, May 2016, doi: 10.1016/j.watres.2016.02.059.
[182] S. Cheng *et al.*, "Comparison of activated carbon and iron/cerium modified activated carbon to remove methylene blue from wastewater," *J. Environ. Sci.*, vol. 65, pp. 92–102, Mar. 2018, doi: 10.1016/j.jes.2016.12.027.
[183] M. Park, S. Wu, I. J. Lopez, J. Y. Chang, T. Karanfil, and S. A. Snyder, "Adsorption of perfluoroalkyl substances (PFAS) in groundwater by granular activated carbons: Roles of hydrophobicity of PFAS and carbon characteristics," *Water Res.*, vol. 170, p. 115364, Mar. 2020, doi: 10.1016/j.watres.2019.115364.
[184] P. N. Omo-Okoro, C. J. Curtis, P. Karásková, L. Melymuk, O. A. Oyewo, and J. O. Okonkwo, "Kinetics, Isotherm, and Thermodynamic Studies of the Adsorption Mechanism of PFOS and PFOA Using Inactivated and Chemically Activated Maize Tassel," *Water. Air. Soil Pollut.*, vol. 231, no. 9, p. 485, Sep. 2020, doi: 10.1007/s11270-020-04852-z.

[185] M.-J. Chen *et al.*, "Influence of crystal topology and interior surface functionality of metal-organic frameworks on PFOA sorption performance," *Microporous Mesoporous Mater.*, vol. 236, pp. 202–210, Dec. 2016, doi: 10.1016/j.micromeso.2016.08.046.
[186] C. A. Clark, K. N. Heck, C. D. Powell, and M. S. Wong, "Highly Defective UiO-66 Materials for the Adsorptive Removal of Perfluorooctanesulfonate," *ACS Sustain. Chem. Eng.*, vol. 7, no. 7, pp. 6619–6628, Apr. 2019, doi: 10.1021/acssuschemeng.8b05572.
[187] J. Pala, T. Le, M. Kasula, and M. Rabbani Esfahani, "Systematic investigation of PFOS adsorption from water by Metal Organic Frameworks, Activated Carbon, Metal Organic Framework@Activated Carbon, and functionalized Metal Organic Frameworks," *Sep. Purif. Technol.*, vol. 309, p. 123025, Mar. 2023, doi: 10.1016/j.seppur.2022.123025.
[188] J. Wang *et al.*, "Critical Review of Thermal Decomposition of Per- and Polyfluoroalkyl Substances: Mechanisms and Implications for Thermal Treatment Processes," *Environ. Sci. Technol.*, vol. 56, no. 9, pp. 5355–5370, May 2022, doi: 10.1021/acs.est.2c02251.
[189] A. Maimaiti *et al.*, "Competitive adsorption of perfluoroalkyl substances on anion exchange resins in simulated AFFF-impacted groundwater," *Chem. Eng. J.*, vol. 348, pp. 494–502, Sep. 2018, doi: 10.1016/j.cej.2018.05.006.
[190] C. Thanh Vu and T. Wu, "Adsorption of short-chain perfluoroalkyl acids (PFAAs) from water/wastewater," *Environ. Sci. Water Res. Technol.*, vol. 6, no. 11, pp. 2958–2972, 2020, doi: 10.1039/D0EW00468E.
[191] H. Son, T. Kim, H.-S. Yoom, D. Zhao, and B. An, "The Adsorption Selectivity of Short and Long Per- and Polyfluoroalkyl Substances (PFASs) from Surface Water Using Powder-Activated Carbon," *Water*, vol. 12, no. 11, Art. no. 11, Nov. 2020, doi: 10.3390/w12113287.
[192] P. McCleaf, S. Englund, A. Östlund, K. Lindegren, K. Wiberg, and L. Ahrens, "Removal efficiency of multiple poly- and perfluoroalkyl substances (PFASs) in drinking water using granular activated carbon (GAC) and anion exchange (AE) column tests," *Water Res.*, vol. 120, pp. 77–87, Sep. 2017, doi: 10.1016/j.watres.2017.04.057.
[193] J. Hu, J. Wu, Q. Yao, C. Wang, L. Li, and C. Li, "Research and Selection of Sorbents for Volatile Organic Compounds (VOC) Sampling Tubes," *E3S Web Conf.*, vol. 441, p. 02008, 2023, doi: 10.1051/e3sconf/202344102008.
[194] P. Wolkoff, "Volatile Organic Compounds Sources, Measurements, Emissions, and the Impact on Indoor Air Quality," *Indoor Air*, vol. 5, pp. 5–73, Dec. 1995, doi: 10.1111/j.1600-0668.1995.tb00017.x.
[195] Y. Wang, C. Wang, X. Huang, Q. Zhang, T. Wang, and X. Guo, "Guideline for modeling solid-liquid adsorption: Kinetics, isotherm, fixed bed, and thermodynamics," *Chemosphere*, vol. 349, p. 140736, Feb. 2024, doi: 10.1016/j.chemosphere.2023.140736.
[196] Z. Zhang, D. Sarkar, R. Datta, and Y. Deng, "Adsorption of perfluorooctanoic acid (PFOA) and perfluorooctanesulfonic acid (PFOS) by aluminum-based drinking water treatment residuals," *J. Hazard. Mater. Lett.*, vol. 2, p. 100034, Nov. 2021, doi: 10.1016/j.hazl.2021.100034.
[197] P. M. Rodrigo *et al.*, "Batch and fixed bed sorption of low to moderate concentrations of aqueous per- and poly-fluoroalkyl substances (PFAS) on Douglas fir biochar and its Fe3O4 hybrids," *Chemosphere*, vol. 308, p. 136155, Dec. 2022, doi: 10.1016/j.chemosphere.2022.136155.
[198] K. L. Tan and B. H. Hameed, "Insight into the adsorption kinetics models for the

removal of contaminants from aqueous solutions," *J. Taiwan Inst. Chem. Eng.*, vol. 74, pp. 25–48, May 2017, doi: 10.1016/j.jtice.2017.01.024.
[199] H. Son and B. An, "Investigation of Adsorption Kinetics for Per- and Poly-fluoroalkyl substances (PFAS) Adsorption onto Powder Activated Carbon (PAC) in the Competing Systems," *Water. Air. Soil Pollut.*, vol. 233, no. 4, p. 129, Apr. 2022, doi: 10.1007/s11270-022-05599-5.
[200] D. Zhang, Q. Luo, B. Gao, S.-Y. D. Chiang, D. Woodward, and Q. Huang, "Sorption of perfluorooctanoic acid, perfluorooctane sulfonate and perfluoroheptanoic acid on granular activated carbon," *Chemosphere*, vol. 144, pp. 2336–2342, Feb. 2016, doi: 10.1016/j.chemosphere.2015.10.124.
[201] S. Deng *et al.*, "Enhanced adsorption of perfluorooctane sulfonate and perfluorooctanoate by bamboo-derived granular activated carbon," *J. Hazard. Mater.*, vol. 282, pp. 150–157, Jan. 2015, doi: 10.1016/j.jhazmat.2014.03.045.
[202] P. Meng, X. Fang, A. Maimaiti, G. Yu, and S. Deng, "Efficient removal of perfluorinated compounds from water using a regenerable magnetic activated carbon," *Chemosphere*, vol. 224, pp. 187–194, Jun. 2019, doi: 10.1016/j.chemosphere.2019.02.132.
[203] M. Park, K. D. Daniels, S. Wu, A. D. Ziska, and S. A. Snyder, "Magnetic ion-exchange (MIEX) resin for perfluorinated alkylsubstance (PFAS) removal in groundwater: Roles of atomic charges for adsorption," *Water Res.*, vol. 181, p. 115897, Aug. 2020, doi: 10.1016/j.watres.2020.115897.
[204] A. K. Ilango *et al.*, "Enhanced Adsorption of Mixtures of Per- and Polyfluoroalkyl Substances in Water by Chemically Modified Activated Carbon," *ACS EST Water*, vol. 3, no. 11, pp. 3708–3715, Nov. 2023, doi: 10.1021/acsestwater.3c00483.
[205] G. Niarchos, L. Georgii, L. Ahrens, D. B. Kleja, and F. Fagerlund, "A systematic study of the competitive sorption of per- and polyfluoroalkyl substances (PFAS) on colloidal activated carbon," *Ecotoxicol. Environ. Saf.*, vol. 264, p. 115408, Oct. 2023, doi: 10.1016/j.ecoenv.2023.115408.
[206] M. A. Al-Ghouti and D. A. Da'ana, "Guidelines for the use and interpretation of adsorption isotherm models: A review," *J. Hazard. Mater.*, vol. 393, p. 122383, Jul. 2020, doi: 10.1016/j.jhazmat.2020.122383.
[207] N. Tzabar and H. J. M. ter Brake, "Adsorption isotherms and Sips models of nitrogen, methane, ethane, and propane on commercial activated carbons and polyvinylidene chloride," *Adsorption*, vol. 22, no. 7, pp. 901–914, Oct. 2016, doi: 10.1007/s10450-016-9794-9.
[208] F. Li *et al.*, "Adsorption of perfluorinated acids onto soils: Kinetics, isotherms, and influences of soil properties," *Sci. Total Environ.*, vol. 649, pp. 504–514, Feb. 2019, doi: 10.1016/j.scitotenv.2018.08.209.
[209] A. C. Umeh *et al.*, "Multicomponent PFAS sorption and desorption in common commercial adsorbents: Kinetics, isotherm, adsorbent dose, pH, and index ion and ionic strength effects," *Sci. Total Environ.*, vol. 904, p. 166568, Dec. 2023, doi: 10.1016/j.scitotenv.2023.166568.
[210] A. C. Umeh, R. Naidu, E. Olisa, Y. Liu, F. Qi, and D. Bekele, "A systematic investigation of single solute, binary and ternary PFAS transport in water-saturated soil using batch and 1-dimensional column studies: Focus on mixture effects," *J. Hazard. Mater.*, vol. 461, p. 132688, Jan. 2024, doi: 10.1016/j.jhazmat.2023.132688.

[211] P. S. Pauletto and T. J. Bandosz, “Activated carbon versus metal-organic frameworks: A review of their PFAS adsorption performance,” *J. Hazard. Mater.*, vol. 425, p. 127810, Mar. 2022, doi: 10.1016/j.jhazmat.2021.127810.
[212] A. C. Umeh *et al.*, “Multicomponent PFAS sorption and desorption in common commercial adsorbents: Kinetics, isotherm, adsorbent dose, pH, and index ion and ionic strength effects,” *Sci. Total Environ.*, vol. 904, p. 166568, Dec. 2023, doi: 10.1016/j.scitotenv.2023.166568.
[213] Z. Du *et al.*, “Removal of perfluorinated carboxylates from washing wastewater of perfluorooctanesulfonyl fluoride using activated carbons and resins,” *J. Hazard. Mater.*, vol. 286, pp. 136–143, Apr. 2015, doi: 10.1016/j.jhazmat.2014.12.037.
[214] N. Liu, C. Wu, G. Lyu, and M. Li, “Efficient adsorptive removal of short-chain perfluoroalkyl acids using reed straw-derived biochar (RESCA),” *Sci. Total Environ.*, vol. 798, p. 149191, Dec. 2021, doi: 10.1016/j.scitotenv.2021.149191.
[215] E. Kumarasamy, I. M. Manning, L. B. Collins, O. Coronell, and F. A. Leibfarth, “Ionic Fluorogels for Remediation of Per- and Polyfluorinated Alkyl Substances from Water,” *ACS Cent. Sci.*, vol. 6, no. 4, pp. 487–492, Apr. 2020, doi: 10.1021/acscentsci.9b01224.
[216] S. Kancharla, P. Alexandridis, and M. Tsianou, “Sequestration of per- and polyfluoroalkyl substances (PFAS) by adsorption: Surfactant and surface aspects,” *Curr. Opin. Colloid Interface Sci.*, vol. 58, p. 101571, Apr. 2022, doi: 10.1016/j.cocis.2022.101571.
[217] D. Li *et al.*, “Efficient removal of short-chain and long-chain PFAS by cationic nanocellulose,” *J. Mater. Chem. A*, vol. 11, no. 18, pp. 9868–9883, 2023, doi: 10.1039/D3TA01851B.
[218] A. Yang, C. Ching, M. Easler, D. E. Helbling, and W. R. Dichtel, “Cyclodextrin Polymers with Nitrogen-Containing Tripodal Crosslinkers for Efficient PFAS Adsorption,” *ACS Mater. Lett.*, vol. 2, no. 9, pp. 1240–1245, Sep. 2020, doi: 10.1021/acsmaterialslett.0c00240.
[219] G. Gałęzowska, J. Rogowska, E. Olkowska, W. Ratajczyk, and L. Wolska, “Environmental Risk Assessment Resulting from Sediment Contamination with Perfluoroalkyl Substances,” *Molecules*, vol. 26, no. 1, Art. no. 1, Jan. 2021, doi: 10.3390/molecules26010116.
[220] A. Spyrou, D. Vlastos, and M. Antonopoulou, “Evidence on the genotoxic and ecotoxic effects of PFOA, PFOS and their mixture on human lymphocytes and bacteria,” *Environ. Res.*, vol. 248, p. 118298, May 2024, doi: 10.1016/j.envres.2024.118298.
[221] S. E. Fenton *et al.*, “Per- and Polyfluoroalkyl Substance Toxicity and Human Health Review: Current State of Knowledge and Strategies for Informing Future Research,” *Environ. Toxicol. Chem.*, vol. 40, no. 3, pp. 606–630, 2021, doi: 10.1002/etc.4890.
[222] M. Abbas *et al.*, “*Vibrio fischeri* bioluminescence inhibition assay for ecotoxicity assessment: A review,” *Sci. Total Environ.*, vol. 626, pp. 1295–1309, Jun. 2018, doi: 10.1016/j.scitotenv.2018.01.066.
[223] M. Wielsøe *et al.*, “Xeno-estrogenic activity of real-life mixtures of perfluoroalkylated substances in human placenta homogenates,” *Reprod. Toxicol.*, vol. 120, p. 108444, Sep. 2023, doi: 10.1016/j.reprotox.2023.108444.
[224] A. M. Temkin, B. A. Hocevar, D. Q. Andrews, O. V. Naidenko, and L. M. Kamendulis, “Application of the Key Characteristics of Carcinogens to Per and Polyfluoroalkyl Substances,” *Int. J. Environ. Res. Public. Health*, vol. 17, no. 5, Art. no. 5, Jan. 2020, doi:

10.3390/ijerph17051668.
[225] R. Crebelli *et al.*, “Can sustained exposure to PFAS trigger a genotoxic response? A comprehensive genotoxicity assessment in mice after subacute oral administration of PFOA and PFBA,” *Regul. Toxicol. Pharmacol.*, vol. 106, pp. 169–177, Aug. 2019, doi: 10.1016/j.yrtph.2019.05.005.
[226] “PhysChemProp_Table_July2023-FINAL.xlsx.” Accessed: Aug. 12, 2024. [Online]. Available: https://view.officeapps.live.com/op/view.aspx?src=https%3A%2F%2Fpfas-1.itrcweb.org%2Fwp-content%2Fuploads%2F2022%2F01%2FPhysChemProp_Table_July2023-FINAL.xlsx&wdOrigin=BROWSELINK

Appendix A Supplementary Material to Materials and Methods

Appendix A.1 Experimental setup of jar tester for mixing

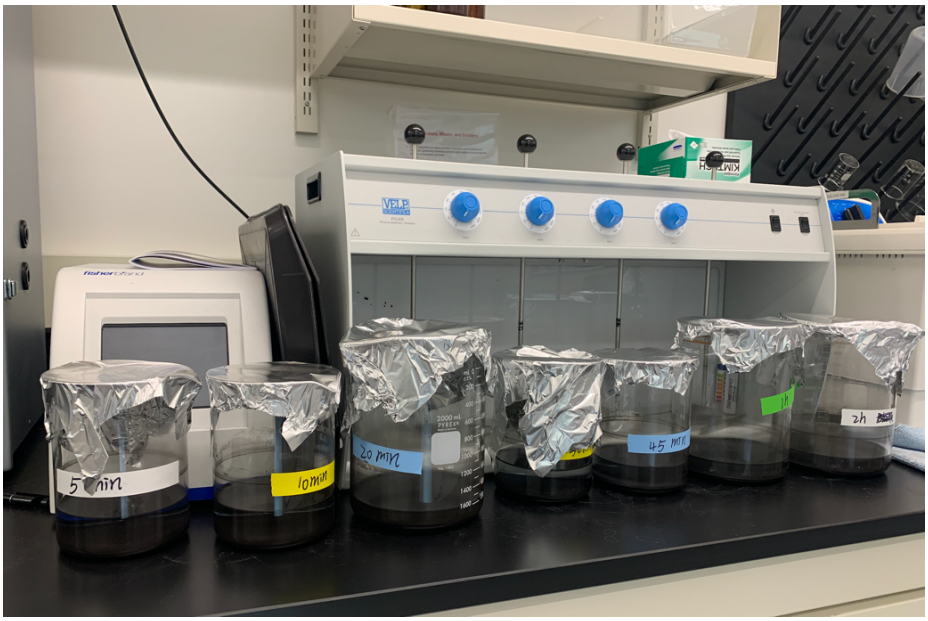

Figure A.1.1. *Jar tester employed in this study and ABR solutions after treatment.*

Appendix A.2 Visual comparison of raw bauxite residue and activated bauxite residue (ABR)

Figure A.2.1. *Raw bauxite residue (left) and activated bauxite residue (right).*

Appendix A.3 YES assay stock solution preparation

The preparation of reagents used for GOLD solution, other stock solutions, GOLD medium, and Minimal medium were listed in **Table A.3.1**, **Table A.3.2**, **Table A.3.3**, and **Table A.3.4**, respectively. GOLD Solution, GOLD Medium, and Minimal medium need to be stored in a 4°C fridge as well. Note that all the solid substances should be dissolved using a magnetic stirrer to ensure thorough mixing and all the stock solution needs to be filtered sterilize using the 0.2 μm filter unit before storage.

Table A.3.1. *Reagents for GOLD solution preparation adapted from Barrow et al. RT = room temperature. [148]*

Compound	Concentration (g/L)	Preparation	Storage	Amount for Gold Solution (mL)
Adenine hydrochloride hydrate	1.2	Autoclave	RT	75
L-Histidine-HCl	2.4	Autoclave	4°C	50
L-Arginine-HCl	2.4	Autoclave	4°C	25
L-Methionine	2.4	Autoclave	4°C	25
L-Tyrosine	0.9	Autoclave	RT	25
L-Isoleucine	3.6	Autoclave	4°C	25
L-Lysine-HCl	3.6	Autoclave	4°C	100
L-Phenylalanine	4	Autoclave	RT	25
L-Glutamic Acid	6	Autoclave	RT	25
L-Aspartic Acid	4	Autoclave	RT	25
L-Valine	18	Autoclave	4°C	25
L-Threonine	24	Autoclave	4°C	25
L-Serine	45	Autoclave	4°C	50
L-Leucine	3.6	Autoclave	RT	25
L-Tryptophan	4.8	Filter Sterilize	4°C	50
Uracil	2.4	Autoclave	RT	25

Table A.3.2. *Other stock solutions preparation adapted from Barrow et al. RT = room temperature. [148]*

Stock Solution	Ingredients	Preparation	Storage
10X YNB solution without amino acids	67g YNB without amino acids 1L ultrapure water	Filter Sterilize	4°C
20% Dextrose	200g Dextrose 1L ultrapure water	Add dextrose slowly Filter Sterilize	4°C
$CuSO_4$ Pentahydrate	250mg copper sulfate pentahydrate 100mL ultrapure water	Filter Sterilize	4°C
30% Glycerol	30mL Glycerol 70mL ultrapure water	Autoclave	RT

Table A.3.3. *GOLD medium preparation adapted from Barrow et al. [148]*

Solution	Volume (mL)
20% Dextrose Stock	60
10X YNB solution without amino acids	60
GOLD solution	110
Ultrapure water	370

Table A.3.4. *Minimal medium preparation adapted from Barrow et al. [148]*

Solution	Volume (mL)
20% Dextrose Stock	100
10X YNB solution without amino acids	100
L-Lysine-HCl	10
Ultrapure water	790

Appendix B Supplementary Material to Results and Discussions

Appendix B.1 Bond type analysis from XPS

Table B.1.1. *Fluorine bond types from XPS spectra in samples of various dosages for 0.1 mg/L individual PFAS.*

ABR Dosage (g/L)	PFAS concentration (mg/L)	Fluorine bonds energy position (eV)	Bond Type
2	0	684.9	Metal bond
2	0.1	685.2, 688.1, 692.1	Metal bond, Carbon bond, no-matching
6	0.1	685.9	Metal or Carbon bond
10	0.1	685.5	Metal bond

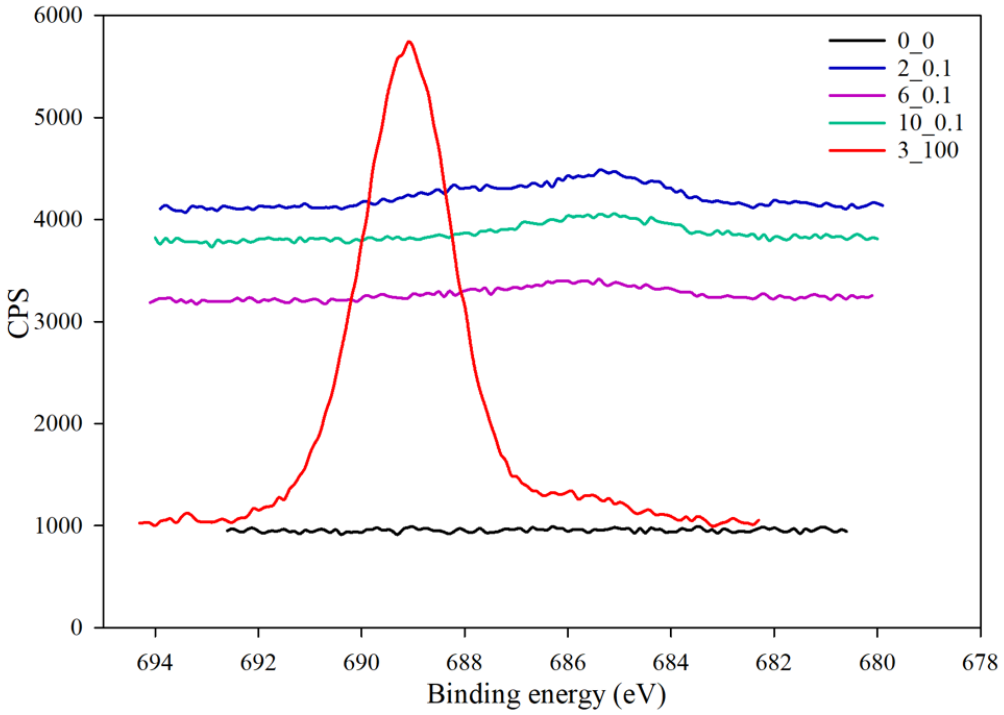

Figure B.1.1. *Florine spectra from different ABR sludge samples. The nomenclature is dosage(g/L)_concentration of individual PFAS (mg/L).*

Appendix B.2 SEM/EDX images of ABR samples

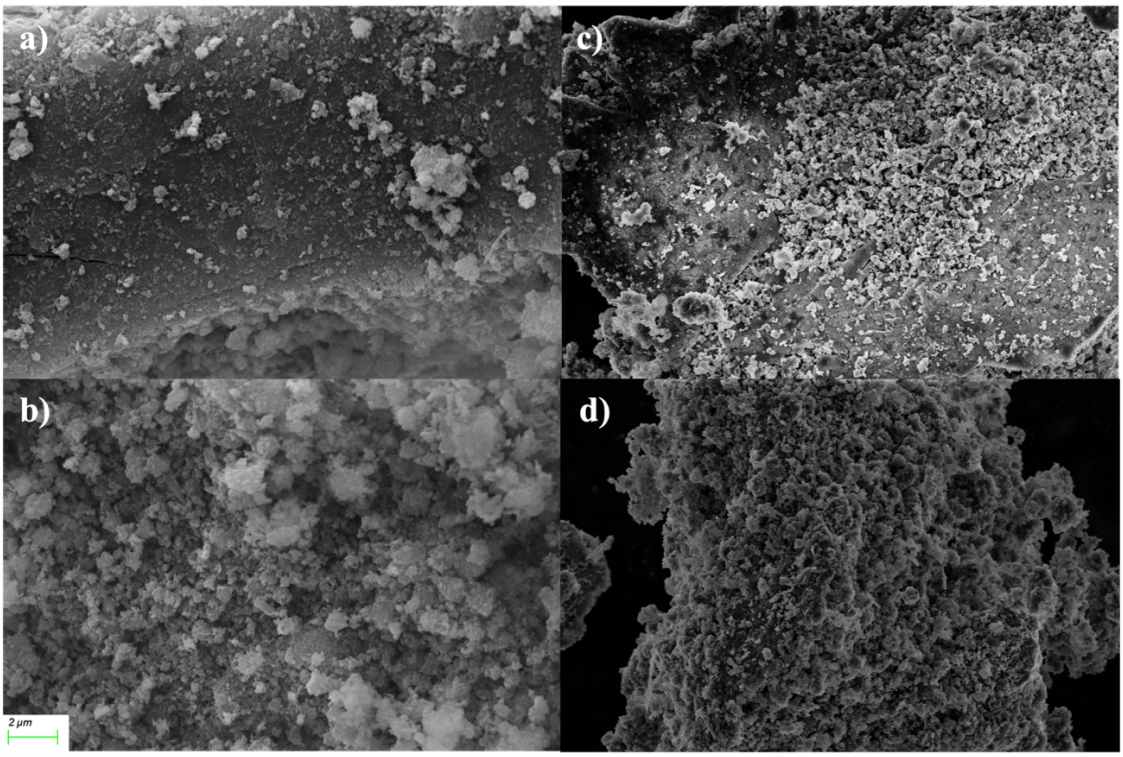

Figure B.2.1. *Scanning electron microscope (SEM) images of* ***(a), (b)*** *"virgin" ABR (e.g., ABR without treatment) and* ***(c), (d)*** *"spent" ABR (e.g., ABR saturated with two PFAS). These images were taken at a magnification of 5000× and a working distance of 7.3–8 mm.*

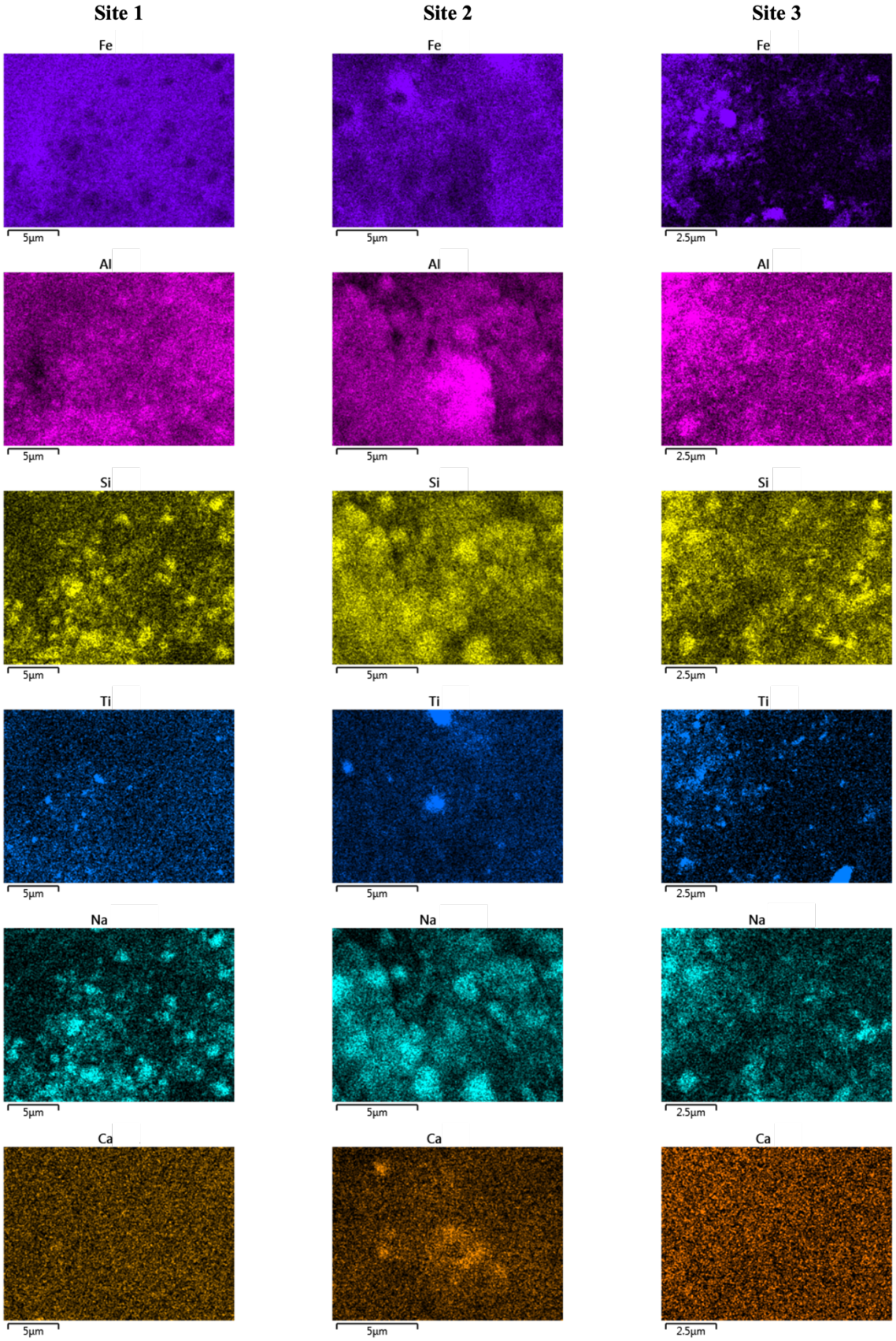

Figure B.2.2. *Distribution mapping of other abundant elements (Fe, Al, Si, Ti, Na, Ca) on the ABR surface from three sites.*

Appendix B.3 Raw data and reporting detection limits of removal efficiency experiments for various dosages and exposure periods

Table B.3.1. *Raw data of removal efficiency of PFAS after application of ABR at various dosages and exposure periods. All the unit for PFAS concentration is µg/L. RDL = reporting detection limit.*

PFAS substance	Blank 1	50 g/L ABR - 24h	100 g/L ABR - 24h	Blank 2	50 g/L ABR - 1h	100 g/L ABR - 1h	10 g/L ABR	15g/L ABR	25 g/L ABR	RDL
PFBA	0.6	0.42	0.48	0.69	0.44	0.38	0.43	0.55	0.42	0.02
PFPeA	0.58	0.15	0.11	0.63	0.21	0.13	0.18	0.28	0.14	
PFHxA	0.61	0.054	0.029	0.67	0.065	0.039	0.045	0.086	0.06	
PFHpA	0.51	0.02	<0.020	0.54	0.022	<0.020	<0.020	0.024	0.039	
PFOA	0.58	<0.020	<0.020	0.56	<0.020	<0.020	<0.020	0.021	0.035	
PFNA	0.64	<0.020	<0.020	0.66	<0.020	<0.020	<0.020	<0.020	0.025	
PFDA	0.58	<0.020	<0.020	1	<0.020	<0.020	0.032	0.037	0.061	
PFUnA	0.54	<0.020	<0.020	0.9	<0.020	<0.020	0.095	0.084	0.14	
PFTEDA	0.44	<0.020	<0.020	0.048	<0.020	<0.020	<0.020	<0.020	<0.020	
PFBS	0.61	0.039	0.023	0.68	0.066	0.038	0.038	0.069	0.03	

Appendix B.4 Raw data and reporting detection limits of kinetics experiments

Table B.4.1. *Raw data of adsorption kinetic experiments of PFAS treated by ABR. All the unit for PFAS concentration is µg/L. RDL = reporting detection limit.*

PFAS Substance	0 min	RDL	5 min	10 min	RDL	20 min	30 min	45 min	1 h	RDL	2 h	RDL	2 h no treatment control	RDL
PFBA	<2.0		<1.0	<1.0		<0.40	<0.40	<0.40	<0.40		<0.20		<2.0	
PFPeA	13		9.7	8.9		7.4	7.3	7.4	6.7		6.0		12	
PFHxA	58		28	22		15	14	14	11		8.8		54	
PFHpA	<2.0		<1.0	<1.0		<0.4	<0.40	<0.40	<0.40		<0.20		<2.0	
PFOA	91	2.0	5.8	3.5	1.0	2.2	1.5	1.9	1.6	0.40	1.1	0.20	83	2.0
PFNA	100		1.6	1.4		0.86	0.49	0.52	0.79		0.43		87	
PFDA	90		<1.0	1.3		0.62	<0.40	<0.40	0.52		0.27		55	
PFUnA	100		<1.0	1.0		1.1	<0.40	<0.40	0.56		0.32		20	
PFTEDA	25		<1.0	<1.0		<0.40	<0.40	<0.40	<0.40		<0.20		21	
PFBS	150		70	55		38	39	39	29		23		130	

Appendix B.5 Parameters for evaluating the trend of PFAS transfer from aqueous to gas phase

Table B.5.1. *Summary of vapor pressure and Henry's Law constants of PFAS used in this study. All values are average from [226].*

PFAS substance	Vapor Pressure (Pa)	Henry's Law Kaw (Dimensionless)	Henry's Law Kaw (atm-m^3/mol)
PFBA	1443.11	0.25	0.00628
PFPeA	827.90	1.80	0.04501
PFHxA	164.06	3.39	0.08294
PFHpA	310.96	11.19	0.26896
PFOA	169.60	28.94	7.00802
PFNA	99.93	199.91	4.92702
PFDA	244.80	730.92	17.93720
PFUnA	40.16	2242.04	54.79052
PFTEDA	0.52	185000.34	4534.00903
PFBS	158.10	2.50	0.06502

Appendix B.6 Estimation of ABR optimal dosage from adsorption isotherm study

As the morphology of ABR is similar to that of PAC, the approximate value of the required dosage can be calculated using the usage rate equation for the Freundlich isotherm model of PAC (**(Equation B.*6.1*** and **(Equation B.*6.2***). PFHpA as an example here, K_F is 1.52 and 1/n was 1.42.

$$D_{PAC} = \frac{C_{inf} - C_{eff}}{q_e|C_{eff}} \textbf{\textit{(Equation B.6.1)}}$$

$$q_e|C_{eff} = KC_{eff}^{\frac{1}{n}} \textbf{\textit{(Equation B.6.2)}}$$

Table B.6.1. *Dosages of ABR are required for various target removal efficiency of PFHpA.*

Initial Concentration (C_{inf}) (μg/L)	Target removal efficiency (treatment goal) (%)	C_{eff} (μg/L)	q_e (μg/g)	Dosage (g/L)
100	99	1	1.52	64.99
	95	5	14.88	6.39
	90	10	39.69	2.27
	50	50	387.59	0.13
	30	70	624.13	0.05
	10	90	890.87	0.01

Appendix B.7 LC_{50} and EC_{50} dose-response curves from *Daphnia magna* acute toxicity test

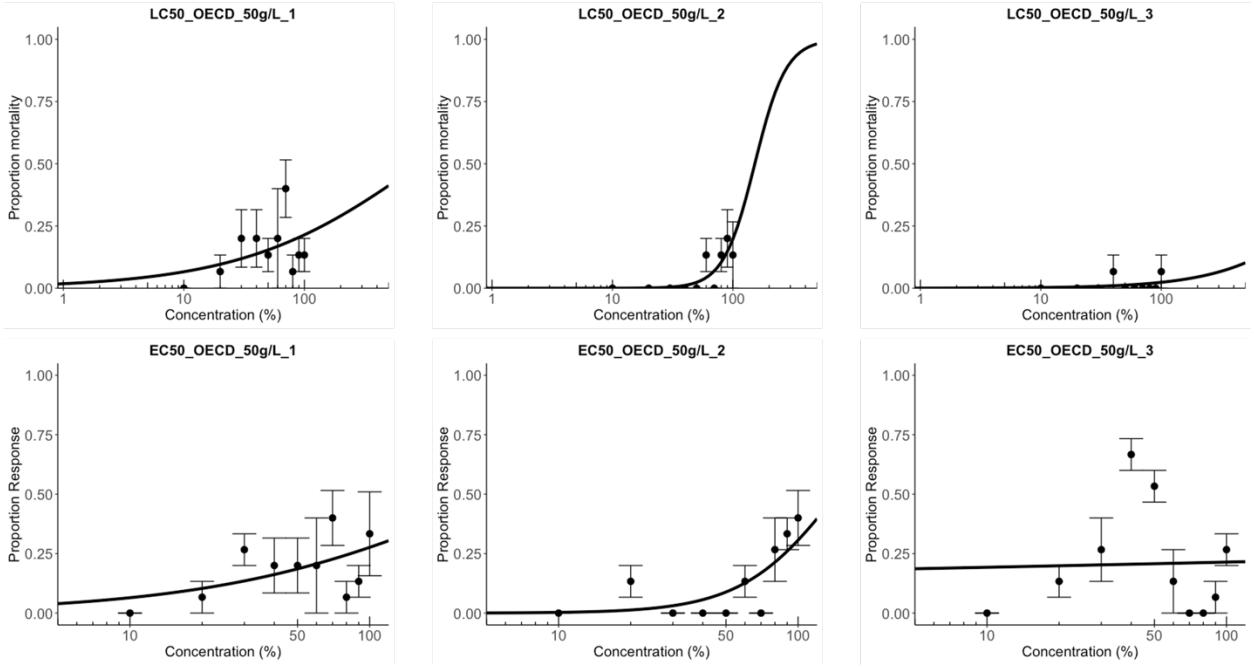

Figure B.7.1. *LC_{50} and EC_{50} dose-response curves of OECD water treated with 50 g/L ABR for Daphnia magna acute toxicity test.*